

MICROCOPY RESOLUTION TEST CHART  
NATIONAL BUREAU OF STANDARDS-1963-A

**LEVEL III**

12

AD

AD A110441

CONTRACT REPORT ARBRL-CR-00475

IMPROVED SAFETY OF RAILROAD CAR WHEELS

Prepared by

IIT Research Institute  
10 West 35th Street  
Chicago, Illinois 60616

SDTIC  
SELECTED  
FEB 3 1982  
H

December 1981



**US ARMY ARMAMENT RESEARCH AND DEVELOPMENT COMMAND  
BALLISTIC RESEARCH LABORATORY  
ABERDEEN PROVING GROUND, MARYLAND**

Approved for public release; distribution unlimited.

ENC FILE COPY

82 08 02 033

UNCLASSIFIED

SECURITY CLASSIFICATION OF THIS PAGE (When Data Entered)

REPORT DOCUMENTATION PAGE		READ INSTRUCTIONS BEFORE COMPLETING FORM
1. REPORT NUMBER CONTRACT REPORT ARBRL-CR-00475	2. GOVT ACCESSION NO. ADA110 441	3. RECIPIENT'S CATALOG NUMBER
4. TITLE (and Subtitle) IMPROVED SAFETY OF RAILROAD CAR WHEELS	5. TYPE OF REPORT & PERIOD COVERED Final Report Draft	
	6. PERFORMING ORG. REPORT NUMBER T6005	
7. AUTHOR(s) Milton R. Johnson Rhees R. Robinson	8. CONTRACT OR GRANT NUMBER(s) DAAK11-78-C-0046	
9. PERFORMING ORGANIZATION NAME AND ADDRESS IIT Research Institute 10 West 35th Street Chicago, Illinois 60616	10. PROGRAM ELEMENT, PROJECT, TASK AREA & WORK UNIT NUMBERS	
11. CONTROLLING OFFICE NAME AND ADDRESS US Army Armament Research & Development Command US Army Ballistic Research Laboratory (DRDAR-BL) Aberdeen Proving Ground, MD 21005	12. REPORT DATE December 1981	
	13. NUMBER OF PAGES 96	
14. MONITORING AGENCY NAME & ADDRESS (if different from Controlling Office)	15. SECURITY CLASS. (of this report) Unclassified	
	15a. DECLASSIFICATION/DOWNGRADING SCHEDULE	
16. DISTRIBUTION STATEMENT (of this Report)  Approved for public release; distribution unlimited.		
17. DISTRIBUTION STATEMENT (of the abstract entered in Block 2 - if different from Report)		
18. SUPPLEMENTARY NOTES		
19. KEY WORDS (Continue on reverse side if necessary and identify by block number)  railroad wheels railroad wheel failure thermal cracks railroad safety		
20. ABSTRACT (Continue on reverse side if necessary and identify by block number)  The safety of rail transportation would be improved by reducing the failure rate of railroad car wheels. Changes in design, materials, or operating limits need to be considered, but before such changes can be recommended one needs to have a better understanding of the factors which lead to wheel failures.		

(Continued)

115350

UNCLASSIFIED

SECURITY CLASSIFICATION OF THIS PAGE(When Data Entered)

20. ABSTRACT (concl)

As a result of evaluating the state of the art of railroad wheel failure analysis it was concluded that detailed studies should be made of the conventional curved plate and straight plate designs relating to crack initiation and growth as an aid to evaluating the advantages of different wheel designs. Results from thermal stress analyses of drag braking showed that the stress distributions in curved plate and straight plate wheel designs can be substantially different. While the thermal stresses at the conclusion of the braking period are larger in straight plate wheels the residual stresses following the subsequent cooling of the wheel are about the same magnitude in both types of wheel.

Stresses calculated from vertical and lateral loads at the wheel/rail interface were generally quite low, except near the contact zone. When the cyclic stress ranges from these loads were combined with the residual stresses from severe thermal loads, it was shown that the stress ranges often occur in combination with high stress ratios. The stress range data were reviewed to estimate the conditions under which thermal crack propagation may be expected, but the significance of the calculations is restricted by the limited amount of applicable crack growth data. Crack growth is associated with small stress changes superimposed on large residual stress fields. These are conditions where limited material property test data are available.

Although analytic techniques are helpful in establishing the relative importance of certain parameters affecting the initiation and development of wheel failures, results from full-scale experiments are required before a complete understanding of failure phenomenology can be expected. Facilities are required where wheels can be subjected to severe thermal loadings in combination with simulated vertical and lateral wheel/rail loads. The test fixture should be constructed in such a way that a wheel can be allowed to fail during a test.



UNCLASSIFIED

SECURITY CLASSIFICATION OF THIS PAGE(When Data Entered)

## EXECUTIVE SUMMARY

→ The work described in this report was directed at the improvement in the safety of rail transportation by reducing the failure rate of railroad car wheels. Changes in design, materials, or operating limits need to be considered. Before such changes can be recommended, however, one needs to have a better understanding of the factors which lead to wheel failures.

Railroad freight car wheels must be designed to fulfill a wide range of service requirements. They must transmit the high mechanical loads accompanying modern high speed train operations and also serve as a heat sink for the energy dissipated by the tread brake system. Railroad wheels are generally expected to provide at least 160,000 km (100,000 miles) of service. A high reliability against failure is necessary because failure of a wheel is likely to result in a train derailment with serious consequences. Railroad wheels must also be tolerant to a considerable amount of wear which results in large cross-sectional changes in the wheel rim over the lifetime of the wheel.

To obtain an improvement in wheel performance one must consider changes in wheel material specifications and wheel design configurations. Wheel failures are inhibited by the use of steels with higher fracture toughness. Within the present grades of wheel steel, the use of the steels with lower carbon content will increase fracture toughness, but lower the resistance to wear. One must therefore strike a balance between wear and fracture resistance. Various alloys have been developed with improved fracture toughness and wear properties, but their use has not gained acceptance on U.S. railroads, primarily because of their additional cost.

The feasibility of using different wheel plate designs to reduce the stresses associated with thermal and mechanical loads has been the subject of past investigations. These studies have generally indicated that the so-called deep-dish curved plate design and the straight plate design, both of which are in common use, maintain satisfactory stress levels in response to normal loadings. Some individuals express preference for the deep dish curved plate design because it exhibits lower plate stresses in response to thermal loads.



Accession For	
NTIS GRA&I	<input checked="" type="checkbox"/>
DTIC TAB	<input type="checkbox"/>
Unannounced	<input type="checkbox"/>
Justification	
By	
Distribution/	
Availability Codes	
Avail and/or	Special
Dist	<b>A</b>

As a result of evaluating these data and other relevant information it was concluded that the detailed analysis work should emphasize comparisons of the conventional curved plate and straight plate designs which are presently in use on U.S. railroads. It was apparent that more detailed stress analyses were required relating to crack initiation and growth before one could make general statements about the advantages of different wheel designs.

A number of analytical studies were conducted to determine the conditions under which wheels are most susceptible to thermal crack development. A two-dimensional elastic-plastic code was used to calculate the shifts in the residual stress field of wheels due to severe thermal load. An elastic three-dimensional code was also used to calculate the stresses which are due to vertical and lateral wheel/rail forces. The cyclic nature of these stresses resulting from the rotation of the wheel were also determined. Results from the two types of calculations were combined by superimposing the cyclic stresses on the residual stress fields calculated from the thermal analysis.

The results from the thermal stress analyses showed that the stress distributions in curved plate and straight plate wheel designs can be substantially different when the wheels are subjected to the same thermal load. While the thermal stresses at the conclusion of the braking period are larger in the straight plate wheel design than in the curved plate design, the residual stresses following the subsequent cooling of the wheel are about the same magnitude in each type of wheel. From one standpoint the residual stress field in the curved plate design may be less satisfactory because of the high tensile stresses on the inside face of the rim, which is a common site for the initiation of thermal cracks.

The wheel stresses calculated for vertical and lateral loads at the wheel/rail interface were generally quite low. When the cyclic stress ranges from these loads were combined with the residual stresses from severe thermal loads, it was shown that the stress ranges often occur in combination with high stress ratios. The largest stress ratio conditions were generally calculated for the flange and inside rim positions. The results also indicated that the combination of outwardly directed lateral loads and vertical loads produced the largest mechanical stress ranges, but this is a relatively rare service load condition which is unlikely to result in a large number of stress cycles. The combined data from the stress calculations did not indicate any significant advantages for either the curved plate or straight plate wheel configurations.

The stress range data for mechanical load stresses combined with thermally induced residual stresses, were reviewed to estimate the conditions under which thermal crack propagation may be expected. The data indicated that the most severe condition occurs on one wear wheels at the inside rim position. Minimum threshold crack depth dimensions for crack extension were calculated. The case where lateral load acts in conjunction with the vertical load, but is directed away from the flange gave the smallest threshold crack size. However, this loading condition would not be representative of conditions where a large number of stress cycles can be anticipated. Excluding these cases the smallest critical crack depth was 2.5 mm (0.098 inch) for a vertical edge load with no lateral load.

The significance of the threshold crack calculations is restricted by the limited amount of applicable crack growth data. Crack growth is associated with high stress ratios and low changes in stress intensity resulting from small stress changes imposed on large residual stress fields. This is a condition where limited material property test data are available. The assumed characteristics of the material in this region was extrapolated from test data obtained at larger stress intensity ranges and at  $R=0$ . The extrapolation of the data reduces the confidence in its accuracy. Therefore, the results should be used primarily as an indication of the trends that can be expected.

Another limitation associated with the application of analytical procedures to the study of wheel failure phenomena is the lack of material property data at elevated temperatures. The lack of data describing the modification of the yield point and the definition of the stress-strain curve at high temperatures is especially critical. The modification of the residual stress field in the wheels will depend to a large extent on the degree of yielding that takes place during severe thermal loads.

Although analytic techniques are helpful in establishing the relative importance of certain parameters affecting the initiation and development of wheel failures, results from full-scale experiments are required before a complete understanding of failure phenomenology can be expected. Facilities are required where wheels can be subjected to severe thermal loadings in combination with simulated vertical and lateral wheel/rail loads. The test fixture should be constructed in such a way that a wheel can be allowed to fail during a test. The equipment should be capable of subjecting wheels to thermal loads in excess of 37 kW (50 bhp) and 222 kN (50,000 lb) wheel/rail loads. The results from such tests could establish the safety margins in the operation of present wheel designs. The test work should be coordinated with wheel analysis programs in order to gain guidance for the specification of test conditions. Tests could be used to verify the analytic procedures.



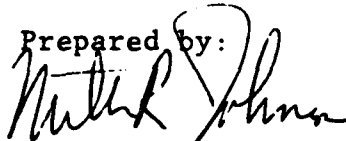
## PREFACE

The work described in this report was conducted by IIT Research Institute (IITRI) under the authorization of Contract DAAK11-78-C-0046 for the Ballistic Research Laboratory (BRL) of Aberdeen Proving Ground, Maryland. The work involved the study of factors which lead to railroad wheel failures as an aid to the determination of ways for reducing these failures and thereby making rail transportation safer.

Dr. M. R. Johnson was the IITRI project manager for this work. Mr. C. Mancillus of IITRI's Electronics Division assisted the authors in developing the computer programs for wheel analysis.

Dr. Charles Anderson was the cognizant BRL technical monitor. His helpful suggestions and guidance throughout the course of the work are gratefully acknowledged.

Prepared by:

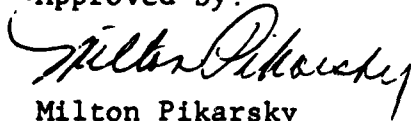


Milton R. Johnson  
Senior Engineering Advisor  
Transportation Research Division



Rhee R. Robinson  
Senior Research Engineer  
Engineering Division

Approved by:



Milton Pikarsky  
Director of Research  
Transportation Research Division

## TABLE OF CONTENTS

	<u>Page</u>
EXECUTIVE SUMMARY	3
TABLE OF CONTENTS	9
LIST OF ILLUSTRATIONS	11
LIST OF TABLES	13
1. OBJECTIVE	15
2. BACKGROUND	16
3. CONSIDERATIONS IN THE DESIGN AND USE OF RAILROAD CAR WHEELS	18
3.1 Wheel Loadings	18
3.2 Materials	19
3.3 Types of Wheel Failures	19
3.3.1 Thermal Cracks	19
3.3.2 Plate Cracks	21
3.4 Complexity of Wheel Failure Phenomena	22
3.5 Analysis of Wheels	23
3.5.1 Previous Studies	23
3.5.2 Analytic Procedures Used in This Program	23
3.6 Approach	24
4. RESULTS: THERMAL STRESS ANALYSIS	25
4.1 Wheel Types	25
4.2 Cases Considered	25
4.3 Summary of Results	27
4.4 Detailed Results Associated With 37 kW Cases	27
4.5 Repeated Severe Thermal Load Applications	42
4.6 Cyclic Stresses Due to Service Braking	45
4.7 Simplifying Assumptions	45
4.7.1 Axisymmetric Heat Impact	45
4.7.2 Heat Conducted to Brake Shoe and Brake Head	48
4.7.3 Heat Conducted to Rail	48
5. RESULTS: WHEEL REVOLUTION STRESS VARIATIONS	50
5.1 Vertical Load Stresses	50
5.1.1 Circumferential Variation	50
5.1.2 Stress Variation with Load Position, One and Two Wear Straight Plate Wheels	50
5.1.3 Stress Variations from Dynamic Effects	53
5.1.4 Factors Affecting Accuracy of Calculations	54

## LIST OF ILLUSTRATIONS

<u>Figure</u>	<u>Page</u>
1. Load Positions and Stress Data Locations	26
2. Temperature Distribution, °C (°F), One Wear Straight Plate Wheel after 60 minutes of 37 kW (50 bhp) Drag Brake Application	29
3. Temperature Distribution, °C (°F), One Wear Curved Plate Wheel after 60 minutes of 37 kW (50 bhp) Drag Brake Application	30
4. Extent of Yielded Region, One Wear Straight Plate Wheel after 60 minutes of 37 kW (50 bhp) Drag Brake Application	31
5. Extent of Yielded Region, One Wear Curved Plate Wheel after 60 minutes of 37 kW (50 bhp) Drag Brake Application	32
6. Distribution of Circumferential Stress ( $\sigma_{\theta}$ ) in MPa (ksi), One Wear Straight Plate Wheel after 60 minutes of 37 kW (50 bhp) Drag Brake Application	34
7. Distribution of Circumferential Stress ( $\sigma_{\theta}$ ) in MPa (ksi), One Wear Curved Plate Wheel after 60 minutes of 37 kW (50 bhp) Drag Brake Application	35
8. Distribution of Residual Circumferential Stresses ( $\sigma_{\theta}$ ) in MPa (ksi), One Wear Straight Plate Wheel Following 37 kW (50 bhp) Drag Brake Application for 1 hour (cooled wheel)	36
9. Distribution of Residual Circumferential Stresses ( $\sigma_{\theta}$ ) in MPa (ksi), One Wear Curved Plate Wheel Following 37 kW (50 bhp) Drag Brake Application for 1 hour (cooled wheel)	37
10. Displacement of Hot One Wear Straight Plate Wheel after 60 minutes of 37 kW (50 bhp) Drag Brake Application	38
11. Displacement of Hot One Wear Curved Plate Wheel after 60 minutes of 37 kW (50 bhp) Drag Brake Application	39
12. Displacement Configuration of Cool, One Wear Straight Plate Wheel Following 37 kW (50 bhp) Drag Brake Application for 1 hour	40

## LIST OF ILLUSTRATIONS (concl)

<u>Figure</u>	<u>Page</u>
13. Displacement Configuration of Cool, One Wear Curved Plate Wheel Following 37 kW (50 bhp) Drag Brake Application for 1 hour	41
14. Rim and Hub Fillet Radial Stresses, in MPa (ksi) for Two 60-minute 37 kW (50 bhp) Thermal Loads	43
15. Circumferential Rim Stress in MPa (ksi) for Two 60-minute 37 kW (50 bhp) Thermal Loads	44
16. Estimate of Brake Power as a Function of Time for Service Braking from 96 km/h (60 mph)	46
17. Circumferential Rim Stresses as a Function of Time for Service Braking Thermal Load	46
18. Radial Hub Plate Fillet Stresses as a Function of Time for Service Braking Thermal Load	47
19. Representation of Wheel/Rail Contact Zone	49
20. Finite Element Mesh for Two Wear Straight Plate Wheel	51
21. Octahedral Shear Stress as a Function of Angle from Radial Plane of Load Application, 142 kN (32,000 lb) Vertical Wheel Load	52
22. Element Locations Used for Study of Convergence of Modal Solution	55
23. Radial Stress versus Number of Modes	56
24. Circumferential Stress versus Number of Modes	57
25. Octahedral Shear Stress as a Function of Angle from Radial Plane of Load Application, 44 kN (10,000 lb) Lateral Wheel Load	59
26. Estimated Crack Growth Curves for Class BR Wheel Steel	74
27. Threshold Stress Intensity Factor Range as a Function of Stress Ratio, R	78
28. Strain Gage Positions for Induction Heating Test	85

## LIST OF TABLES

	<u>Page</u>
1. Material Properties of Wheel Steels	20
2. Residual Circumferential Stresses in Rim Following 60 minute Drag Braking	28
3. Predicted Heat Flow at Wheel/Rail Interface	49
4. Circumferential Stress Variations Caused by Vertical Wheel Load of 142 kN (32 klb)	53
5. Index of Tabulated Stresses for Combined Loads	60
Circumferential Rim Stresses, Residual Stresses from Thermal Load Combined with Stresses from Mechanical Load	
6a. Vertical tape line load, no lateral load and 30 kW (40 bhp) thermal load	61
6b. Vertical tape line load, no lateral load and 37 kW (50 bhp) thermal load	62
7a. Vertical edge load, no lateral load and 30 kW (40 bhp) thermal load	63
7b. Vertical edge load, no lateral load and 37 kW (50 bhp) thermal load	64
8a. Vertical tape line load, outwardly directed lateral load and 30 kW (40 bhp) thermal load	65
8b. Vertical tape line load, outwardly directed lateral load and 37 kW (50 bhp) thermal load	66
9a. Vertical tape line load, inwardly directed lateral load and 30 kW (40 bhp) thermal load	67
9b. Vertical tape line load, inwardly directed lateral load and 37 kW (50 bhp) thermal load	68
10a. Vertical edge load, outwardly directed lateral load and 30 kW (40 bhp) thermal load	69
10b. Vertical edge load, outwardly directed lateral load and 37 kW (50 bhp) thermal load	70

LIST OF TABLES (concl)

	<u>Page</u>
11a. Vertical edge load, inwardly directed lateral load and 30 kW (40 bhp) thermal load	71
11b. Vertical edge load, inwardly directed lateral load and 37 kW (50 bhp) thermal load	72
12. Conditions for Crack Extension Associated with Stress Variations from Combined Loads	77
13. Conditions for Crack Extension with Inclusion of Service Braking Stresses	80
14. Crack Growth Analysis	82
15. Temperature Dependent Material Properties	86
16. Comparison of Calculated and Experimental Thermal Strains for 37 kW (50 bhp) Induction Coil Thermal Load Tests using IITRI Material Properties	88
17. Comparison of Calculated and Experimental Thermal Strains for 37 kW (50 bhp) Induction Coil Thermal Load Tests using AAR Material Properties	89

## 1. OBJECTIVE

The objective of the work performed under this program was the improvement in the safety of rail transportation through a reduction in the failure rate of railroad car wheels. Changes in design, materials, and operating limits may be considered to improve wheel performance, but before specific changes can be recommended one needs to have a better understanding of the factors which lead to wheel failures. Accordingly, the major purpose of this program was to utilize analytical procedures for the investigation of these factors. The use of an elastic-plastic finite-element analytical code was to be included for the calculation of changes in the residual stress fields of a wheel as a result of severe thermal loading (e.g., a long tread brake application). Residual stress changes are likely to be influential in development of thermal cracks, which is one of the most serious types of wheel failures. With the proper understanding of the factors affecting failure mechanisms it is possible to evaluate design changes or operational limits which are proposed to reduce the probability of wheel failures.

## 2. BACKGROUND

Railroad freight car wheels must fulfill a wide range of service requirements. They must transmit the high mechanical loads accompanying modern high speed train operations and also serve as a heat sink for the energy dissipated by the tread brake system. Railroad wheels are generally expected to provide at least 160,000 km (100,000 miles) of service. A high reliability against failure is necessary because failure of a wheel is likely to result in a train derailment with serious consequences. Railroad wheels must also be tolerant to a considerable amount of wear which results in large cross-sectional changes in the wheel rim over the lifetime of the wheel.

In recent years the use of high capacity cars has placed greater demands on the performance of railroad freight car wheels. In the early 1960's a 64 Mg (70 ton) car was the most common high-capacity car. It allowed a 930 kN (210,000 lb) rail load and utilized 840 mm (33 inch) diameter wheels. Today the allowable vertical wheel loads have been increased by approximately 5 percent and a significant proportion of new cars are of 91 Mg (100 ton) capacity allowing a 1.17 MN (263,000 lb) rail load.

In spite of the demands on wheel performance the failure rate of wheels has remained relatively low when one considers the large number of wheels in service. With U.S. railroad operations of approximately 30 billion car miles per year, the number of wheels which have failed by fracture leading to Federal Railroad Administration (FRA) reportable derailments has averaged slightly over 100 per year. This is an indicated accident rate from wheel failures of less than 0.5 derailments per billion wheel miles.

To obtain an improvement in wheel performance one must consider changes in wheel material specifications and wheel design configurations. A recent discussion of alternatives for obtaining better failure resistance in wheels (Ref 1) noted that the use of steels with higher fracture toughness properties would inhibit wheel failures. Within the present grades of wheel steel, the use of the steels with lower carbon content will increase fracture toughness, but lower resistance to wear. One must therefore strike a balance between wear and fracture resistance. A radical restructuring of the alloy content of the wheel would have to be considered to maintain the desired degree of hardness at increased fracture toughness. Reference 1 concludes that the best potential for improving the fracture resistance of wheels is to consider design changes which will reduce stresses.



Various studies have been conducted to examine potential benefits of modified wheel materials. An illustration is provided by the high alloy steel developed by Italisider Spa of Italy (Ref 2). Their 5CR alloy, which contains 4.85 percent chromium, is reported to have excellent wear and fracture resistance properties. The use of alloys of this type has not gained acceptance on U.S. railroads primarily because of their additional cost.

The feasibility of using different wheel plate designs to reduce the stresses associated with thermal and mechanical loads has been the subject of several investigations. The most detailed study is reported by Wetenkamp (Ref 3) which included five different wheel cross sections: deep dish curved plate, conventional straight plate, S-plate, sharp fillet S-plate, and offset straight plate designs. The wheels were subjected to drag tests using a wheel dynamometer and the wheel stresses under severe thermal loading were analyzed using the finite element method. The test results indicated that the two S-plate designs and the offset straight plate designs had a greater tendency for the development of permanent deformations (measured by axial rim movement) than the curved plate and conventional straight plate designs. The results of the analyses showed that the lowest stresses were associated with the deep dish curved plate design and that the highest stresses were associated with the S-plate designs.

As a result of evaluating these data and other relevant information it was concluded that the detailed analysis work should emphasize comparisons of the conventional curved plate and straight plate designs which are presently in use on U.S. railroads. It was apparent that more detailed stress analyses were required relating to crack initiation and growth before one could make general statements about the advantages of different wheel designs.

### 3. CONSIDERATIONS IN THE DESIGN AND USE OF RAILROAD CAR WHEELS

#### 3.1 Wheel Loadings

The major mechanical load on the wheel is the vertical load which is applied between the wheel/rail contact point. The magnitude of this load depends on the weight of the car and it is modified by transient factors, such as rail irregularities, suspension system oscillations, wheel flat spots, etc.

Lateral loads are also applied at the wheel/rail interface. This load is due to flange contacts during the normal hunting motion of the wheel-axle set and lateral creep and slip forces which are built up during the traversal of curved track. Under normal conditions these forces are directed toward the flange. Occasionally, large transient forces can be directed in the opposite lateral direction due to guardrail contacts.

Wheels are also subjected to radial load when tread brakes are applied. The effects of this load are similar to the vertical load except that the total load is smaller and it is active for a relatively short period in the life of the wheel. Circumferential wheel loads are developed at the tread as a result of creep and slip forces built up during the traversal of curved track and as a result of brake shoe frictional forces. Another type of loading results from the press fit of the wheel on the axle.

Wheels are also subjected to thermal loading when tread brake shoes are applied. The deposition of this energy in the rim leads to temperature gradients within the wheel. The differential heating causes an expansion and twisting of the rim relative to the plate, which results in the development of large stresses in the wheel. If high temperatures are reached at the tread, metallurgical changes can be produced, which may affect the ability of the material to resist damage.

There are two distinct types of severe braking service. The first is drag braking which is associated with the descent of a long grade. On some of the long grades in the western mountainous regions this might involve braking for over an hour at moderate rates of energy deposition (e.g., 15 kW (20 bhp)). The relatively long duration of the brake application allows the heat to penetrate through the rim down into the plate. The second type of service is emergency braking. This condition is particularly severe in high-speed passenger operations where tread brakes are used. Energy deposition rates may exceed 150 kW (200 bhp) for time periods exceeding 2 minutes. The relatively short time of brake application means that most of the heat is retained near the surface of the tread.

### 3.2 Materials

Railroad wheels are manufactured in accordance with Association of American Railroads (AAR) specification M107 (Ref 4) for wrought steel wheels or AAR specification M208 (Ref 5) for cast steel wheels. There are five classes of wheel steels defined in the specifications: U, L, A, B, and C. The classifications are defined on the basis of carbon content and hardness, as summarized in Table 1. Typical values of yield strength and ultimate strength for these steel classifications are also indicated in the table. Design stresses are not specified for wheels. Instead various geometric configurations are specified by stating dimensional requirements. Minimum dimensions are specified at critical locations (e.g., plate thicknesses at hub and rim fillets).

### 3.3 Types of Wheel Failures

The AAR Field Manual of Interchange Rules (Ref 6) lists 19 defects which require removal of wheels from service:

Slid Flat	Grooved Tread
Shattered Rim	Cracked or Broken Flange
Spread Rim	Cracked or Broken Rim
Shelled Tread	Thin Rim
Thin Flange	Cracked or Broken Plate
Vertical Flange	Holes in Plate
Thermal Cracks	Loose
Built Up Tread	Out of Gauge
Overheated	Scrape, Dent or Gouge in
High Flange	Wheel Plate

Some of these defects are the result of normal service wear (e.g., thin flange or thin rim); other defects are due to malfunctioning equipment (e.g., slid flat). From the standpoint of ensuring the structural adequacy of the wheel, the most serious of these defects are thermal (radial rim) cracks and plate cracks.

3.3.1 Thermal Cracks-A thermal crack is a radial crack which develops on the periphery of the wheel and propagates inward toward the hub. Once these cracks propagate through the rim they will often turn and propagate as a circumferential plate crack. The crack may then turn again and propagate through the rim in a radial direction separating a large segment from the wheel. A thermal crack might be initiated and propagate over an extended period of time or the crack may develop rapidly causing a sudden failure of the wheel.

TABLE 1. MATERIAL PROPERTIES OF WHEEL STEELS

Class	Carbon Content (percent)	Rim Hardness (BHN)	Typical Values	
			Yield Strength MPa (ksf)	Ultimate Strength MPa (ksf)
U	0.65 - 0.80		380 (55)	760 (110)
L	0.47 max.	197/277	430 (63) rim	720 (105) rim
A	0.47 - 0.57	255/321	450 (65) rim	720 (105) rim
B	0.57 - 0.67	277/341	310 (45) plate	620 (90) plate
			550 (80) rim	930 (135) rim
C	0.67 - 0.77	321/363	380 (55) plate	760 (110) plate
			620 (90) rim	970 (140) rim
			380 (55) plate	760 (110) plate

Note: Classes L, A, B, and C are heat treated, rim quenched, or entire wheel quenched and tempered.

The thermal crack mode of failure is probably the most severe problem in present day railroad car wheel operation. Thermally cracked wheels often lead to serious train derailments. The thermal crack may cause a sudden separation of the wheel leading to an immediate derailment or it may lead to a loose wheel, which would move inward on the axle causing a derailment.

Thermal crack development is associated with modifications in the residual stress field within the wheel which are caused by severe tread braking. Under these conditions the periphery of the wheel is heated to a relatively high temperature, but is restrained from expanding by the colder plate and hub of the wheel. This causes the development of circumferential compressive stresses in the rim and radial tensile stresses in the plate. The plate stresses are greatest in the outside hub fillet and the inside rim fillet. If the thermal gradient is large enough, plastic deformation will take place first in the highly stressed plate fillet regions and, with increasing severity of the thermal load, in the rim adjacent to the surface of the tread. Plastic deformation causes a change in the residual stress field of the wheel when it cools. The change puts circumferential tensile stress in the rim and compressive radial stresses in the plate. The existence of tensile stress in the rim will promote thermal crack growth.

A limited survey of wheels which have failed by thermal cracking showed that approximately 50 percent of the failures were initiated in the flange, 30 percent were initiated on the back face of the rim, 15 percent were initiated at the outside corner of the tread, and 5 percent were initiated on the face of the tread.

3.3.2 Plate Cracks-Cracks that initiate in the plate of the wheel and propagate circumferentially around the plate are commonly referred to as plate cracks. They normally develop and propagate as fatigue cracks from a point of initiation in the outside plate hub fillet. Plate crack development is believed to be caused by the effects of both thermal and mechanical loads. The highest stresses in the regions of crack initiation result from the thermal effect, but there is a relatively small number of cycles of high stresses over the life of the wheel. Mechanical wheel loads produce an alternating stress pattern within the critical fillet regions of the wheel once per wheel revolution, but the stress levels are of relatively low magnitude. The relative importance of these stress cycles has not yet been established. An additional factor affecting plate crack growth is that the wheel is more sensitive to fatigue damage from mechanical loads if the rim of the wheel is heated by tread brake application (Ref 7 and 8). This results from the steady tensile stresses in the regions where the maximum fluctuating stresses are developed.

### 3.4 Complexity of Wheel Failure Phenomena

A complete understanding of wheel failure phenomena is required before one can propose cost-effective changes in design and operating requirements to improve wheel reliability. One should be able to state the specific sets of conditions which will lead to wheel failure and be able to demonstrate these by tests as a means for verifying the methods of analysis. There are a number of reasons for the complexity of wheel failure analysis. Some of the more significant of these are summarized:

- The wheel is subjected to both mechanical (wheel/rail) and thermal (tread brake heating) loads.
- Residual stress fields can both promote and inhibit wheel crack growth phenomena.
- The fact that wheel/rail loads are transmitted across a relatively small "contact zone" where unit stresses are quite large as defined by the Hertzian deformations of the wheel and rail.
- The fact that considerable wear must be tolerated, which results in large cross sectional changes in the rim over the life of the wheel; this in turn causes changes in the wheel stress patterns resulting from mechanical and thermal loads.
- The fact that cyclic stresses can occur due to wheel rotation and wheel/rail loads while certain regions of the wheel are being strained beyond the yield point due to thermal (brake) loads.
- The type of brake shoe affects the way the tread braking thermal load is introduced into the wheel. The use of cast iron shoes can lead to hot spots on the surface of the tread whereas the composition shoe results in the transmission of a greater percentage of the total brake energy into the rim.
- The fact that some wheels are manufactured in such a way that they possess complex residual stress fields.

### 3.5 Analysis of Wheels

3.5.1 Previous Studies-The development of modern computational techniques has made possible the calculation of wheel response to thermal and mechanical loads. Finite element analysis techniques have made possible more efficient solution of wheel temperature and stress calculations and the treatment of a broad range of load conditions. The finite element technique has been used by Novak, Eck, et al, (Ref 9, 10, and 11) and Nishioka and Morita (Ref 12) for calculation of wheel stresses resulting from discrete loads acting on the wheel. Wetenkamp (Ref 3) and others (Ref 13 and 14) have used this technique for the calculation of thermal stresses resulting from tread brake applications.

Finite element analyses have been used to determine the relative stresses caused by vertical (radial) and lateral mechanical loads and thermal loads due to braking (Ref 11, 12, and 15). They have also been used to compare the thermal stresses caused by emergency and drag braking (Ref 15); to examine the effects on thermal stresses of different wheel configurations, such as deep dish, straight plate, and S-plate designs (Ref 3); to determine the tendency for the wheel press fit to loosen as the wheel temperature rises (Ref 3); and to determine the effect of rim thickness on stresses from vertical wheel loads (Ref 10).

3.5.2 Analytic Procedures Used in This Program-Two types of finite element analyses have been utilized on this program for the study of wheel stresses. A linear code was used for the study of the effects of mechanical (e.g., wheel/rail) loads. The code is capable of determining the effects of three-dimensional loads on an axisymmetric (two-dimensional) body through the use of harmonic analysis.

A two-dimensional elastic-plastic code was used for the study of severe thermal loads. Its use assumes axisymmetric heat input to the wheel. The use of the code is preceded by a separate finite element analysis to predict the temperature distribution throughout the wheel as a function of time from the brake energy deposited in the tread of the wheel.

The analytic codes have been previously described in Ref 20.

### 3.6 Approach

Since one of the principal objectives of the program was to determine the conditions under which wheels are most susceptible to thermal crack development, the following approach was adopted to define these conditions. The two-dimensional elastic-plastic code was used to calculate the shifts in the residual stress field of wheels due to severe thermal load. The elastic three-dimensional code was then used to calculate the stresses which are due to vertical and lateral wheel/rail forces. The cyclic nature of these stresses resulting from the rotation of the wheel were also determined. In addition the variations in the cyclic stresses caused by changes in the position of the point of load application were calculated. Results from the two types of calculations were combined. It was assumed that the cyclic stresses were elastic and could be superimposed on the residual stress fields calculated from the thermal analysis. The results were used to determine if the stresses caused by mechanical loadings, which fluctuate at any one point in the wheel due to wheel rotation, can cause thermal crack propagation under certain residual stress field conditions. Fracture mechanics crack growth models were used for these studies.



#### 4. RESULTS: THERMAL STRESS ANALYSES

This section presents results of analyses which have been made with the elastic-plastic two-dimensional code to determine the changes in the residual stress field resulting from severe thermal loading. The major interest was in braking conditions where the thermal load is large enough to cause the yield point to be exceeded with a consequent shift in the residual stress field when the wheel cools. This requires a relatively long brake application (30 to 60 minutes) where the rate of energy input to the wheel exceeds 22 kW (30 bhp).

Of particular importance in these calculations is the residual circumferential stress which is developed within the rim of the wheel, because a tensile stress in this direction promotes the initiation and growth of radial cracks.

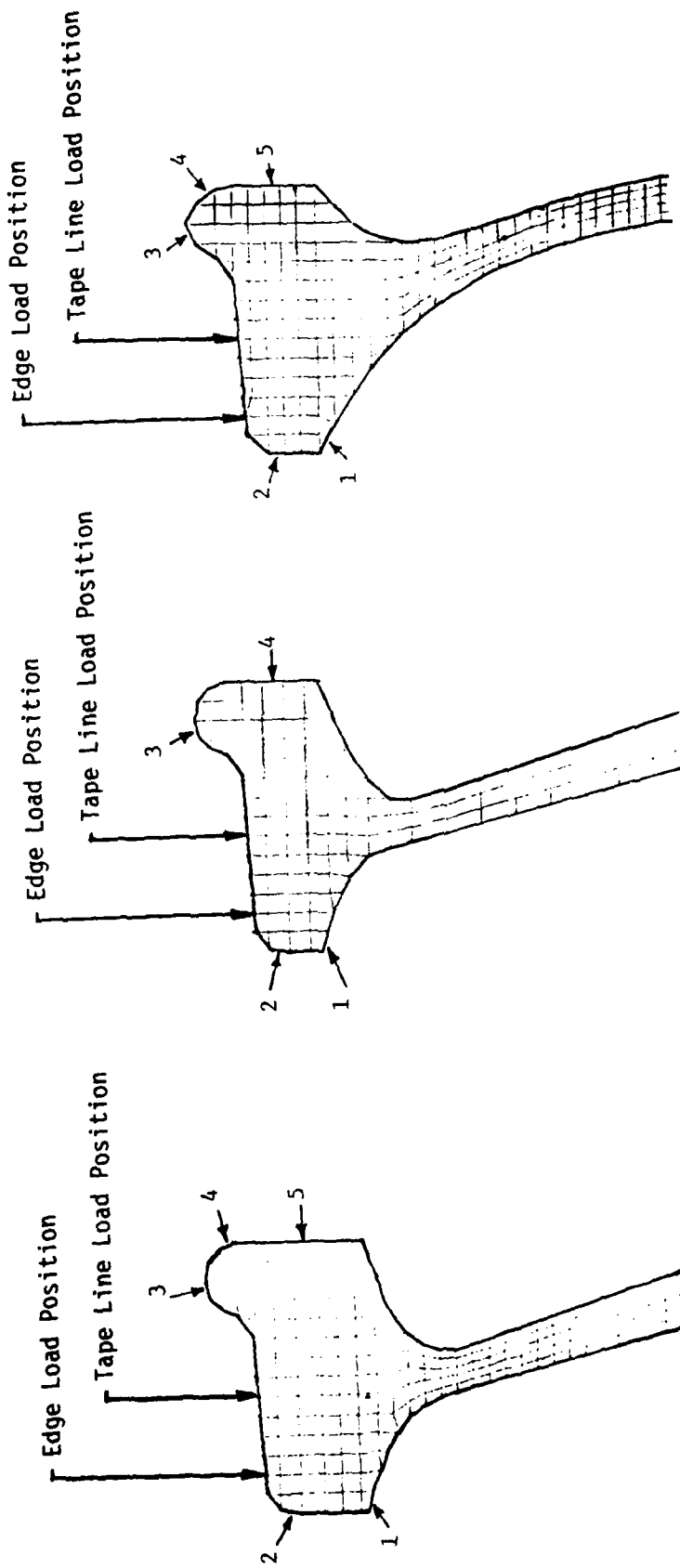
##### 4.1 Wheel Types

Figure 1 shows the three types of wheels which have been analyzed. The wheels are 914 mm (36 inch) diameter freight car wheels, two having a straight plate cross section and one having a curved plate cross section. The curved plate wheel and one of the straight plate wheels have the rim cross section representative of a one wear wheel design. The other straight plate design has a rim cross section representative of a two wear wheel design. Figure 1 also defines positions around the rims where stress results are reported. These are common sites for the initiation of thermal cracks.

##### 4.2 Cases Considered

Two levels of severe thermal load input to the wheel have been considered, namely, 30 and 37 kW (40 and 50 bhp) for 1 hour. These are representative of severe drag braking conditions.

The significance of the location of the heat input to the wheel on the development of thermal stress has also been investigated. Two cases are considered, one representing the brake shoe centered on the tape line of the wheel and the other with the brake shoe centered about 25 mm (1 inch) outside of the tape line, which represents a brake shoe overhanging the outside corner of the wheel. It is assumed that the thermal load is applied to the wheel through a 75 mm (3 inch) wide area on the tread.



(a) Two Wear Straight Plate Wheel      (b) One Wear Straight Plate Wheel      (c) One Wear Curved Plate Wheel

Figure 1 Load Positions and Stress Data Locations

### 4.3 Summary of Results

Results of the analyses are tabulated in Table 2. The compressive stresses for the hot wheel and the residual stresses following the subsequent cooling of the wheel are shown. In all cases the assumption is made that there are no initial residual stresses within the wheel prior to the application of the thermal load.

The results show that the residual stresses from the 37 kW (50 bhp) thermal load are more severe than from the 30 kW (40 bhp) thermal load. The results also show that there are only minor differences in the stresses for an off center brake load in comparison with a centered brake load.

The results in Table 2 indicate that there is a larger variation in the residual stresses in the rim of the curve plate wheel than in either of the two straight plate designs. This difference is most pronounced for the 37 kW (50 bhp) case and leads to large tensile stresses on the inside face of the rim.

### 4.4 Detailed Results Associated with 37 kW Cases

The phenomena associated with the application of the thermal brake load to the wheels are illustrated by comparing the responses of the one wear straight plate and curved plate designs to a 60 minute, 37 kW (50 bhp) drag brake load. These cases are selected to provide additional information on the differences in response of straight plate and curved plate wheel designs.

The elastic-plastic two-dimensional code was used for these calculations. It utilizes a bilinear representation of the stress strain curve for the material. Values were selected to represent the properties of a Class U wheel steel having a yield point of 400 MPa (57 ksi). The modulus of elasticity was assumed to be reduced to 22 percent of its initial value above the yield point stress.

Figures 2 and 3 compare the temperature distribution after 60 minutes of braking. The temperature distributions are quite similar for both wheels. Figures 4 and 5 show the extent of the regions in the wheels where the yield point has been exceeded. Note that the straight plate wheel shows greater areas of yielding on the plate whereas the curved plate wheel shows more yielding in the region about the flange.

TABLE 2. RESIDUAL CIRCUMFERENTIAL STRESSES IN RIM  
FOLLOWING 60 MINUTE DRAG BRAKING

Wheel	Brake Power kW (bhp)	Position of Stress Value (See Fig. 1)	Residual Circumferential Stress MPa (ksi)			
			Centered Brake Load		Edge Brake Load	
One Wear Straight Plate	30 (40)	1	-2.8	(-0.4)	-43	(-2.0)
		2	1.4	(0.2)	-43	(-6.2)
		3	40	(5.8)	39	(5.7)
		4	50	(8.1)	57	(8.3)
	37 (50)	1	-34	(-5.0)	-55	(-8.0)
		2	-18	(-2.6)	41	(5.9)
		3	57	(8.2)	78	(11.3)
		4	123	(17.3)	145	(21.0)
Two Wear Straight Plate	30 (40)	1	-2.1	(-0.3)	8.3	(1.2)
		2	3.4	(0.5)	3.4	(0.5)
		3	32	(4.7)	30	(4.3)
		4	42	(6.1)	40	(5.8)
		5	49	(7.1)	47	(6.8)
	37 (50)	1	-22	(-3.2)	-43	(-6.2)
		2	-8.3	(-1.2)	2.1	(0.3)
		3	57	(8.2)	56	(8.1)
		4	78	(11.3)	82	(11.9)
		5	94	(13.6)	105	(15.3)
One Wear Curved Plate	30 (40)	1	-19	(-2.7)	-22	(-3.2)
		2	-17	(-2.5)	-18	(-2.6)
		3	17	(2.4)	13	(1.9)
		4	23	(3.4)	19	(2.8)
		5	77	(11.2)	66	(9.6)
	37 (50)	1	-56	(-8.1)	-69	(-10.0)
		2	-28	(-4.1)	-32	(-4.7)
		3	26	(3.7)	12	(1.7)
		4	135	(19.6)	112	(16.2)
		5	208	(30.1)	196	(28.5)

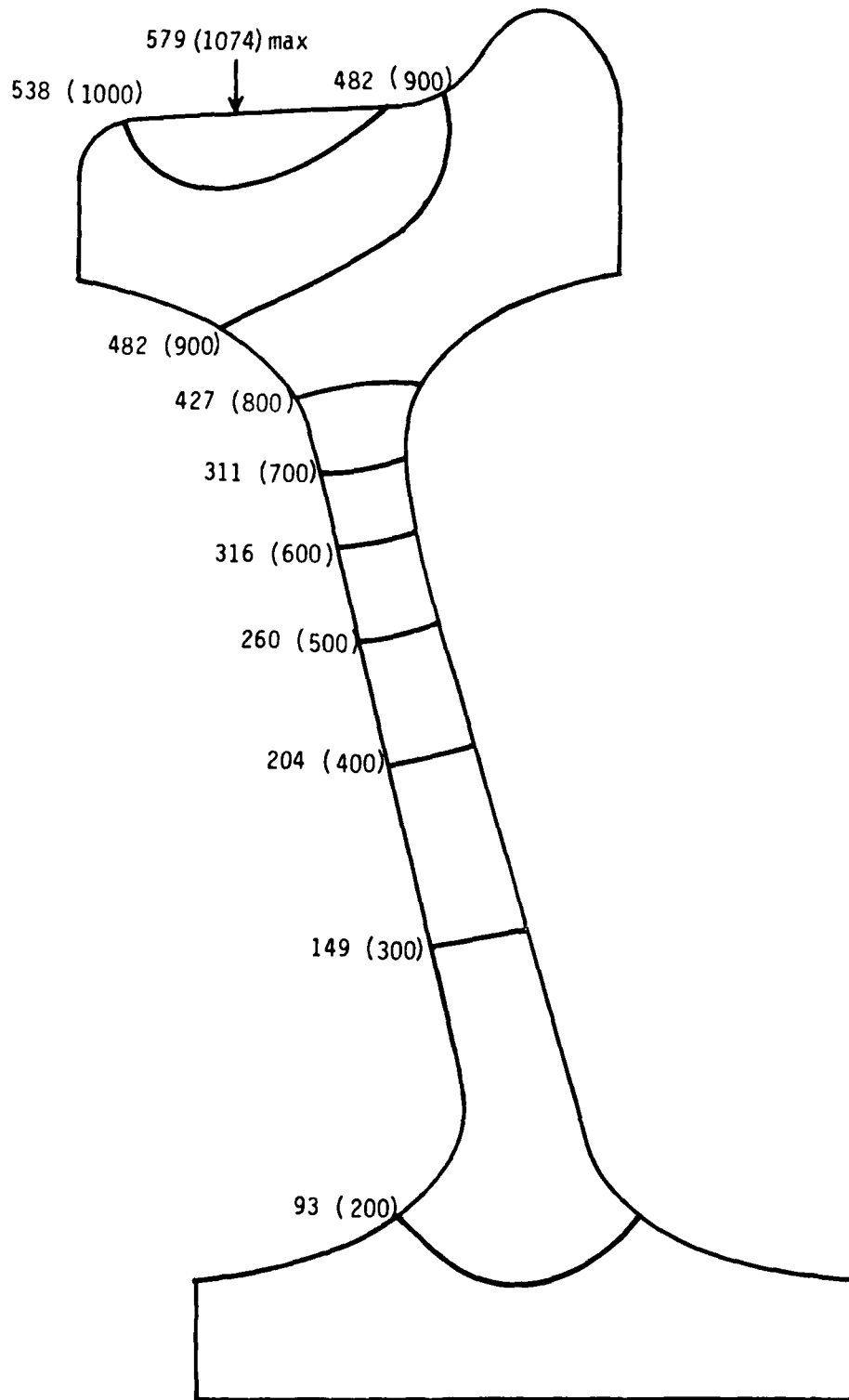


Figure 2 Temperature Distribution, °C (°F), One Wear Straight Plate Wheel after 60 minutes of 37 kW (50 bhp) Drag Brake Application

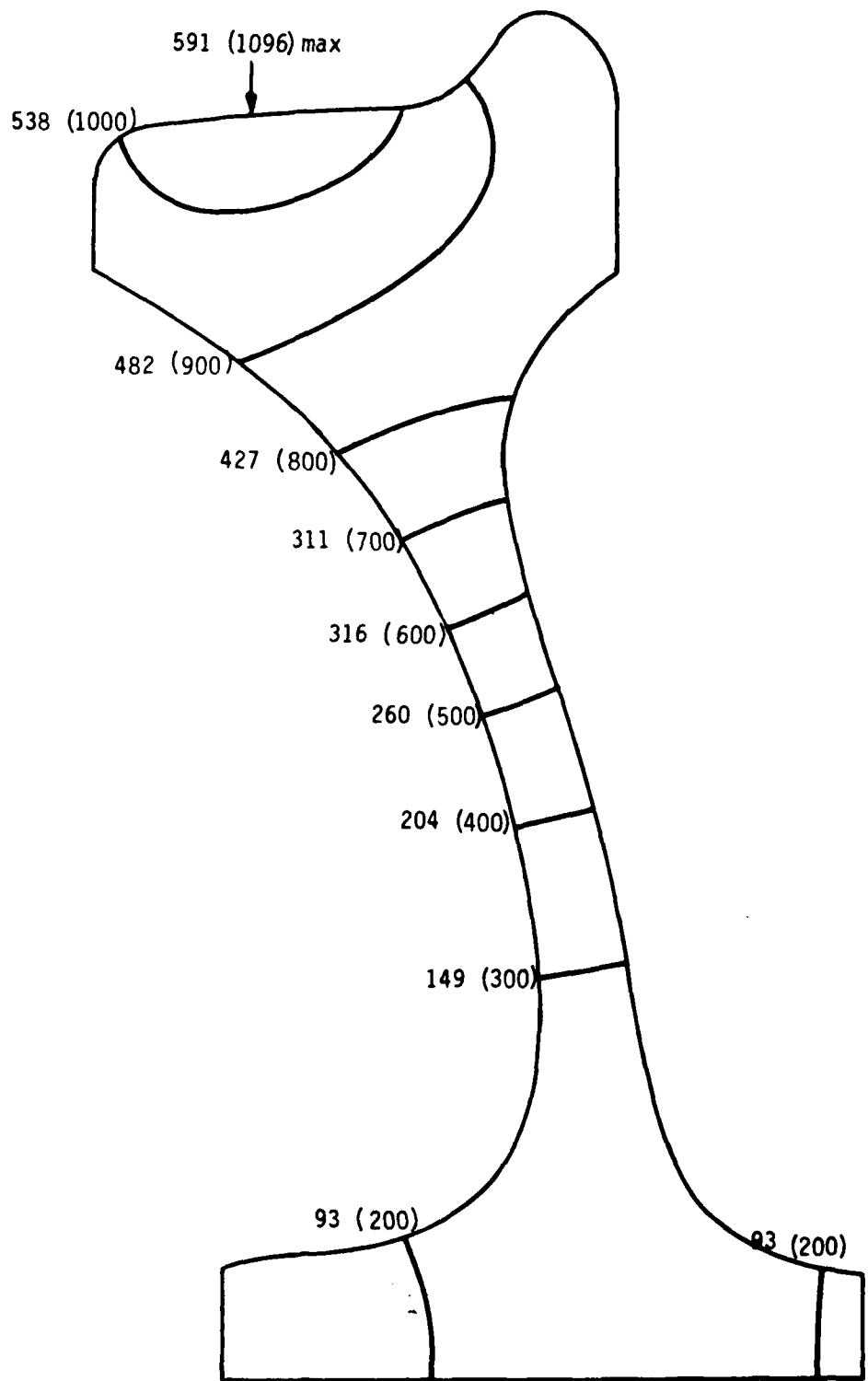


Figure 3 Temperature Distribution, °C (°F), One Wear Curved Plate Wheel after 60 minutes of 37 kW (50 bhp) Drag Brake Application

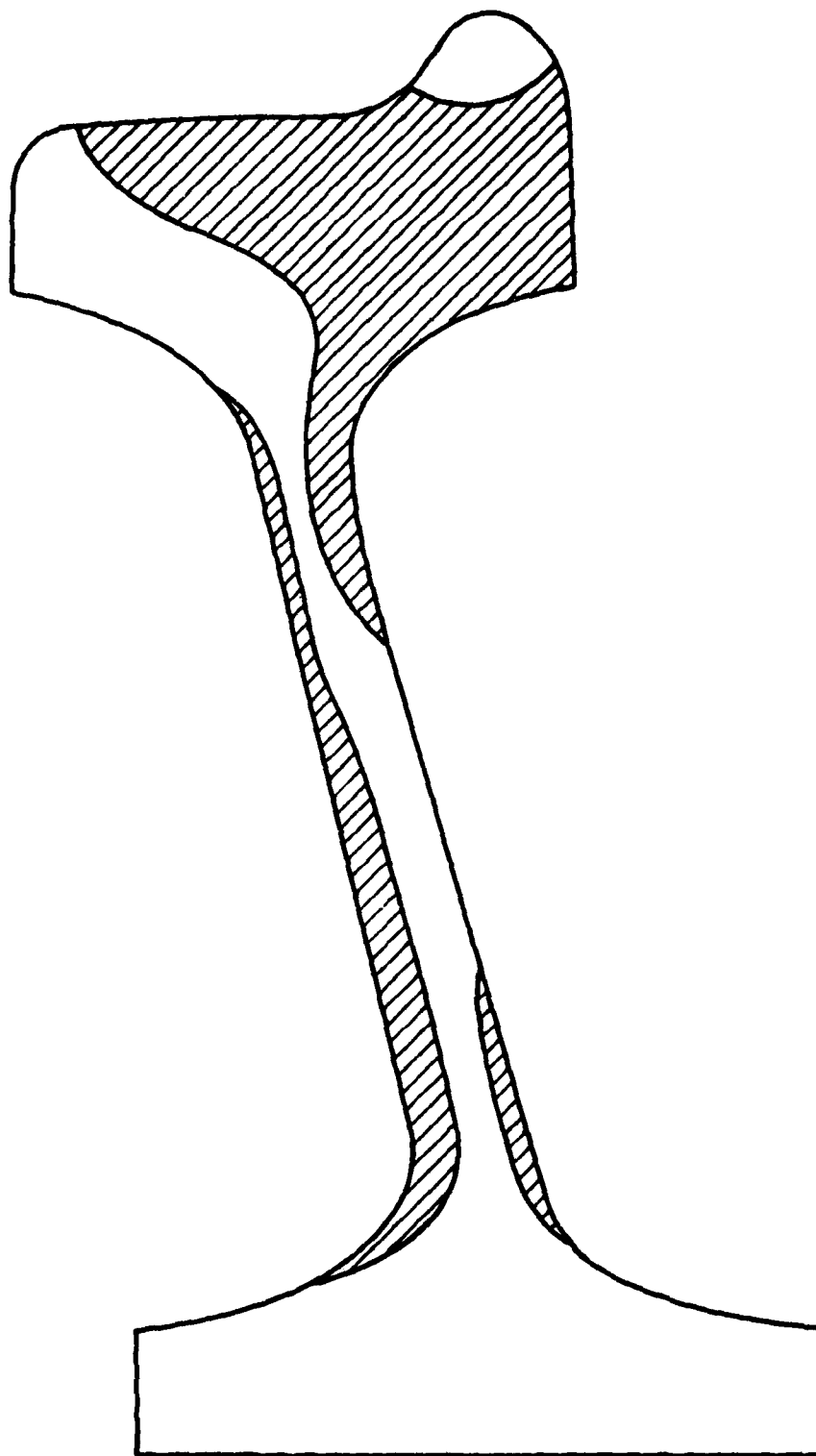


Figure 4 Extent of Yielded Region, One Wear Straight Plate Wheel after 60 minutes of 37 kW (50 bhp) Drag Brake Application

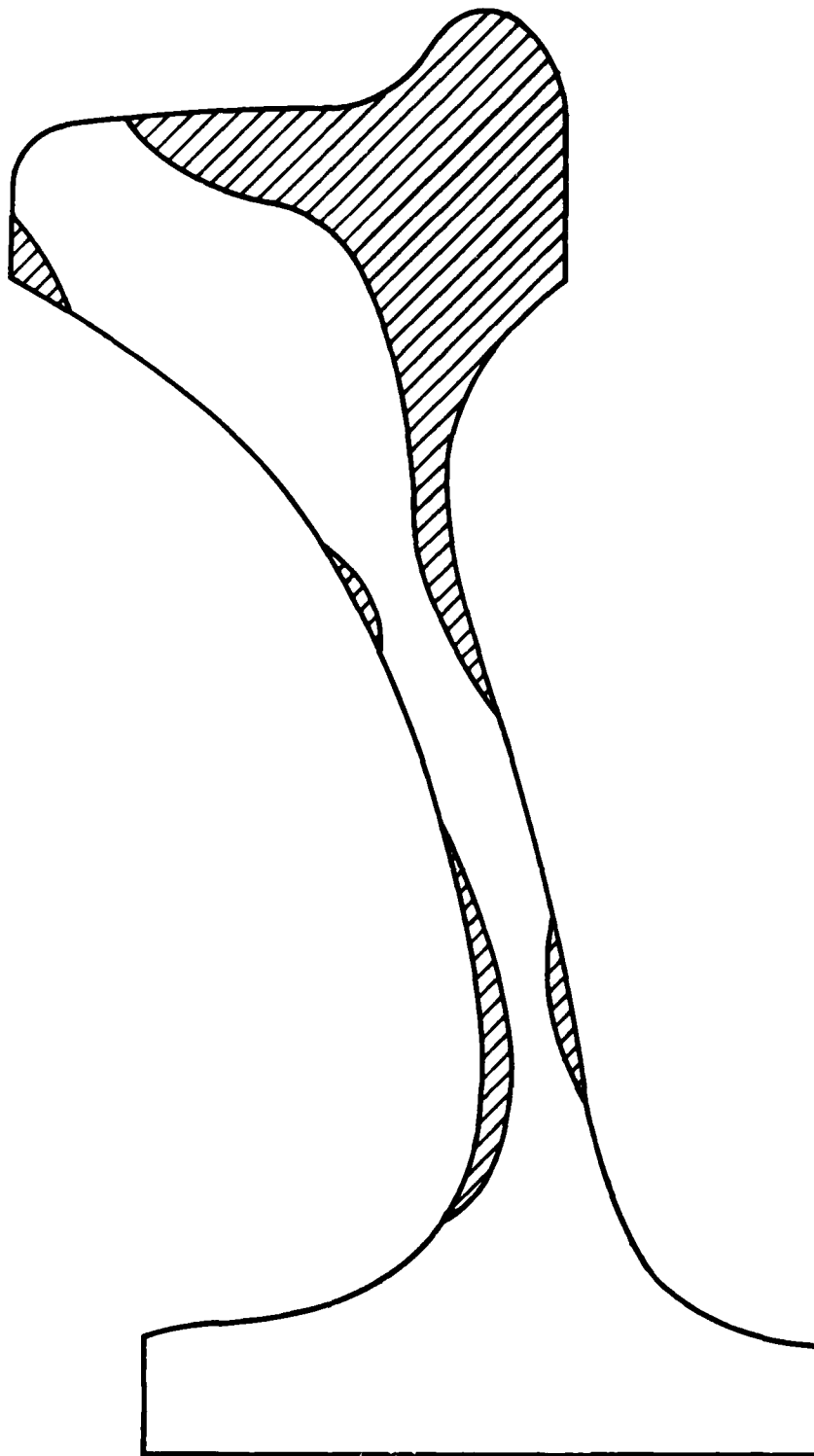


Figure 5 Extent of Yielded Region, One Wear Curved Plate Wheel after 60 minutes of 37 kW (50 bhp) Drag Brake Application



Figures 6 and 7 compare the maximum circumferential stresses within the wheels at the completion of the drag brake loading period. There is a greater stress variation across the rim of the curved plate wheel than across the rim of the straight plate wheel, although the maximum value of compressive stress is approximately the same. These figures also show that there are larger stresses in the plate of the straight plate wheel than the plate of the curved plate wheel.

Similar trends are observed if one compares radial stresses in the plates of these wheels. The radial component of stress in the hub fillet region is 691 MPa (100 ksi) in the curved plate wheel and 818 MPa (119 ksi) in the straight plate wheel. Similarly the radial component of stress in the rim fillet is 377 MPa (55 ksi) in the curved plate wheel and 594 MPa (86 ksi) in the straight plate wheel. The values for the stress in the hub plate fillet regions are well above the yield point of the steel indicating that considerable yielding has taken place.

Figures 8 and 9 compare the residual circumferential stress distributions following cooling of the wheel. The straight plate wheel shows the highest stresses near the tread of the wheel where the thermal load is applied. The curved plate wheel shows the highest stresses on the inside surface of the rim.

The difference in response of the two types of wheels to the thermal load can also be shown by a comparison of displacements. Figures 10 and 11 compare the displacements of the wheel under the maximum temperature conditions. Little difference in response is indicated. However, the comparison of residual displacement conditions (after the wheel cools) as shown in Figures 12 and 13, reveals considerable differences in displacement. The straight plate wheel rim shows a slight counterclockwise distortion, whereas the curved plate wheel shows a slight clockwise distortion. The differences are not unexpected in view of the different patterns of the residual stress fields.

The results illustrate the differences in the way the two types of wheels respond to the severe thermal load. The curved plate wheel allows slightly larger outward expansion of the rim than the straight plate wheel resulting in slightly lower plate stresses. On the other hand, the larger curved plate wheel expansion causes larger compressive stresses in the rim which contributes to greater yielding in the rim. When the wheels cool a larger range of residual stresses is indicated across the rim of the curved plate wheel. Also, the residual stress is larger at the inside surface of the rim.

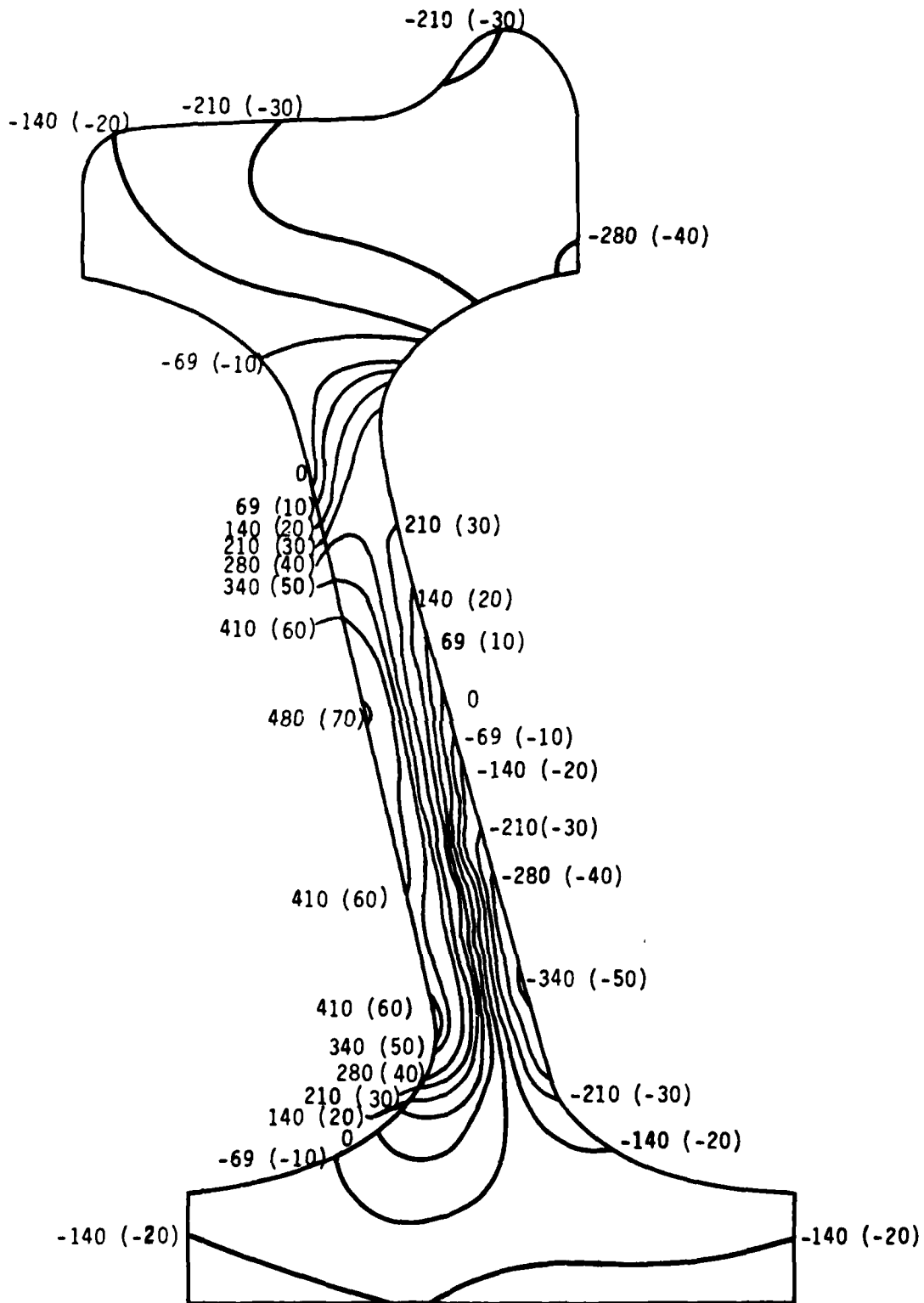


Figure 6 Distribution of Circumferential Stress ( $\sigma_\theta$ ) in MPa (ksi),  
 One Wear Straight Plate Wheel after 60 minutes of 37 kW (50 bhp)  
 Drag Brake Application

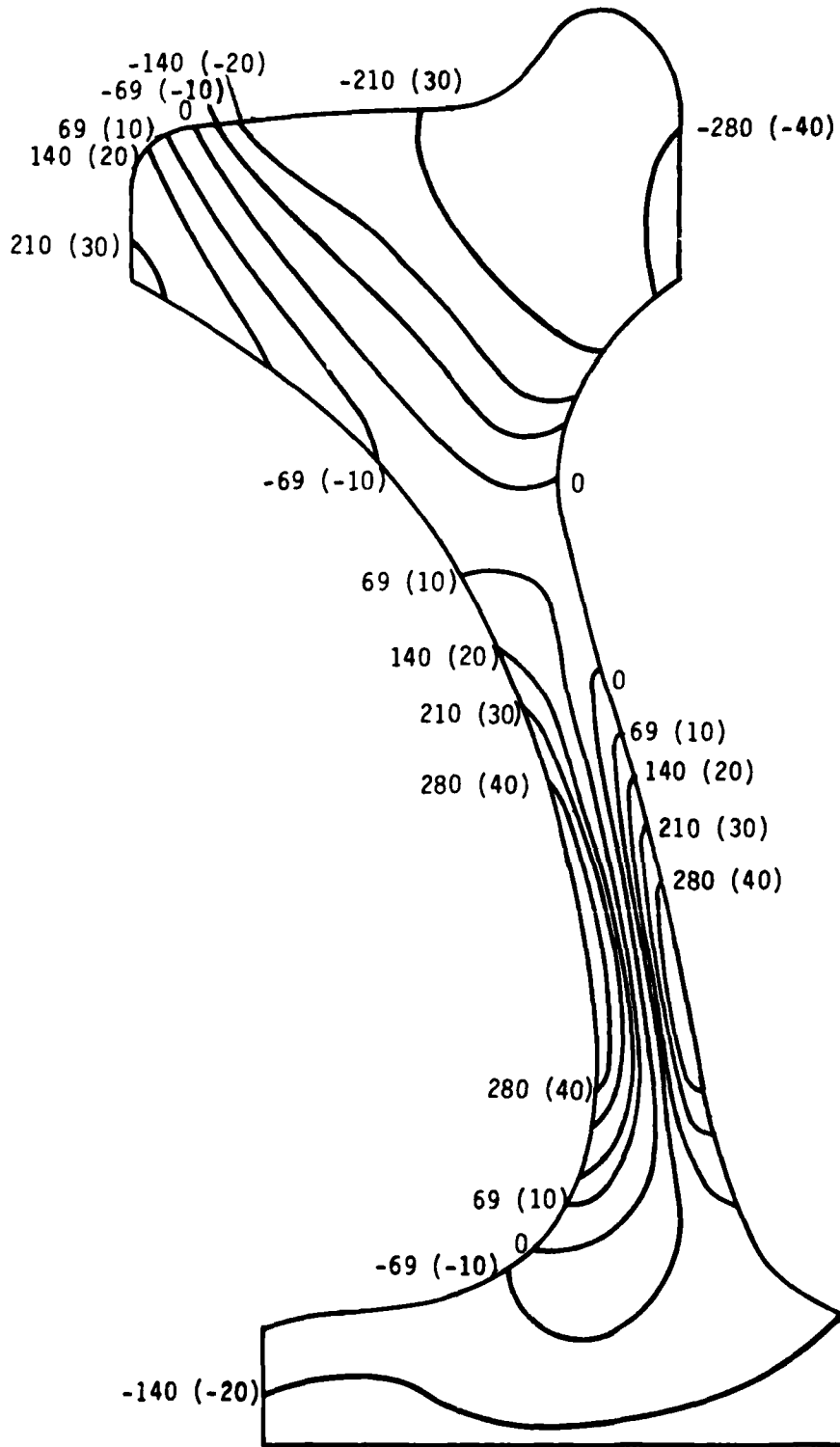


Figure 7 Distribution of Circumferential Stresses ( $\sigma_{\theta}$ ) in MPa (ksi),  
 One Wear Curved Plate Wheel after 60 minutes of 37 kW (50 bhp)  
 Drag Brake Application

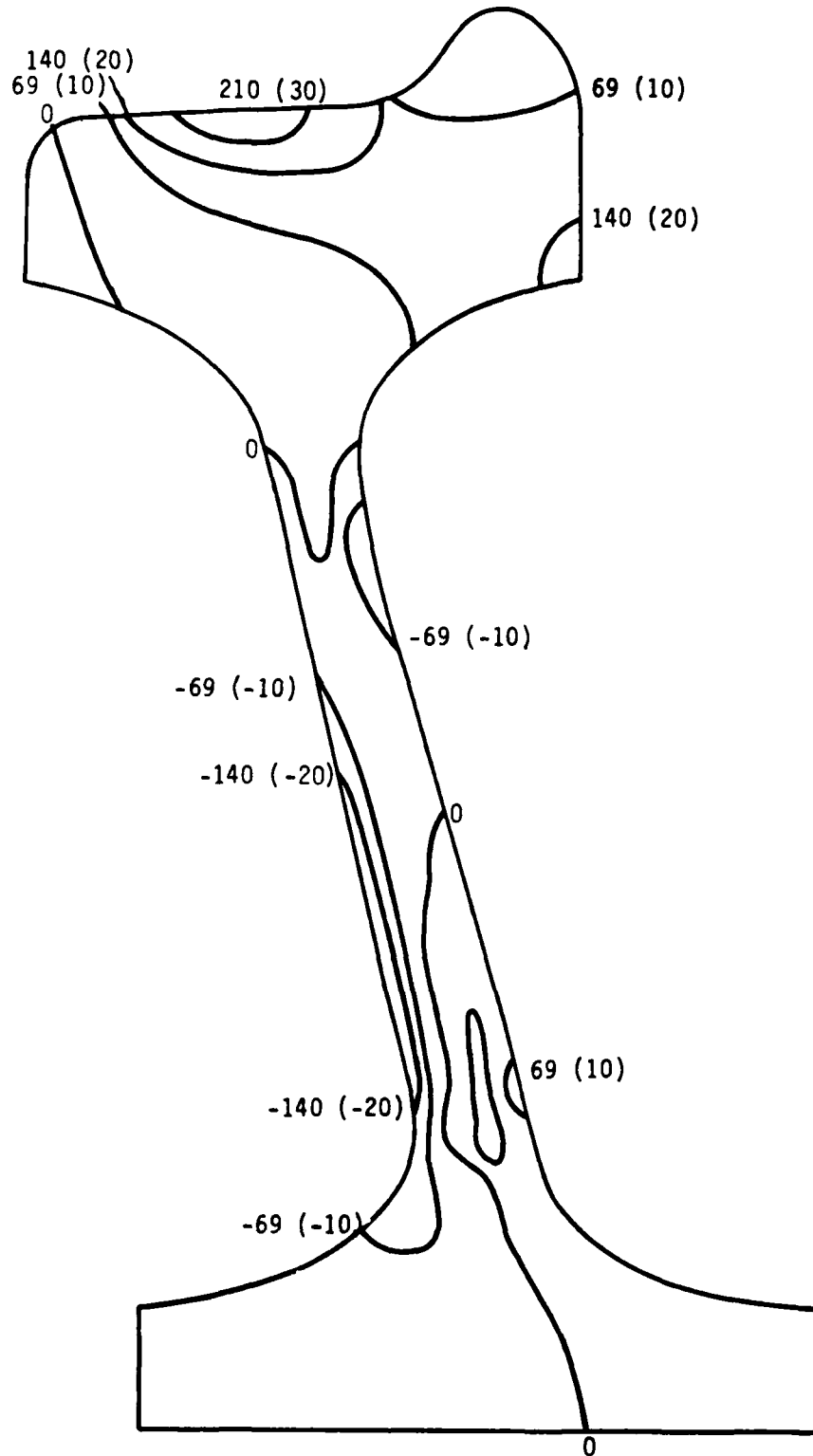


Figure 8 Distribution of Residual Circumferential Stresses ( $\sigma_{\theta}$ ) in MPa (ksi), One Wear Straight Plate Wheel Following 37 kW (50 bhp) Drag Brake Application for 1 hour (cooled wheel)

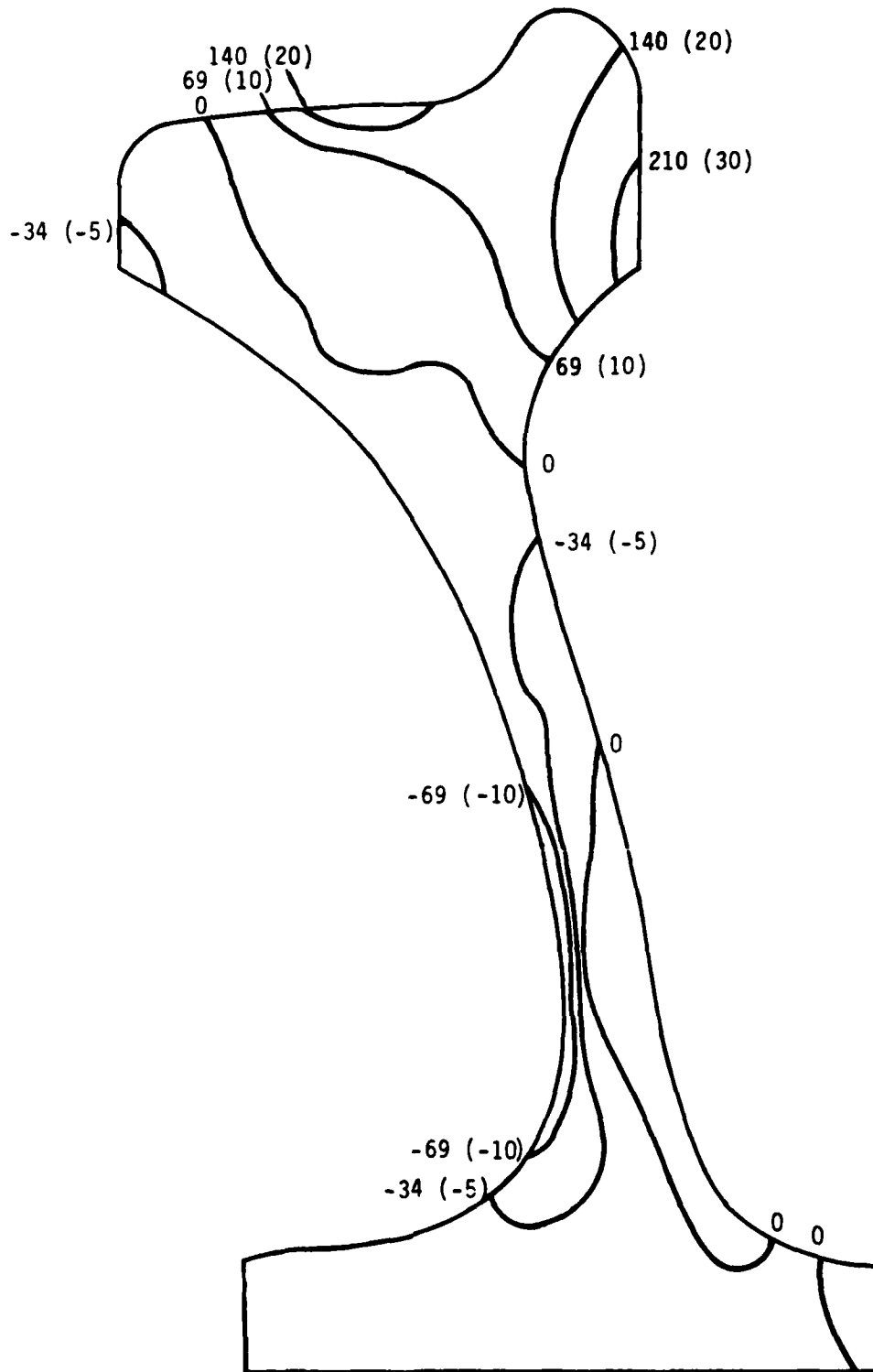


Figure 9 Distribution of Residual Circumferential Stresses ( $\sigma_{\theta}$ ) in MPa (ksi), One Wear Curved Plate Wheel Following 37 kW (50 bhp) Drag Brake Application for 1 hour (cooled wheel)

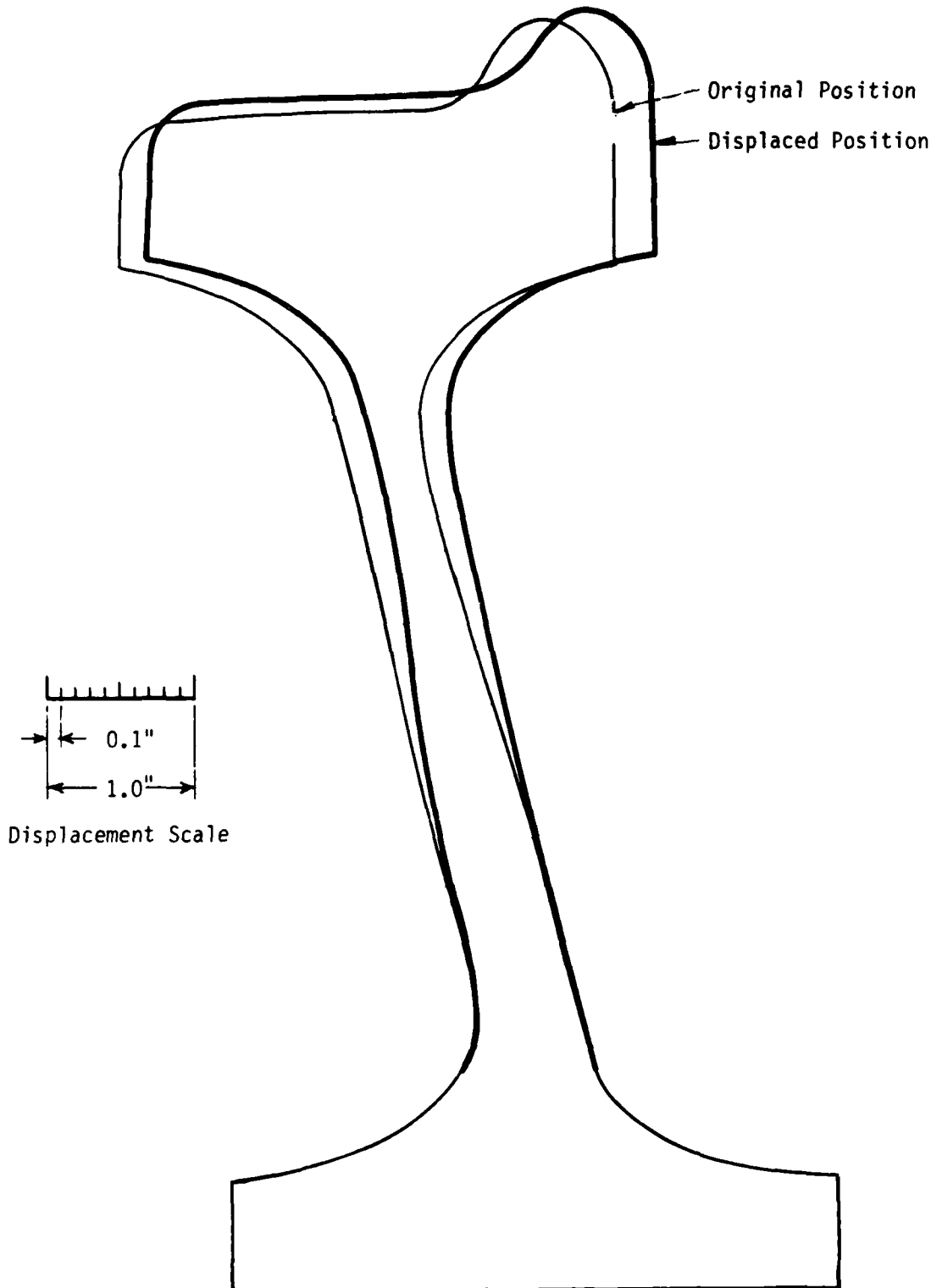


Figure 10 Displacement of Hot One Wear Straight Plate Wheel after 60 minutes of 37 kW (50 bhp) Drag Brake Application

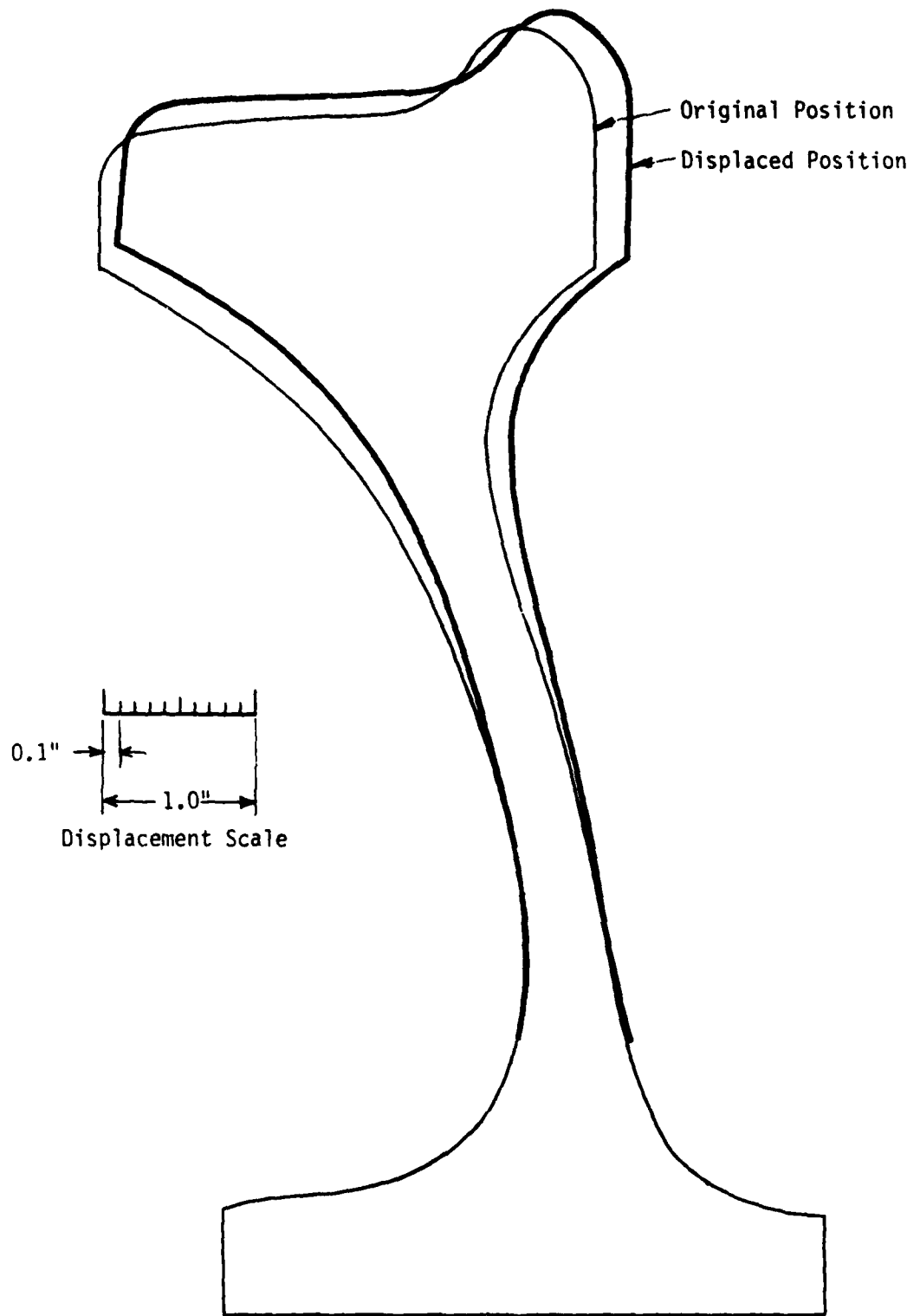


Figure 11 Displacement of Hot One Wear Curved Plate Wheel after 60 minutes of 37 kW (50 bhp) Drag Brake Application

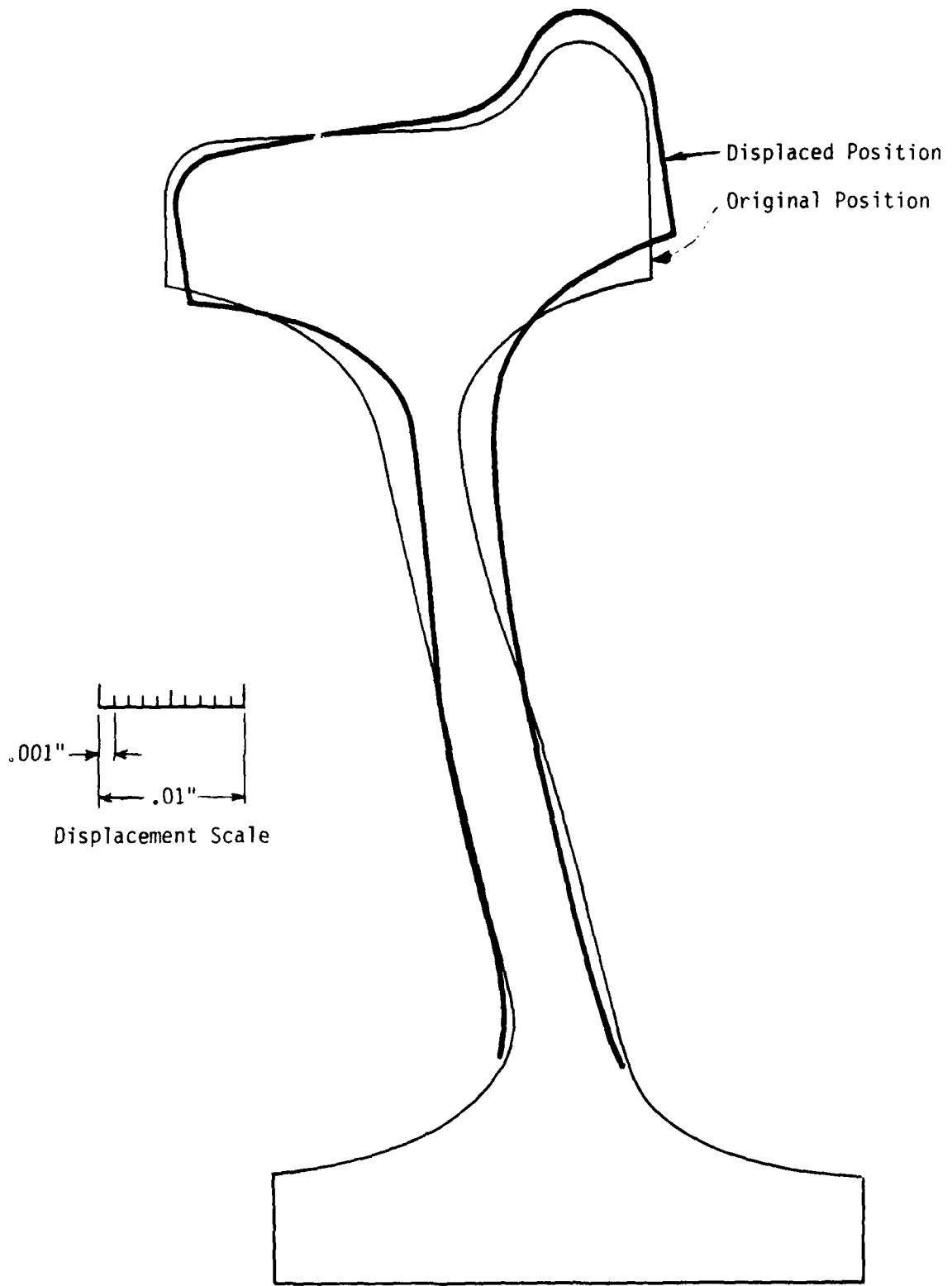


Figure 12 Displacement Configuration of Cool, One Wear Straight Plate Wheel Following 37 kW (50 bhp) Drag Brake Application for 1 hour



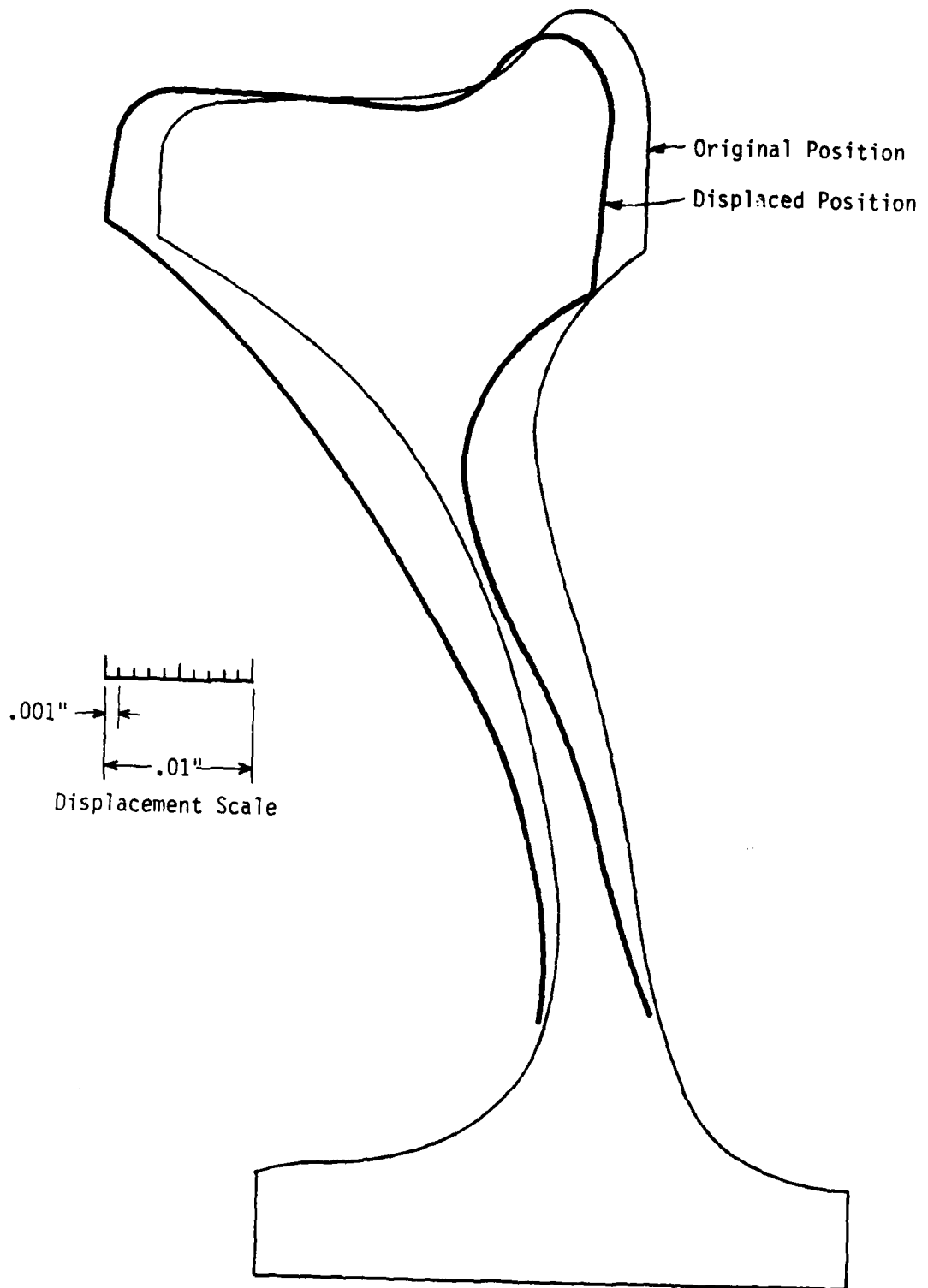


Figure 13 Displacement Configuration of Cool, One Wear Straight Plate Wheel Following 37 kW (50 bhp) Drag Brake Application for 1 hour

#### 4.5 Repeated Severe Thermal Load Applications

The calculation of major changes in the residual stress field following a severe thermal load raises the question of whether or not subsequent applications of a severe thermal load would cause further changes in the residual stress field. A partial answer to this question has been provided by an analysis of a one wear straight plate wheel to two drag brake applications of 37 kW (50 bhp) which are separated by an intermediate cool down period.

Results are shown in Figures 14 and 15. Figure 14 shows the radial component of stress at the inside rim fillet and outside hub fillet. The hub fillet stress reaches a maximum of 820 MPa (119 ksi) at the end of the first 60 minute thermal load. Subsequent cooling causes the stress to become a residual compressive stress of 620 MPa (90 ksi). A slightly lower stress of 765 MPa (111 ksi) is reached after the second thermal load. Subsequent cooling of the wheel leads to a compressive stress of 680 MPa (98 ksi). Similar behavior is noted for the rim fillet stress. The rim fillet stress reaches a maximum of 590 MPa (86 ksi) at the end of the first 60 minute thermal load. Subsequent cooling causes the stress at this location to become a residual compressive stress of 470 MPa (68 ksi). A slightly lower tensile stress of 520 MPa (75 ksi) is reached after the second thermal load. Subsequent cooling leads to a compressive stress of 540 MPa (79 ksi).

The behavior of the stress in the rim is indicated in Figure 15. Data are shown for the central region of the tread because this is where the highest rim stresses are developed. The circumferential component of stress is the most significant parameter in this region. The results plotted in the figure show that a compressive stress of 211 MPa (30.6 ksi) is reached at the end of the first thermal load. Subsequent cooling causes a residual tensile stress of 225 MPa (32.6 ksi). At the end of the second thermal load the compressive stress is 161 MPa (23.4 ksi) which is modified to a residual tensile stress of 274 MPa (39.8 ksi) by subsequent cooling.

These results show that the largest change in residual stresses are caused by the first severe thermal load. They also indicate that after the second thermal loading the residual stress condition is more severe than after the first thermal load. It is quite possible that subsequent application of severe thermal loads would cause further shifts in the residual stress field, but that a steady state condition would be approached asymptotically.

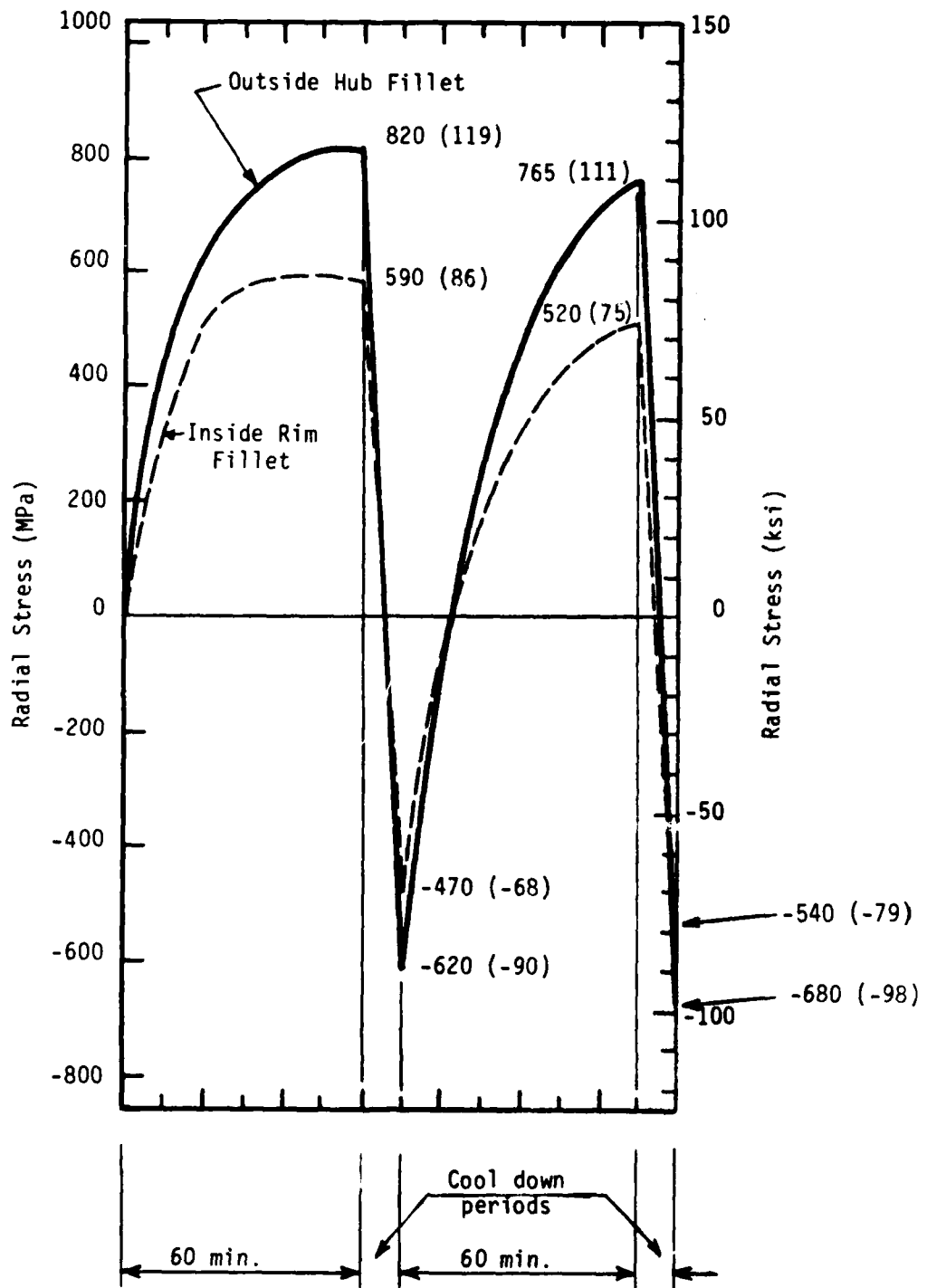


Figure 14 Rim and Hub Fillet Radial Stresses, in MPa (ksi) for Two 60-minute 37 kW (50 bhp) Thermal Loads

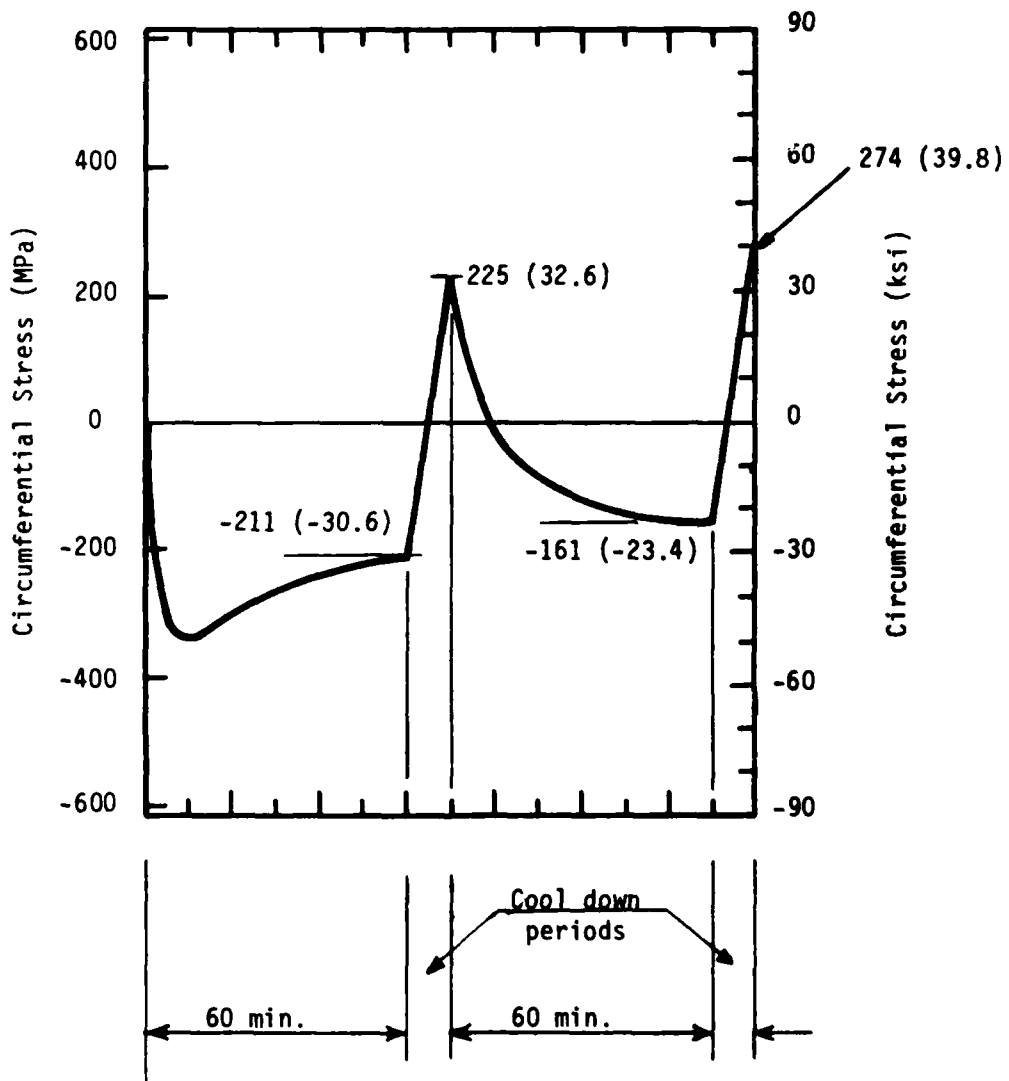


Figure 15 Circumferential Rim Stress in MPa (ksi) for Two 60-minute 37 kW (50 bhp) Thermal Loads

#### 4.6 Cyclic Stresses Due to Service Braking

Service braking generally results in much lower levels of thermal load input to the wheels than drag braking, but the associated stress cycles can be significant. The magnitudes of representative stress cycles have been determined by analyzing the response of a one wear straight plate wheel to an approximate representation of the thermal brake load from a full service brake application at 96 km/h (60 mph). The thermal load is applied at the tread of the wheel and is shown as a function of time in Figure 16. The resulting stresses are plotted for several positions (defined in Figure 1) within the wheel in Figures 17 and 18. Figure 17 shows variations in the circumferential rim stresses as a function of time. Note that there is a cyclic circumferential stress at certain positions within the rim which is due to the transient nature of the heat flow into the rim. The surface layer at the tread is heated by the deposition of the brake energy, but there is insufficient time for the heat to be conducted all the way down through the rim. Therefore, the thermal gradient is quite steep resulting in a circumferential compressive stresses in the outer layer of the rim and tensile stresses in the colder material below. As the heat penetrates into the rim and becomes more uniformly distributed the tensile stresses disappear and the entire rim cross section is in compression.

Figure 18 shows plots of the radial component of stress as a function of time in the hub and rim fillet locations. Here the stress cycle is one of a moderate tensile stress due to the overall temperature gradient in the wheel. The transient stresses introduced at these locations, while moderate, are still higher than the cyclic stresses caused by mechanical load effects.

#### 4.7 Simplifying Assumptions

When making comparisons between the results of thermal stress analyses and actual braking cycles one must recognize certain simplifying assumptions which are made in the analyses.

4.7.1 Axisymmetric Heat Impact-First, the assumption is made that the heat is introduced axisymmetrically around the tread of the wheel, when actually the heat is introduced in a localized manner at the brake head. The fairly rapid rotation of the wheel (e.g., approximately five revolutions per second at 16 m/s (35 mph)) along with a relatively slow change in wheel temperature (approximately 34°C (62°F) per minute at the tread for a 37 kW (50 bhp) input) should result in small calculational errors using the axisymmetric heat input assumption.

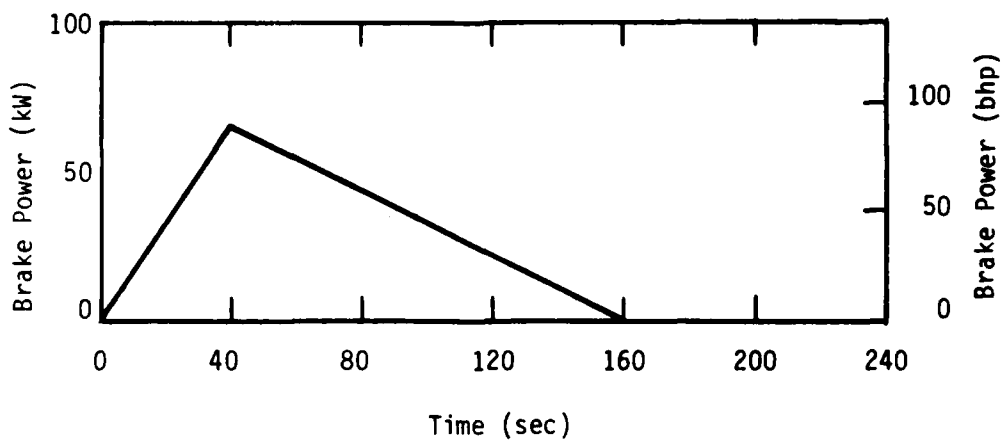


Figure 16 Estimate of Brake Power as a Function of Time for Service Braking from 96 km/h (60 mph)

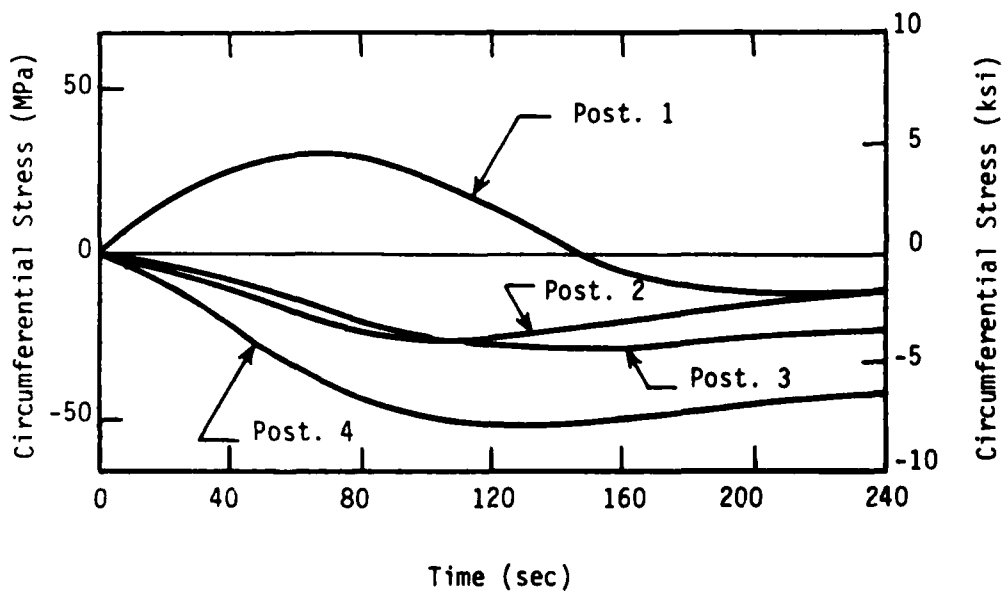


Figure 17 Circumferential Rim Stresses as a Function of Time for Service Braking Thermal Load

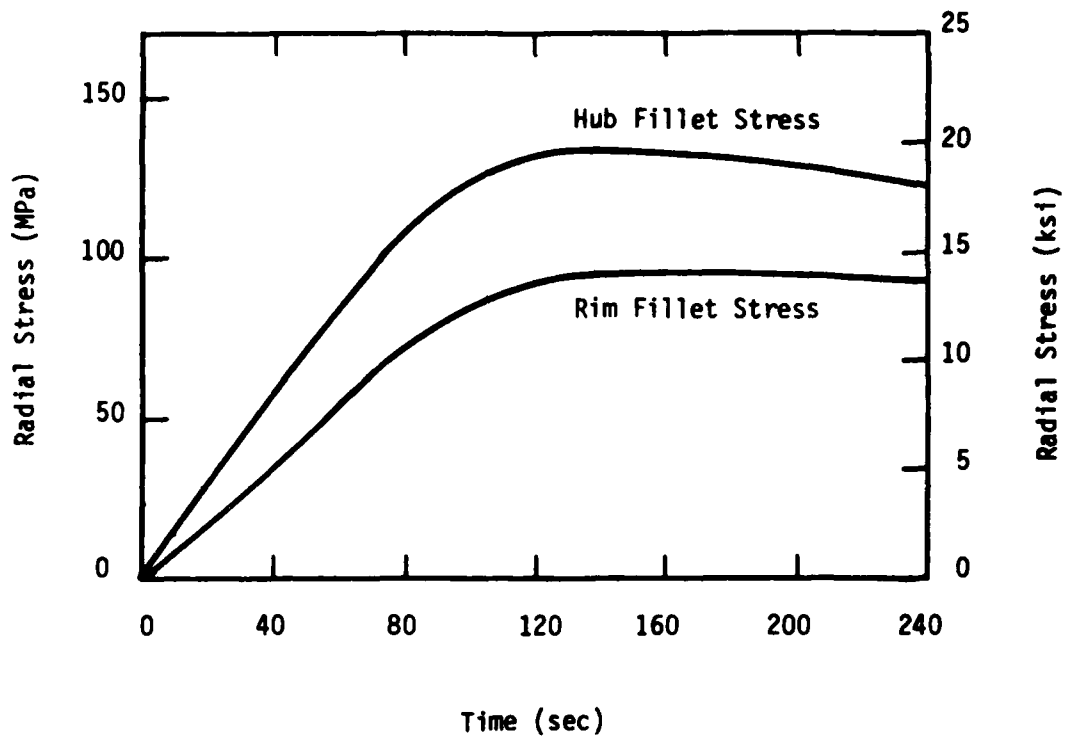


Figure 18 Radial Hub Plate Fillet Stresses as a Function of Time for Service Braking Thermal Load

4.7.2 Heat Conducted to Brake Shoe and Brake Head-Second, it must be recognized that the analyses are made on the basis of the heat input to the wheel. This is less than the total braking energy per wheel because some of the energy is conducted into the brake shoe, the brake head, and its supporting structure. Less heat would be conducted thru a composition brake shoe than an iron shoe. It has been estimated that up to 25 percent of the braking energy is conducted through a metal shoe. This results in significantly lower wheel temperatures.

4.7.3 Heat Conducted to Rail-Another factor that should be considered is the reduction in the thermal brake load due to the heat conducted from the wheel to the rail thru the wheel/rail contact point. The significance of this effect was noted on recent tests with the U.S. Steel wheel/rail dynamometer. This test machine is used for railroad wheel braking experiments and is the only dynamometer of its kind which uses a load wheel to simulate the wheel/rail contact. Tests showed that thermal strains and wheel temperatures were depressed approximately 55°C (100°F) when the load wheel was in contact with the test wheel. This is equivalent to an approximate reduction of 20 percent in the brake energy.

The possible magnitude of this effect has been examined by analyzing a simplified representation of the transient wheel/rail contact. A given position on the tread of the wheel, which is at high temperature because of the brake heating, comes into momentary contact with the cold rail at the wheel/rail contact zone. The cold rail has the effect of quenching the rim of the wheel, because the large temperature difference will result in a high rate of heat flow. The major limitation on the heat flow is the thermal resistance of the interface itself.

Calculations were made assuming that the effect can be represented by a one-dimensional calculation where two bodies of different temperature are brought into momentary contact. The wheel/rail contact zone, which is approximately elliptical in shape, was represented by two rectangles as illustrated in Figure 19. A wheel speed of 15.7 m/s (35 mph) was assumed which implies that a point on the wheel will be in contact with the rail for 1.25 or 0.71 ms respectively for the large and small rectangles. It was further assumed that the thermal resistance of boundary itself is zero. This would give an upper bound to the predicted rate of heat flow.

Results from the analysis are presented in Table 3. They are shown in terms of the predicted heat flow for 100°C (180°F) increments of temperature difference between wheel and rail at an operating speed of 15.7 m/s (35 mph).



The results show that large heat flows across the wheel/rail contact zone are plausible. In the real case there will be some thermal resistance between the wheel and rail and this will limit heat flow to values less than those indicated in the table.

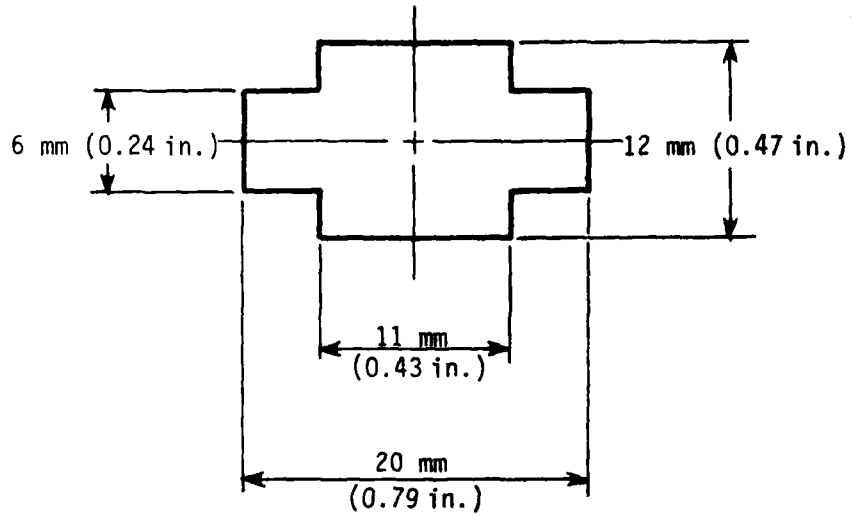


Figure 19 Representation of Wheel/Rail Contact Zone

TABLE 3. PREDICTED HEAT FLOW AT WHEEL/RAIL INTERFACE  
(NO THERMAL RESISTANCE AT BOUNDARY ASSUMED)

Temperature Difference Between Wheel Tread and Rail		Heat Flow	
°C	(°F)	kW	(bhp)
100	(180)	8.7	(11.6)
200	(360)	17.4	(23.3)
300	(540)	26.0	(34.9)
400	(720)	34.7	(46.5)

## 5. RESULTS: WHEEL REVOLUTION STRESS VARIATIONS

This section presents results of analyses which have been made with the elastic three-dimensional code to determine the wheel stresses caused by forces at the wheel/rail interface and their variation due to rotation of the wheel. Data are presented for 914 mm (36 inch) diameter wheels.

### 5.1 Vertical Load Stresses

Stress data are presented for an assumed vertical wheel load of 142 kN (32,000 lb), which is the nominal wheel load for a fully loaded 91 Mg (100 ton) capacity car.

5.1.1 Circumferential Variation-Figure 20 shows a typical finite element configuration (the two wear straight plate wheel case) that was used for the analysis of stresses caused by a vertical load application (radial with respect to the wheel) centered on the tape line. The load was assumed distributed over elements 275 and 276 for a 25 mm (1 inch) circumferential direction. Figure 21 presents typical results which show the variation of stress as a function of the angular position with respect to the point of load application. Note that the maximum stresses occur in the radial cross section of the wheel which is centered on the area of load application (0 deg).

5.1.2 Stress Variation with Load Position, One and Two Wear Straight Plate Wheels-Circumferential rim stress variations are presented in Table 4 from the analyses of one and two wear straight plate wheels. The positions around the cross section of the rim where stress results are recorded are shown in Figure 1. Table 4 presents the mechanical stress ranges (as the wheel rotates) for loads centered at two different positions on the tread of the wheel, the tape line and near the outer edge, as defined in Figure 1.

The results presented in Table 4 show that stress variations in the rim are relatively small. The largest stress range is associated with the edge load condition and it occurs at the outside back of rim (position 1). The stress ranges for the two wear wheel are significantly lower than the corresponding stress ranges for the one wear wheel. The stress ranges on the inside rim face, Positions 4 and 5, are relatively small.

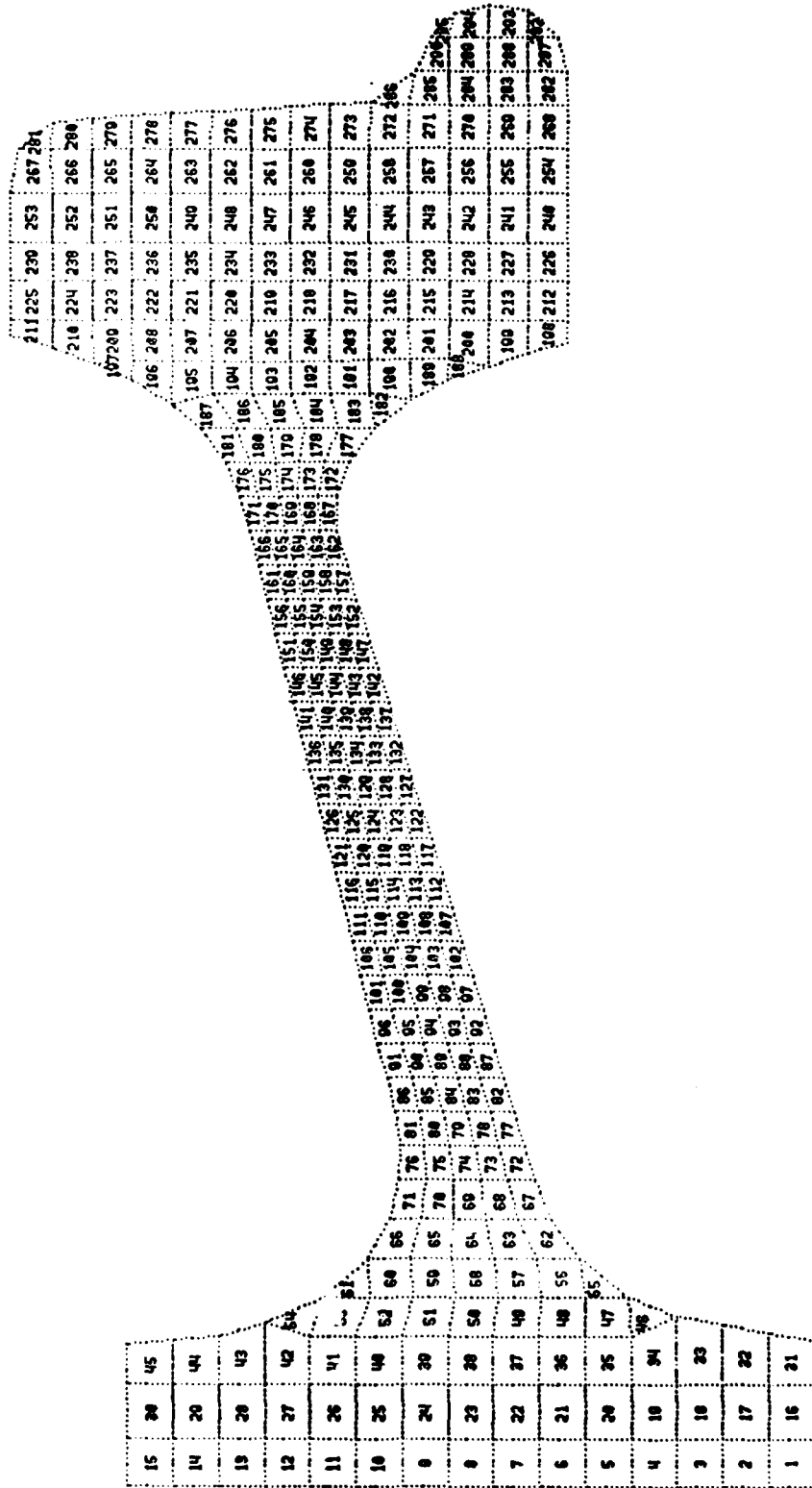


Figure 20 Finite Element Mesh for Two Wear Straight Plate Wheel

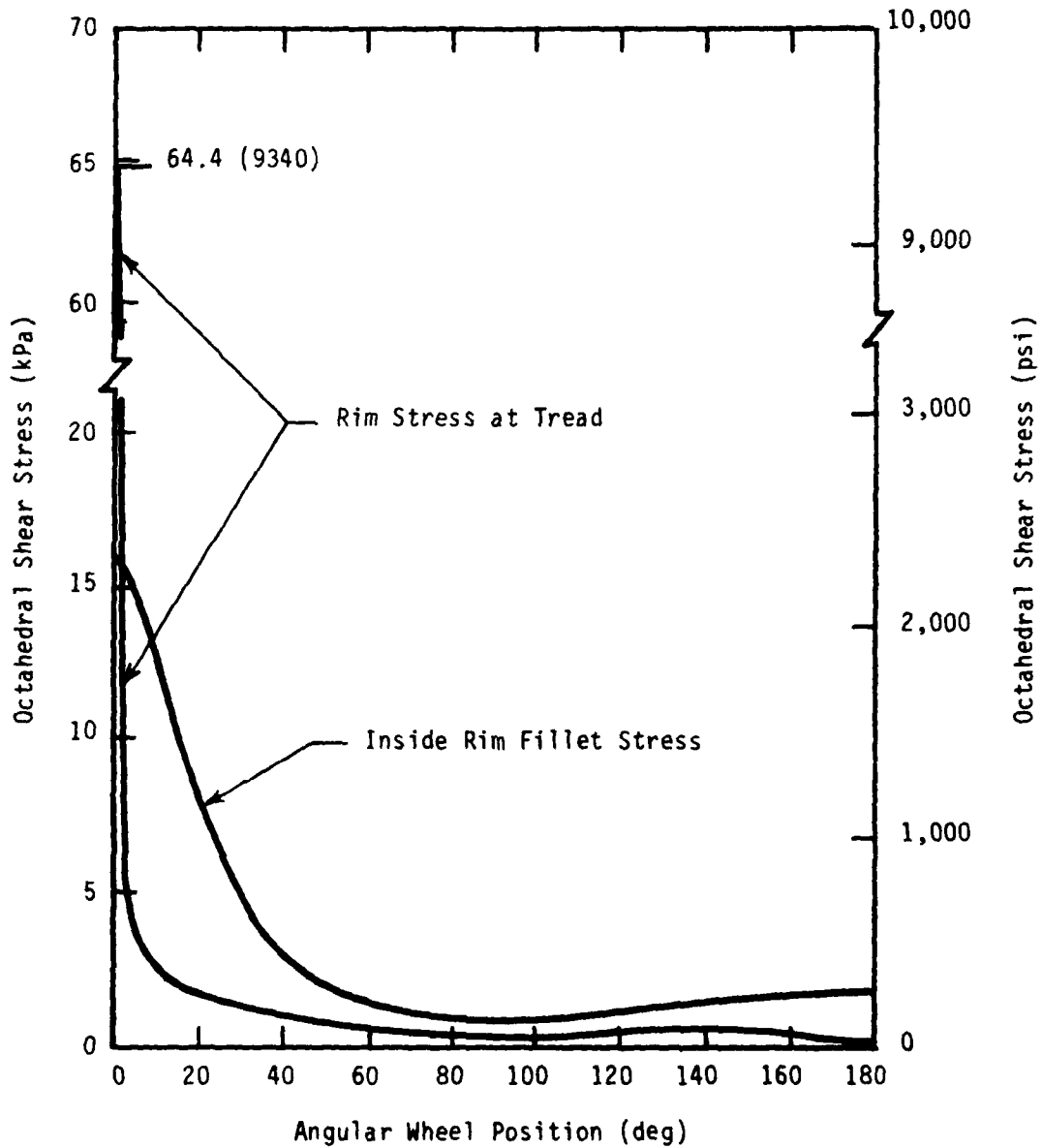


Figure 21 Octahedral Shear Stress as a Function of Angle from Radial Plane of Load Application, 142 kN (32,000 lb) Vertical Wheel Load

TABLE 4. CIRCUMFERENTIAL STRESS VARIATIONS CAUSED BY VERTICAL WHEEL LOAD OF 142 kN (32,000 lb)

Wheel Type and Load Position	Position of Stress Value (See Fig. 1 straight plate wheels)	Mechanical Stress, MPa (ksi)	
		Minimum	Maximum
Two-Wear Center Load	1	-0.7 (-0.1)	15.2 ( 2.2)
	2	-6.9 (-1.0)	-2.8 (-0.4)
	3	-15.2 (-2.2)	-6.2 (-0.9)
	4	-13.8 (-2.0)	-6.2 (-0.9)
	5	-3.4 (-0.5)	-1.4 (-0.2)
Two-Wear Edge Load	1	-11.7 (-1.7)	33.8 ( 4.9)
	2	-18.6 (-2.7)	-9.6 (-1.4)
	3	-6.2 (-0.9)	-2.1 (-0.3)
	4	-9.0 (-1.3)	-2.8 (-0.4)
	5	-3.4 (-0.5)	-0.7 (-0.1)
One-Wear Center Load	1	-6.9 (-1.0)	10.3 ( 1.5)
	2	-10.3 (-1.5)	2.1 ( 0.3)
	3	-20.6 (-3.0)	1.4 ( 0.2)
	4	-6.9 (-1.0)	2.8 ( 0.4)
One-Wear Edge Load	1	-24.1 (-3.5)	49.6 ( 7.2)
	2	-26.9 (-3.9)	4.1 ( 0.6)
	3	-6.2 (-0.9)	4.1 ( 0.6)
	4	-9.0 (-1.3)	9.6 ( 1.4)

5.1.3 Stress Variations from Dynamic Effects-The interpretation of the results presented in Table 4 should also consider that the mechanical load stresses are based on the nominal static load capacity of the wheel. This load value is often exceeded during normal operations because of the dynamic interaction between the wheel and rail and because of oscillations of the primary suspension system of the car. A recent analysis of wheel/rail load data obtained on high quality track has shown that a 13 percent increase in load can be expected at least 10 percent of the time. Larger increases would be expected on lower quality track. The mechanical stress range would be proportionately increased during these high load situations.

5.1.4 Factors Affecting Accuracy of Calculations-The stresses in wheels resulting from loads acting at the wheel/rail interface were calculated using the elastic three-dimensional finite element code. As described in the appendix this analytical procedure makes use of a Fourier series representation of the load in the circumferential direction. The stress results are obtained by the summation of the effects of each term in the series. The accuracy of the solution is dependent on the number of terms which are used to represent the load. Generally speaking, the closer one gets to the load point the larger the number of terms required for an accurate solution. Similarly, the variation in stress across a radial section of the wheel is represented by the stress calculations for elements in a finite element mesh. Greater accuracy is obtained at higher computational expense by reducing the size and increasing the number of elements in the mesh.

It was of considerable importance in this study to determine the relationship between a number of Fourier components and the accuracy of the results because of the interest in determining the rim stresses. Therefore, a series of computations were made to determine the influence of the number of Fourier components (modes) on the accuracy of the results. Figure 22 shows the loading that was assumed for these calculations. The load is two elements wide, 20 mm (0.8 inch), and is uniform in the circumferential direction of the wheel over a length of 25 mm (1.0 inch). The stresses were obtained for the elements surrounding the point of load application. Results were compared for locations directly below the load, a position to the side of the load, and at similar positions 10 degrees away. Figure 22 also defines these positions of interest.

The results are shown in Figures 23 and 24 which present calculated stresses as a function of a number of modes which are used in the summation. Figure 23 shows radial stress data and Figure 24 presents circumferential stress data. Note that directly under the load (position 1, Figures 23 and 24) approximately 100 terms are required to get an accurate indication of the radial and circumferential stresses. The final value is approached in an asymptotic manner as a function of the number of modes. At a point deeper within the rim under the load (position 3, 29 mm (1.1 inch), deep) the radial stress is approached in approximately 50 modes (Figure 23), whereas about 100 terms are required to approach the circumferential stress (Figure 24) at this location.

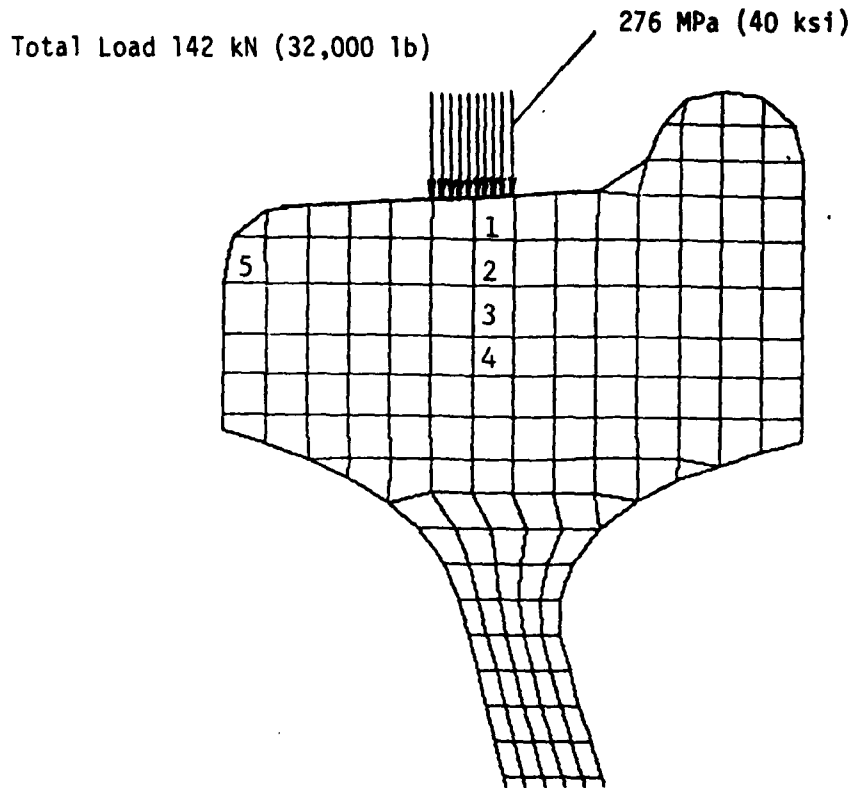


Figure 22 Element Locations Used for Study of Convergence of Modal Solution

At a point 10 degrees away from the point of load application the radial stress in the outer element would be expected to be negligible. Note (Figure 23) that this value is approached in an alternating manner as a function of the number of modes. At least 100 terms are required to come close to the final value. At position 3 the convergence is more rapid and a reasonable approximation of the load is obtained with 60 terms (Figure 23). The rate of convergence of the circumferential stress is approximately the same at this position as illustrated in Figure 24.

Figure 25 shows the convergence of the solution for circumferential stress at a point on the outside face of the rim (position 5). Note that in both the plane of loading ( $\theta=0$  deg) and 10 degrees away ( $\theta=10$  deg) convergence is obtained with approximately 30 modes. This illustrates the principle that convergence requires fewer terms as the position of interest moves further from the point of load application.

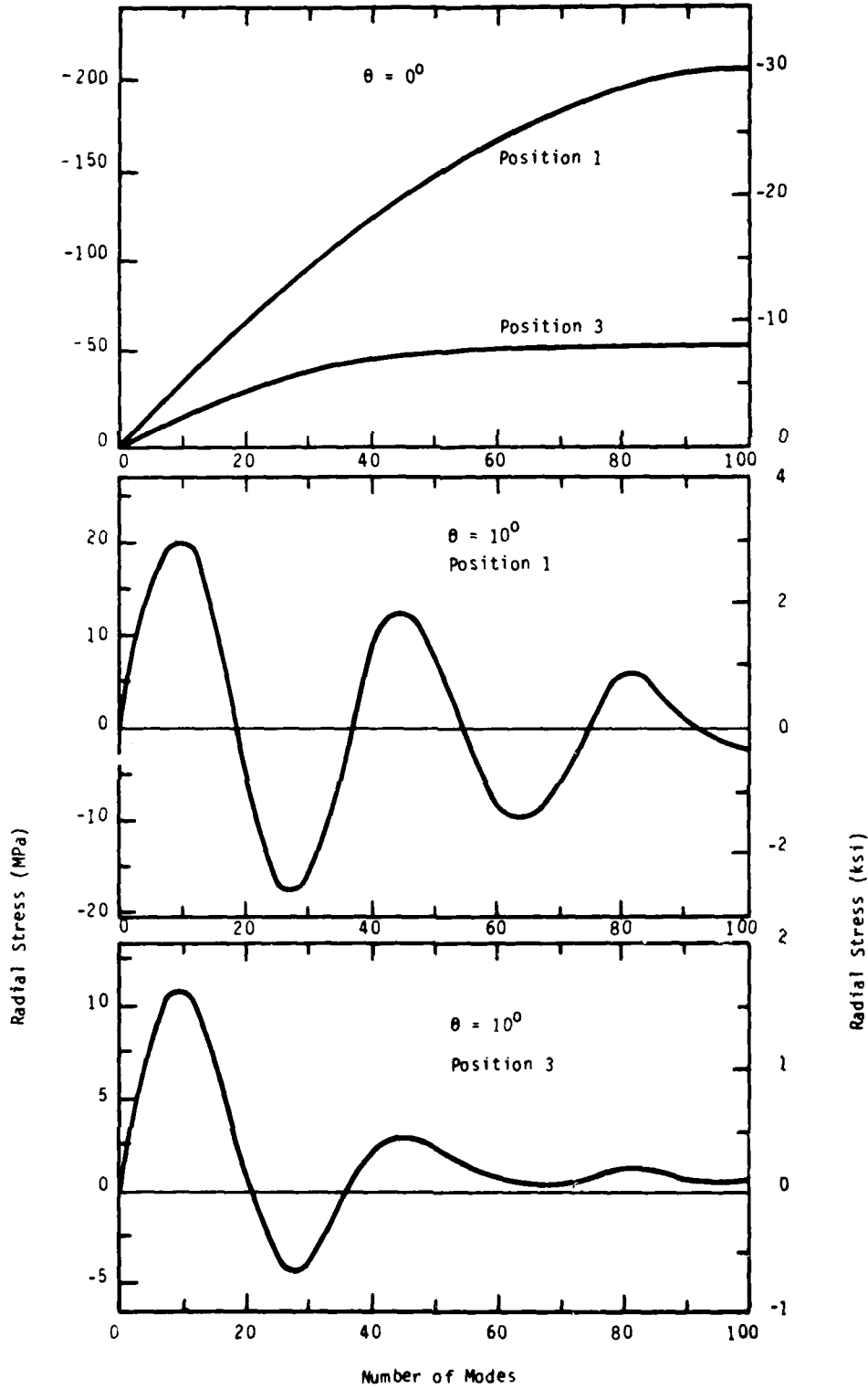


Figure 23 Radial Stress versus Number of Modes



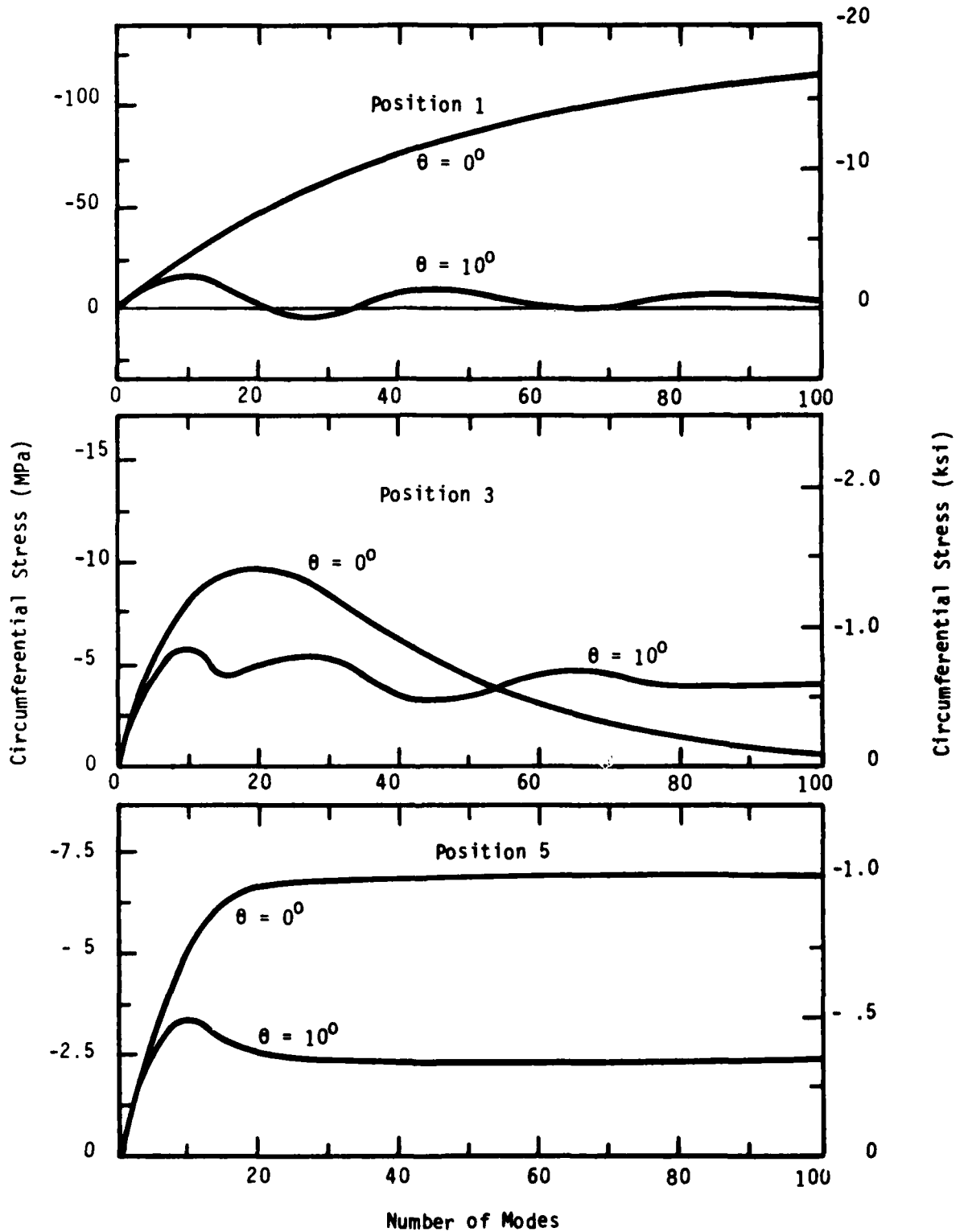


Figure 24 Circumferential Stress versus Number of Modes

## 5.2 Lateral Load

Figure 25 shows typical stress variations as a function of angular position resulting from the application of a 44 kN (10,000 lb) lateral load acting against the flange. The figure presents the radial component of stress at the outside hub fillet and the inside rim fillet of a two wear straight plate wheel. Note that the maximum stress occurs in the radial cross section of the wheel which includes the point of load application (0 deg). Note also that the stress at the inside rim fillet is much lower in magnitude, but also that it undergoes a greater range of variation with position around the wheel. This figure illustrates a general phenomenon with respect to wheel stresses from lateral loading, namely, that the maximum stress is in the plane of loading, but that for some other radial positions, where the maximum stress is lower, the largest stress at that radius may occur at some other position than in the plane of loading.

## 5.3 Combined Loads

This section presents results from analyses of stresses caused by the action of mechanical loads combined with the residual stresses from severe thermal loads. The information is used later in this report for an assessment of the likelihood of crack initiation and growth. Residual stress data from severe thermal loads have been presented in Table 2. Some cyclic mechanical stress data have been presented in Table 4.

The combined stress data are presented in Tables 6 through 10. One and two wear straight plate and one wear curved plate wheels have been considered in these analyses. Stresses are reported for several points in the rims of the wheels as defined in Figure 1. The data in the tables are restricted to circumferential stress data. This component of stress would be expected to be the most significant for thermal crack initiation and growth.

The data presented in the tables give stress ranges (as the wheel rotates) for both tape line and edge positions for the vertical load. Data are shown for the vertical load acting alone and in combination with lateral loads directed both toward the flange and away from the flange. The assumed vertical load is 142 kN (32,000 lb) and the assumed lateral load is 44 kN (10,000 lb). Two levels of thermal load are considered in these analyses, 30 kW (40 bhp) and 37 kW (50 bhp) for 1 hour. The thermal load input was assumed to be centered about the tape line. Table 5 presents an index of the combined stress data presented in Tables 6 through 11.

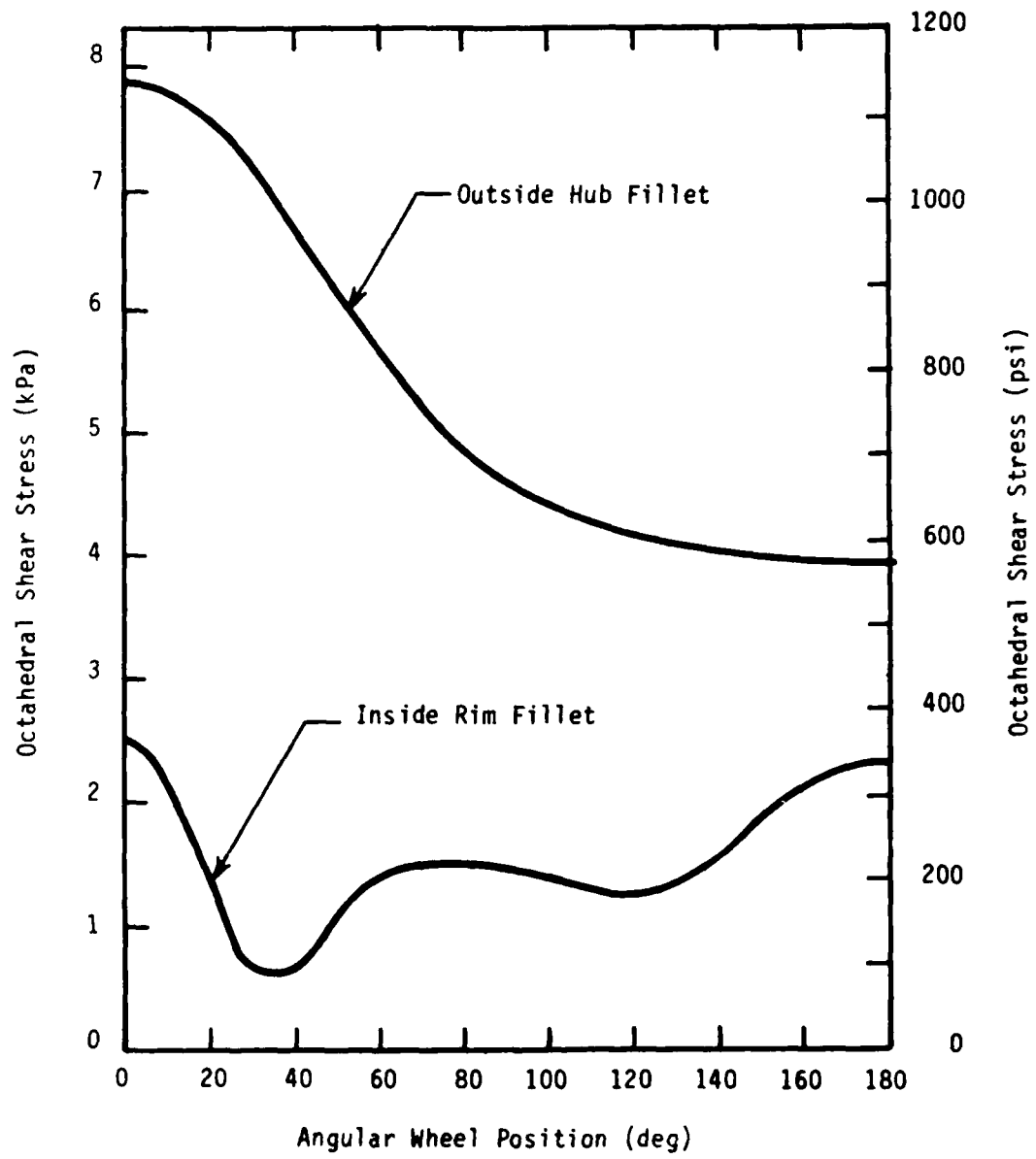


Figure 25 Octahedral Shear Stress as a Function of Angle from Radial Plane of Load Application, 44 kN (10,000 lb) Lateral Wheel Load

TABLE 5. INDEX OF TABULATED STRESSES FOR COMBINED LOADS

Table	Vertical Load Position	Lateral Load Direction	Thermal Load for Residual Stresses kW (bhp)
6a	Tape Line	None	30 (40)
6b			37 (50)
7a	Edge	None	30 (40)
7b			37 (50)
8a	Tape Line	Away From Flange	30 (40)
8b			37 (50)
9a	Tape Line	Toward Flange	30 (40)
9b			37 (50)
10a	Edge	Away From Flange	30 (40)
10b			37 (50)
11a	Edge	Toward Flange	30 (40)
11b			37 (50)

#### 5.4 Interpretation of Results

Thermal crack initiation is most likely to occur under conditions of large stress ranges and stress ratios. An examination of the data contained in Tables 6 to 11 shows that the stress ranges are relatively low, but that in some cases they occur in combination with high stress ratios. The data show that the most severe conditions occur at the flange and inside rim positions where the stress ratios are relatively large. The results also indicate that the combination of outwardly directed lateral loads with vertical loads produced the largest mechanical stress ranges. This is a case which is unlikely to result in a large number of stress cycles during normal operations. The data from the stress calculations do not indicate any significant advantages for either the curved plate or straight plate wheel configuration.

TABLE 6a. CIRCUMFERENTIAL RIM STRESSES, RESIDUAL STRESSES FROM THERMAL LOAD COMBINED WITH STRESSES FROM MECHANICAL LOAD (Vertical tape line load, no lateral load and 30 kW (40 bhp) thermal load)

Type of Wheel	Position	Stress Range for 142 kN (32 kip) Radial Wheel Load Applied at Center of Tread		Residual Stress From 30 kW (40 bhp) Thermal Load	Mechanical Stresses Combined with 30 kW (40 bhp) Residual Thermal Stresses		Stress Ratio
		Circumferential Stress Minimum MPa (ksi)	Maximum MPa (ksi)		Minimum MPa (ksi)	Maximum MPa (ksi)	
Two Wear Straight Plate	1	-4.8 (-0.7)	15 (2.2)	-2.1 (-0.3)	-6.9 (-1.0)	13 (1.9)	-0.53
	2	-6.9 (-1.0)	0.7 (0.1)	3.4 (0.5)	-3.5 (-0.5)	4 (0.6)	-0.83
	3	-15 (-2.2)	2.8 (0.4)	32 (4.7)	17 (2.5)	35 (5.1)	0.49
	4	-14 (-2.0)	2.8 (0.4)	42 (6.1)	28 (4.1)	45 (6.5)	0.63
	5	-3.4 (-0.5)	2.1 (0.3)	49 (7.1)	46 (6.6)	51 (7.4)	0.89
One Wear Straight Plate	1	-7.6 (-1.1)	10 (1.5)	-2.8 (-0.4)	-10 (-1.5)	7 (1.1)	-1.36
	2	-10 (-1.5)	2.1 (0.3)	1.4 (0.2)	-9 (-1.3)	3.5 (0.5)	-2.60
	3	-21 (-3.0)	1.4 (0.2)	40 (5.8)	19 (2.8)	41 (6.0)	0.47
	4	-6.9 (-1.0)	2.8 (0.4)	56 (8.1)	49 (7.1)	59 (8.5)	0.84
One Wear Curved Plate	1	-9.7 (-1.4)	18 (2.6)	-19 (-2.7)	-29 (-4.1)	-1 (-0.1)	-
	2	-7.6 (-1.1)	4.1 (0.6)	-17 (-2.5)	-25 (-3.6)	-13 (-1.9)	-
	3	-17 (-2.5)	4.1 (0.6)	17 (2.4)	-0.7 (-0.1)	21 (3.0)	-0.03
	4	-17 (-2.5)	6.2 (0.9)	23 (3.4)	6 (0.9)	29 (4.3)	.21
	5	-6.9 (-1.0)	5.5 (0.8)	77 (11.2)	70 (10.2)	82 (12.0)	.85

TABLE 6b. CIRCUMFERENTIAL RIM STRESSES, RESIDUAL STRESSES FROM THERMAL LOAD COMBINED WITH STRESSES FROM MECHANICAL LOAD (Vertical tape line load, no lateral load and 37 kW (50 bhp) thermal load)

Type of Wheel	Position	Stress Range for 142 kN (32 kip) Radial Wheel Load Applied at Center of Tread		Residual Stress From 37 kW (50 bhp) Thermal Load		Stress Range MPA (ksi)		Circumferential Stress		Mechanical Stresses Combined with 37 kW (50 bhp) Residual Thermal Stresses		Stress Ratio
		Minimum MPa (ksi)	Maximum MPa (ksi)	Minimum MPa (ksi)	Maximum MPa (ksi)	Minimum MPa (ksi)	Maximum MPa (ksi)	Minimum MPa (ksi)	Maximum MPa (ksi)	Minimum MPa (ksi)	Maximum MPa (ksi)	
Two Wear Straight Plate	1	-4.8 (-0.7)	15 (2.2)	-22 (-3.2)	20 (2.9)	-27 (-3.9)	-7 (-1.0)	-	-	-	-	-
	2	-6.9 (-1.0)	0.7 (0.1)	-8.3 (-1.2)	7.6 (1.1)	-15 (-2.2)	-8 (-1.1)	-	-	-	-	-
	3	-15 (-2.2)	2.8 (0.4)	57 (8.2)	18 (2.6)	42 (6.0)	60 (8.6)	0.70	0.70	60 (8.6)	0.70	0.79
	4	-14 (-2.0)	2.8 (0.4)	78 (11.3)	17 (2.4)	64 (9.3)	81 (11.7)	0.79	0.79	81 (11.7)	0.79	0.94
	5	-3.4 (-0.5)	2.1 (0.3)	94 (13.6)	5.5 (.8)	91 (13.1)	96 (13.9)	0.94	0.94	96 (13.9)	0.94	0.94
One Wear Straight Plate	1	-7.6 (-1.1)	10 (1.5)	-34 (-5.0)	18 (2.6)	-42 (-6.1)	-24 (-3.5)	-	-	-	-	-
	2	-10 (-1.5)	2.1 (0.3)	-18 (-2.6)	12 (1.8)	-28 (-4.1)	-16 (-2.3)	-	-	-	-	-
	3	-21 (-3.0)	1.4 (0.2)	57 (8.2)	22 (3.2)	36 (5.2)	58 (8.4)	0.62	0.62	58 (8.4)	0.62	0.92
	4	-6.9 (-1.0)	2.8 (0.4)	123 (17.8)	9.7 (1.4)	116 (16.8)	126 (18.2)	0.92	0.92	126 (18.2)	0.92	0.92
One Wear Curved Plate	1	-9.7 (-1.4)	18 (2.6)	-56 (-8.1)	28 (4.0)	-66 (-9.5)	-38 (-5.5)	-	-	-	-	-
	2	-7.6 (-1.1)	4.1 (0.6)	-28 (-4.1)	12 (1.7)	-36 (-5.2)	-24 (-3.5)	-	-	-	-	-
	3	-17 (-2.5)	4.1 (0.6)	26 (3.7)	21 (3.1)	9 (1.2)	30 (4.3)	0.83	0.83	30 (4.3)	0.83	0.83
	4	-17 (-2.5)	6.2 (0.9)	135 (19.6)	23 (3.4)	118 (17.1)	141 (20.7)	0.83	0.83	141 (20.7)	0.83	0.94
	5	-6.9 (-1.0)	5.5 (0.8)	208 (30.1)	12 (1.8)	201 (29.1)	214 (30.9)	0.94	0.94	214 (30.9)	0.94	0.94

TABLE 7a. CIRCUMFERENTIAL RIM STRESSES, RESIDUAL STRESSES FROM THERMAL LOAD COMBINED WITH STRESSES FROM MECHANICAL LOAD (Vertical edge load, no lateral load and 30 kW (40 bhp) thermal load)

Type of Wheel	Position	Stress Range for 142 kN (32 kip) Radial Wheel Load Applied at Edge of Tread		Stress Range Mpa (ksi)	Residual Stress From 30 kW (40 bhp) Thermal Load		Mechanical Stresses Combined with 30 kW (40 bhp) Residual Thermal Stresses		Stress Ratio
		Minimum Mpa (ksi)	Maximum Mpa (ksi)		Minimum Mpa (ksi)	Maximum Mpa (ksi)	Minimum Mpa (ksi)	Maximum Mpa (ksi)	
Two Wear Straight Plate	1	-14 (-2.0)	34 (4.9)	48 (6.9)	-2.1 (-0.3)	-16 (-2.3)	32 (4.6)	-0.50	
	2	-19 (-2.7)	3.4 (0.5)	22 (3.2)	3.4 (0.5)	-16 (-2.2)	7 (1.0)	-2.20	
	3	-6.2 (-0.9)	4.8 (0.7)	11 (1.6)	32 (4.7)	26 (3.8)	37 (5.4)	0.70	
	4	-9.0 (-1.3)	7.6 (1.1)	17 (2.4)	42 (6.1)	33 (4.8)	50 (7.2)	0.67	
	5	-3.4 (-0.5)	7.6 (1.1)	11 (1.6)	49 (7.1)	46 (6.6)	57 (8.2)	0.80	
One Wear Straight Plate	1	-24 (-3.5)	50 (7.2)	74 (10.7)	-2.8 (-0.4)	-27 (-3.9)	47 (6.8)	-0.57	
	2	-27 (-3.9)	4.1 (0.6)	31 (4.5)	1.4 (0.2)	-26 (-3.7)	5 (0.8)	-4.63	
	3	-6.2 (-0.9)	4.1 (0.6)	10 (1.5)	40 (5.8)	34 (4.9)	44 (6.4)	0.77	
	4	-9.0 (-1.3)	9.7 (1.4)	19 (2.7)	56 (8.1)	47 (6.8)	66 (9.5)	0.72	
One Wear Curved Plate	1	-17 (-2.4)	41 (6.0)	58 (8.4)	-19 (-2.7)	-35 (-5.1)	23 (3.3)	-1.55	
	2	-17 (-2.5)	5.5 (0.8)	23 (3.3)	-17 (-2.5)	-34 (-5.0)	-11 (-1.7)	-	
	3	-12 (-1.7)	6.2 (0.9)	18 (2.6)	17 (2.4)	5 (0.7)	23 (3.3)	0.21	
	4	-15 (-2.2)	9.7 (1.4)	25 (3.6)	23 (3.4)	8 (1.2)	33 (4.8)	0.25	
	5	-10 (-1.5)	9.7 (1.4)	20 (2.9)	77 (11.2)	67 (9.7)	87 (12.6)	0.77	

TABLE 7b. CIRCUMFERENTIAL RIM STRESSES, RESIDUAL STRESSES FROM THERMAL LOAD COMBINED WITH STRESSES FROM MECHANICAL LOAD (Vertical edge load, no lateral load and 37 kW (50 bhp) thermal load)

Type of Wheel	Position	Stress Range for 142 kN (32 kip) Radial Wheel Load Applied at Edge of Tread		Stress Range MPa (ksi)	Residual Stress From 37 kW (50 bhp) Thermal Load		Circumferential Stresses Combined with 37 kW (50 bhp) Residual Thermal Stresses		Stress Ratio
		Minimum MPa (ksi)	Maximum MPa (ksi)		Minimum MPa (ksi)	Maximum MPa (ksi)			
Two Wear Straight Plate	1	-14 (-2.0)	34 (4.9)	48 (6.9)	-22 (-3.2)	-36 (-5.2)	12 (1.7)	-3.06	
	2	-19 (-2.7)	3.4 (0.5)	22 (3.2)	-8.3 (-1.2)	-27 (-3.9)	-5 (-0.7)	-	
	3	-6.2 (-0.9)	4.8 (0.7)	11 (1.6)	57 (8.2)	51 (7.3)	62 (8.9)	0.82	
	4	-9.0 (-1.3)	7.6 (1.1)	17 (2.4)	78 (11.3)	69 (10.0)	86 (12.4)	0.81	
	5	-3.4 (-0.5)	7.6 (1.1)	11 (1.6)	94 (13.6)	91 (13.1)	102 (14.7)	0.89	
One Wear Straight Plate	1	-24 (-3.5)	50 (7.2)	74 (10.7)	-34 (-5.0)	-58 (-8.5)	16 (2.2)	-3.86	
	2	-27 (-3.9)	4.1 (0.6)	31 (4.5)	-18 (-2.6)	-47 (-6.5)	-14 (-2.0)	-	
	3	-6.2 (-0.9)	4.1 (0.6)	10 (1.5)	57 (8.2)	51 (7.3)	61 (8.8)	0.83	
	4	-9.0 (-1.3)	9.7 (1.4)	19 (2.7)	123 (17.8)	114 (16.5)	133 (19.2)	0.86	
One Wear Curved Plate	1	-17 (-2.4)	41 (6.0)	58 (8.4)	-56 (-8.1)	-73 (-10.5)	-15 (-2.1)	-	
	2	-17 (-2.5)	5.5 (0.8)	23 (3.3)	-28 (-4.1)	-45 (-6.6)	-23 (-3.3)	-	
	3	-12 (-1.7)	6.2 (0.9)	18 (2.6)	26 (3.7)	14 (2.0)	32 (4.6)	0.43	
	4	-15 (-2.2)	9.7 (1.4)	25 (3.6)	135 (19.6)	123 (17.8)	148 (21.4)	0.83	
	5	-10 (-1.5)	9.7 (1.4)	20 (2.9)	208 (30.1)	197 (28.6)	217 (31.5)	0.91	



TABLE 8a. CIRCUMFERENTIAL RIM STRESSES, RESIDUAL STRESSES FROM THERMAL LOAD COMBINED WITH STRESSES FROM MECHANICAL LOAD (Vertical tape line load, outwardly directed lateral load and 30 kW (40 bhp) thermal load)

Type of Wheel	Position	Circumferential Stress		Stress Range MPa (ksi)	Residual Stress From 30 kW (40 bhp) Thermal Load	Circumferential Stresses Combined with 30 kW (40 bhp) Residual Thermal Stresses		Stress Ratio
		Minimum MPa (ksi)	Maximum MPa (ksi)			Minimum MPa (ksi)	Maximum MPa (ksi)	
		Stress Range for 142 kN (32 kip) Radial Wheel Load Applied at Center of Tread and 44 kN (10 kip) Lateral Load Directed Away From Flange						
Two Wear Straight Plate	1	-20 (-2.9)	26 (3.8)	46 (6.7)	-2.1 (-0.3)	-22 (-3.2)	24 (3.5)	-0.92
	2	-14 (-2.1)	5.5 (0.8)	20 (2.9)	3.4 (0.5)	-11 (-1.6)	9.0 (1.3)	-1.22
	3	-17 (-2.4)	5.5 (0.8)	22 (3.2)	32 (4.7)	16 (2.3)	38 (5.5)	0.42
	4	-22 (-3.2)	10 (1.5)	32 (4.7)	42 (6.1)	20 (2.9)	52 (7.6)	0.38
	5	-13 (-1.9)	11 (1.6)	24 (3.5)	49 (7.1)	36 (5.2)	60 (8.7)	0.60
One Wear Straight Plate	1	-19 (-2.7)	21 (3.0)	39 (5.7)	-2.8 (0.4)	-21 (-3.1)	18 (2.6)	-1.17
	2	-15 (-2.2)	7.6 (1.1)	23 (3.3)	1.4 (0.2)	-14 (-2.0)	9.0 (1.3)	-1.56
	3	-23 (-3.3)	4.8 (0.7)	28 (4.0)	40 (5.8)	17 (2.5)	45 (6.5)	0.38
	4	-23 (-3.3)	11 (1.6)	34 (4.9)	56 (8.1)	33 (4.8)	67 (9.7)	0.49
One Wear Curved Plate	1	-23 (-3.4)	33 (4.8)	57 (8.2)	-19 (-2.7)	-42 (-6.1)	14 (2.1)	-3.00
	2	-20 (-2.9)	10 (1.5)	30 (4.4)	-17 (-2.5)	-37 (-5.4)	-6.9 (-1.0)	-
	3	-23 (-3.4)	9.0 (1.3)	32 (4.7)	17 (2.4)	-6.9 (-1.0)	26 (3.7)	-0.27
	4	-30 (-4.4)	14 (2.0)	44 (6.4)	23 (3.4)	-6.9 (-1.0)	37 (5.4)	-0.19
	5	-23 (-3.3)	14 (2.0)	37 (5.3)	77 (11.2)	54 (7.9)	91 (13.2)	0.59

TABLE 8b. CIRCUMFERENTIAL RIM STRESSES, RESIDUAL STRESSES FROM THERMAL LOAD COMBINED WITH STRESSES FROM MECHANICAL LOAD (Vertical tape line load, outwardly directed lateral load and 37 kW (50 bhp) thermal load)

Type of Wheel	Position	Stress Range for 142 kN (32 kip) Radial Wheel Load Applied at Center of Tread and 44 kN (10 kip) Lateral Load Directed Away From Flange		Residual Stress From 37 kW (50 bhp) Thermal Load		Circumferential Stress		Mechanical Stresses Combined with 37 kW (50 bhp) Residual Thermal Stresses		Stress Ratio
		Minimum MPa (ksi)	Maximum MPa (ksi)	Stress Range MPa (ksi)	Minimum MPa (ksi)	Maximum MPa (ksi)	Minimum MPa (ksi)	Maximum MPa (ksi)	Minimum MPa (ksi)	
Two Wear Straight Plate	1	-20 (-2.9)	26 (3.8)	46 (6.7)	-22 (-3.2)	-42 (-6.1)	4.1 (0.6)	-2.8 (-0.4)	-10.24	
	2	-14 (-2.1)	5.5 (0.8)	20 (2.9)	-8.3 (-1.2)	-23 (-3.3)	-2.8 (-0.4)	62 (9.0)	0.65	
	3	-17 (-2.4)	5.5 (0.8)	22 (3.2)	57 (8.2)	40 (5.8)	88 (12.8)	62 (9.0)	0.64	
	4	-22 (-3.2)	10 (1.5)	32 (4.7)	78 (11.3)	56 (8.1)	105 (15.2)	88 (12.8)	0.77	
	5	-13 (-1.9)	11 (1.6)	24 (3.5)	94 (13.6)	81 (11.7)	105 (15.2)	105 (15.2)		
One Wear Straight Plate	1	-19 (-2.7)	21 (3.0)	39 (5.7)	-34 (-5.0)	-53 (-7.7)	-14 (-2.0)	-10 (-1.5)		
	2	-15 (-2.2)	7.6 (1.1)	23 (3.3)	-18 (-2.6)	-33 (-4.8)	-10 (-1.5)	61 (8.9)	0.56	
	3	-23 (-3.3)	4.8 (0.7)	28 (4.0)	57 (8.2)	34 (4.9)	134 (19.4)	61 (8.9)		
	4	-23 (-3.3)	11 (1.6)	34 (4.9)	123 (17.8)	100 (14.5)	134 (19.4)	134 (19.4)		
One Wear Curved Plate	1	-23 (-3.4)	33 (4.8)	57 (8.2)	-56 (-8.1)	-79 (-11.5)	-23 (-3.3)	-18 (-2.6)		
	2	-20 (-2.9)	10 (1.5)	30 (4.4)	-28 (-4.1)	-48 (-7.0)	-18 (-2.6)	34 (5.0)	0.06	
	3	-23 (-3.4)	9.0 (1.3)	32 (4.7)	26 (3.7)	2.1 (0.3)	149 (21.6)	34 (5.0)	0.70	
	4	-30 (-4.4)	14 (2.0)	44 (6.4)	135 (19.6)	105 (15.2)	221 (32.1)	149 (21.6)	0.84	
	5	-23 (-3.3)	14 (2.0)	37 (5.3)	208 (30.1)	185 (26.8)	221 (32.1)	221 (32.1)		

**TABLE 9a. CIRCUMFERENTIAL RIM STRESSES, RESIDUAL STRESSES FROM THERMAL LOAD COMBINED WITH STRESSES FROM MECHANICAL LOAD (Vertical tape line load, inwardly directed lateral load and 30 kW (40 bhp) thermal load)**

Type of Wheel	Position	Stress Range for 142 kN (32 kip) Radial Wheel Load Applied at Center of Tread and 44 kN (10 kip) Lateral Load Directed Toward Flange		Circumferential Stress		Stress Range		Residual Stress From 30 kW (40 bhp) Thermal Load		Mechanical Stresses Combined with 30 kW (40 bhp) Residual Thermal Stresses		Stress Ratio
		Minimum MPa (ksi)	Maximum MPa (ksi)	Minimum MPa (ksi)	Maximum MPa (ksi)	Minimum MPa (ksi)	Maximum MPa (ksi)	Minimum MPa (ksi)	Maximum MPa (ksi)	Minimum MPa (ksi)	Maximum MPa (ksi)	
Two Wear Straight Plate	1	-4.8 (-0.7)	9.7 (1.4)	14 (2.1)	-2.1 (-0.3)	-6.9 (-1.0)	7.6 (1.1)	-0.91				
	2	-12 (-1.7)	9.0 (1.3)	21 (3.0)	3.4 (0.5)	-8.6 (-1.2)	12 (1.8)	-0.67				
	3	-14 (-2.1)	1.4 (0.2)	16 (2.3)	32 (4.7)	18 (2.6)	33 (4.9)	0.53				
	4	-5.5 (-0.8)	2.8 (0.4)	8.3 (1.2)	42 (6.1)	36 (5.3)	45 (6.5)	0.82				
	5	-6.9 (-1.0)	10 (1.5)	17 (2.5)	49 (7.1)	42 (6.1)	59 (8.6)	0.71				
One Wear Straight Plate	1	-18 (-2.6)	2.8 (0.4)	21 (3.0)	-2.8 (-0.4)	-21 (-3.0)	0 (0)					
	2	-27 (-3.9)	1.4 (0.2)	28 (4.1)	1.4 (0.2)	-26 (-3.7)	2.8 (0.4)	-9.25				
	3	-19 (-2.8)	2.8 (0.4)	22 (3.2)	40 (5.8)	21 (3.0)	43 (6.2)	0.48				
	4	-6.9 (-1.0)	8.3 (1.2)	15 (2.2)	56 (8.1)	49 (7.1)	64 (9.3)	0.76				
One Wear Curved Plate	1	-5.5 (-0.8)	6.9 (1.0)	12 (1.8)	-19 (-2.7)	-25 (-3.5)	-12 (-1.7)					
	2	-12 (-1.8)	4.8 (0.7)	17 (2.5)	-17 (-2.5)	-29 (-4.3)	-20 (-2.8)					
	3	-11 (-1.6)	2.8 (0.4)	14 (2.0)	17 (2.4)	6 (-0.8)	20 (2.8)	0.29				
	4	-3.4 (-0.5)	2.1 (0.3)	5.5 (0.8)	23 (3.4)	20 (2.9)	25 (3.7)	0.78				
	5	-2.1 (-0.3)	9.0 (1.3)	11 (1.6)	77 (11.2)	75 (10.9)	86 (12.5)	0.87				

TABLE 9b. CIRCUMFERENTIAL RIM STRESSES, RESIDUAL STRESSES FROM THERMAL LOAD COMBINED WITH STRESSES FROM MECHANICAL LOAD (Vertical tape line load, inwardly directed lateral load and 37 kW (50 bhp) thermal load)

Type of Wheel	Position	Circumferential Stress		Stress Range MPa (ksi)	Residual Stress From 37 kW (50 bhp) Thermal Load		Circumferential Stresses Minimum MPa (ksi)		Combined Circumferential Stresses Maximum MPa (ksi)		Stress Ratio	
		Minimum MPa (ksi)	Maximum MPa (ksi)		Minimum MPa (ksi)	Maximum MPa (ksi)	Minimum MPa (ksi)	Maximum MPa (ksi)				
Stress Range for 142 kN (32 kip) Radial Wheel Load Applied at Center of Tread and 44 kN (10 kip) Lateral Load Directed Toward Flange												
Two Wear Straight Plate	1	-4.8 (-0.7)	9.7 (1.4)	14 (2.1)	-22 (-3.2)	14 (2.1)	-27 (-3.9)	-12 (-1.8)	-	-		
	2	-12 (-1.7)	9.0 (1.3)	21 (3.0)	-8.3 (-1.2)	21 (3.0)	-20 (-2.9)	0.7 (0.1)	-	-		
	3	-14 (-2.1)	1.4 (0.2)	16 (2.3)	57 (8.2)	16 (2.3)	43 (6.1)	58 (8.4)	0.73	0.73		
	4	-5.5 (-0.8)	2.8 (0.4)	8.3 (1.2)	78 (11.3)	8.3 (1.2)	72 (10.5)	81 (11.7)	0.90	0.90		
	5	-6.9 (-1.0)	10 (1.5)	17 (2.5)	94 (13.6)	17 (2.5)	87 (12.6)	104 (15.1)	0.83	0.83		
One Wear Straight Plate	1	-18 (-2.6)	2.8 (0.4)	21 (3.0)	-34 (-5.0)	21 (3.0)	-52 (-7.6)	-31 (-4.6)	-	-		
	2	-27 (-3.9)	1.4 (0.2)	28 (4.1)	-18 (-2.6)	28 (4.1)	-45 (-6.5)	-17 (-2.4)	-	-		
	3	-19 (-2.8)	2.8 (0.4)	22 (3.2)	57 (8.2)	22 (3.2)	38 (5.4)	60 (8.6)	0.63	0.63		
	4	-6.9 (-1.0)	8.3 (1.2)	15 (2.2)	123 (17.8)	15 (2.2)	116 (16.8)	131 (19.0)	0.88	0.88		
One Wear Curved Plate	1	-5.5 (-0.8)	6.9 (1.0)	12 (1.8)	-56 (-8.1)	12 (1.8)	-61 (-8.9)	-49 (-7.1)	-	-		
	2	-12 (-1.8)	4.8 (0.7)	17 (2.5)	-28 (-4.1)	17 (2.5)	-40 (-5.9)	-23 (-3.4)	-	-		
	3	-11 (-1.6)	2.8 (0.4)	14 (2.0)	26 (3.7)	14 (2.0)	15 (2.1)	29 (4.1)	0.51	0.51		
	4	-3.4 (-0.5)	2.1 (0.3)	5.5 (0.8)	135 (19.6)	5.5 (0.8)	132 (19.1)	137 (19.9)	0.96	0.96		
	5	-2.1 (-0.3)	9.0 (1.3)	11 (1.6)	208 (30.1)	11 (1.6)	206 (29.8)	217 (31.4)	0.95	0.95		

**TABLE 10a. CIRCUMFERENTIAL RIM STRESSES, RESIDUAL STRESSES FROM THERMAL LOAD COMBINED WITH STRESSES FROM MECHANICAL LOAD (Vertical edge load, outwardly directed lateral load and 30 kW (40 bhp) thermal load)**

		Stress Range for 142 kN (32 kip) Radial Wheel Load Applied at Edge of Tread and 44 kN (10 kip) Lateral Load Directed Away From Flange			Mechanical Stresses Combined with 30 kW (40 bhp) Residual Thermal Stresses			Combined Stresses			Stress Ratio
Type of Wheel	Position	Minimum MPa (ksi)	Maximum MPa (ksi)	Stress Range MPa (ksi)	Residual Stress From 30 kW Thermal Load	Minimum MPa (ksi)	Maximum MPa (ksi)	Minimum MPa (ksi)	Maximum MPa (ksi)		
Two Wear Straight Plate	1	-28	45 (6.5)	72 (10.5)	-2.1 (-0.3)	-29	43 (6.2)	-29	43 (6.2)	-0.69	
	2	-21	7.6 (1.1)	28 (4.1)	3.4 (0.5)	-17	11 (1.6)	-17	11 (1.6)	-1.56	
	3	-7.6	8.3 (1.2)	9.0 (1.3)	32 (4.7)	25	41 (5.9)	25	41 (5.9)	0.61	
	4	-17	14 (2.1)	18 (2.6)	42 (6.1)	25	57 (8.2)	25	57 (8.2)	0.44	
	5	-15	17 (2.4)	18 (2.6)	49 (7.1)	34	66 (9.5)	34	66 (9.5)	0.52	
One Wear Straight Plate	1	-28	76 (11.0)	104 (15.1)	-2.8 (-0.4)	31	73 (10.6)	31	73 (10.6)	-0.42	
	2	-23	9.7 (1.4)	33 (4.8)	1.4 (0.2)	-22	11 (1.6)	-22	11 (1.6)	-2.00	
	3	-8.3	7.6 (1.1)	16 (2.3)	40 (5.8)	32	48 (6.9)	32	48 (6.9)	0.67	
	4	-28	19 (2.7)	47 (6.8)	56 (8.1)	28	74 (10.8)	28	74 (10.8)	0.37	
One Wear Curved Plate	1	-30	57 (8.3)	88 (12.7)	-19 (-2.7)	-49	39 (5.6)	-49	39 (5.6)	-1.27	
	2	-26	12 (1.7)	37 (5.4)	-17 (-2.5)	-43	-5.5 (-0.8)	-43	-5.5 (-0.8)	-	
	3	-18	11 (1.6)	29 (4.2)	17 (2.4)	-1.4 (-0.2)	28 (4.0)	-1.4 (-0.2)	28 (4.0)	-0.05	
	4	-29	17 (2.5)	46 (6.7)	23 (3.4)	-5.5 (-0.8)	41 (5.9)	-5.5 (-0.8)	41 (5.9)	-0.14	
	5	-26	18 (2.6)	43 (6.3)	77 (11.2)	52 (7.5)	95 (13.8)	52 (7.5)	95 (13.8)	0.54	

TABLE 10b. CIRCUMFERENTIAL RIM STRESSES, RESIDUAL STRESSES FROM THERMAL LOAD COMBINED WITH STRESSES FROM MECHANICAL LOAD (Vertical edge load, outwardly directed lateral load and 37 kW (50 bhp) thermal load)

Type of Wheel	Position	Circumferential Stress		Stress Range MPa (ksi)	Residual Stress From 37 kW (50 bhp) Thermal Load		Mechanical Stresses Combined with 37 kW (50 bhp) Residual Thermal Stresses		Stress Ratio					
		Minimum MPa (ksi)	Maximum MPa (ksi)		Minimum MPa (ksi)	Maximum MPa (ksi)	Minimum MPa (ksi)	Maximum MPa (ksi)						
Stress Range for 142 kN (32 kip) Radial Wheel Load Applied at Edge of Tread and 44 kN (10 kip) Lateral Load Directed Away From Flange														
Two Wear Straight Plate	1	-28	(-4.0)	45	(6.5)	72	(10.5)	-22	(-3.2)	-50	(-7.2)	23	(3.3)	-2.18
	2	-21	(-3.0)	7.6	(1.1)	28	(4.1)	-8.3	(-1.2)	-29	(-4.2)	-0.7	(-0.1)	-
	3	-7.6	(-1.1)	8.3	(1.2)	9.0	(1.3)	57	(8.2)	49	(7.1)	65	(9.4)	0.75
	4	-17	(-2.5)	14	(2.1)	18	(2.6)	78	(11.3)	61	(8.8)	92	(13.4)	0.66
	5	-15	(-2.2)	17	(2.4)	18	(2.6)	94	(13.6)	79	(11.4)	110	(16.0)	0.71
One Wear Straight Flare	1	-28	(-4.1)	76	(11.0)	104	(15.1)	-34	(-5.0)	-63	(-9.1)	41	(6.0)	-1.54
	2	-23	(-3.4)	9.7	(1.4)	33	(4.8)	-18	(-2.6)	-41	(-6.0)	-8.3	(-1.2)	-
	3	-8.3	(-1.2)	7.6	(1.1)	16	(2.3)	57	(8.2)	48	(7.0)	64	(9.3)	0.75
	4	-28	(-4.1)	19	(2.7)	47	(6.8)	123	(17.8)	94	(13.7)	104	(15.1)	0.90
One Wear Curved Plate	1	-30	(-4.4)	57	(8.3)	88	(12.7)	-56	(-8.1)	-86	(-12.5)	1	(0.2)	-
	2	-26	(-3.7)	12	(1.7)	37	(5.4)	-28	(-4.1)	-54	(-7.8)	-17	(-2.4)	-
	3	-18	(-2.6)	11	(1.6)	29	(4.2)	26	(3.7)	7.6	(1.1)	37	(5.3)	0.21
	4	-29	(-4.2)	17	(2.5)	46	(6.7)	135	(19.6)	106	(15.4)	152	(22.1)	0.70
	5	-26	(-3.7)	18	(2.6)	43	(6.3)	208	(30.1)	182	(26.4)	225	(32.7)	0.81

TABLE 11a. CIRCUMFERENTIAL RIM STRESSES, RESIDUAL STRESSES FROM THERMAL LOAD COMBINED WITH STRESSES FROM MECHANICAL LOAD (Vertical edge load, inwardly directed lateral load and 30 kW (40 bhp) thermal load)

Type of Wheel	Position	Circumferential Stress		Stress Range MPa (ksi)	Residual Stress From 30 kW (40 bhp) Thermal Load		Circumferential Stresses Combined with 30 kW (40 bhp) Residual Thermal Stresses		Stress Ratio
		Minimum MPa (ksi)	Maximum MPa (ksi)		Minimum MPa (ksi)	Maximum MPa (ksi)	Minimum MPa (ksi)	Maximum MPa (ksi)	
Two Wear Straight Plate	1	-12 (-1.8)	23 (3.3)	35 (5.1)	-2.1 (-0.3)	-14 (-2.1)	21 (3.0)	-0.67	
	2	-23 (-3.4)	2.8 (0.4)	26 (3.8)	3.4 (0.5)	-20 (-2.9)	6.2 (0.9)	-3.23	
	3	-4.8 (-0.7)	3.4 (0.5)	8.3 (1.2)	32 (4.7)	28 (4.0)	36 (5.2)	0.78	
	4	-1.4 (-0.2)	3.4 (0.5)	4.8 (0.7)	42 (6.1)	41 (5.9)	46 (6.6)	0.89	
	5	-2.1 (-0.3)	7.6 (1.1)	9.7 (1.4)	49 (7.1)	47 (6.8)	57 (8.2)	0.82	
One Wear Straight Plate	1	-34 (-5.0)	24 (3.5)	59 (8.5)	-2.8 (-0.4)	-37 (-5.4)	21 (3.1)	-1.76	
	2	-43 (-6.3)	-1.4 (-0.2)	45 (6.5)	1.4 (0.2)	-42 (-6.1)	0.0 (0.0)	-	
	3	-4.8 (-0.7)	3.4 (0.5)	8.3 (1.2)	40 (5.8)	35 (5.1)	43 (6.3)	0.81	
	4	1.4 (0.2)	9.7 (1.4)	11 (1.6)	56 (8.1)	57 (8.3)	66 (9.5)	0.86	
One Wear Curved Plate	1	-18 (-2.6)	26 (3.7)	43 (6.3)	-19 (-2.7)	-37 (-5.3)	6.9 (1.0)	-5.36	
	2	-21 (-3.0)	1.4 (0.2)	22 (3.2)	-17 (-2.5)	-38 (-5.5)	-16 (-2.3)	-	
	3	-4.8 (-0.7)	4.1 (0.6)	9.0 (1.3)	17 (2.4)	12 (1.7)	21 (3.0)	0.57	
	4	-6.9 (-1.0)	5.5 (0.8)	12 (1.8)	23 (3.4)	17 (2.4)	29 (4.2)	0.59	
	5	-1.7 (-0.1)	5.5 (0.8)	6.2 (0.9)	77 (11.2)	77 (11.1)	83 (12.0)	0.93	

TABLE 11b. CIRCUMFERENTIAL RIM STRESSES, RESIDUAL STRESSES FROM THERMAL LOAD COMBINED WITH STRESSES FROM MECHANICAL LOAD (Vertical edge load, inwardly directed lateral load and 37 kW (50 bhp) thermal load)

Type of Wheel	Position	Circumferential Stress		Stress Range MPa (ksi)	Residual Stress From 37 kW (50 bhp) Thermal Load		Circumferential Stresses Combined with 37 kW (50 bhp) Residual Thermal Stresses		Stress Ratio	
		Minimum MPa (ksi)	Maximum MPa (ksi)		Minimum MPa (ksi)	Maximum MPa (ksi)				
Stress Range for 142 kN (32 kip) Radial Wheel Load Applied at Edge of Tread and 44 kN (10 kip) Lateral Load Directed Toward Flange										
Two Wear Straight Plate	1	-12 (-1.8)	23 (3.3)	35 (5.1)	-22 (-3.2)	-34 (-5.0)	0.7 (0.1)	-		
	2	-23 (-3.4)	2.8 (0.4)	26 (3.8)	-8.3 (-1.2)	-32 (-4.6)	-5.5 (-0.8)	-		
	3	-4.8 (-0.7)	3.4 (0.5)	8.3 (1.2)	57 (8.2)	52 (7.5)	60 (8.7)	0.86		
	4	-1.4 (-0.2)	3.4 (0.5)	4.8 (0.7)	78 (11.3)	77 (11.1)	81 (11.8)	0.95		
	5	-2.1 (-0.3)	7.6 (1.1)	9.7 (1.4)	94 (13.6)	92 (13.3)	101 (14.7)	0.91		
One Wear Straight Plate	1	-34 (-5.0)	24 (3.5)	59 (8.5)	-34 (-5.0)	-69 (-10.0)	-10 (-1.5)	-		
	2	-43 (-6.3)	-1.4 (-0.2)	45 (6.5)	-18 (-2.6)	-61 (-8.9)	-19 (-2.8)	-		
	3	-4.8 (0.7)	3.4 (0.5)	8.3 (1.2)	57 (8.2)	52 (7.5)	60 (8.7)	0.86		
	4	1.4 (0.2)	9.7 (1.4)	11 (1.6)	123 (17.8)	124 (18.0)	132 (19.2)	0.94		
One Wear Curved Plate	1	-18 (-2.6)	26 (3.7)	43 (6.3)	-56 (-8.1)	-74 (-10.7)	-30 (-4.4)	-		
	2	-21 (-3.0)	1.4 (0.2)	22 (3.2)	-28 (-4.1)	-49 (-7.1)	-27 (-3.9)	-		
	3	-4.8 (-0.7)	4.1 (0.6)	9.0 (1.3)	26 (3.7)	21 (3.0)	30 (4.3)	0.70		
	4	-6.9 (-1.0)	5.5 (0.8)	12 (1.8)	135 (19.6)	128 (18.6)	141 (20.4)	0.91		
	5	-1.7 (-0.1)	5.5 (0.8)	6.2 (0.9)	208 (30.1)	207 (30.0)	213 (30.9)	0.97		



## 6. DEVELOPMENT AND PROPAGATION OF THERMAL CRACKS

The analytical techniques of fracture mechanics may be used to predict the likelihood of crack initiation and propagation under various operating conditions. The procedures and limitations of such investigations were discussed in papers presented at the 6th International Wheelset Congress (Ref 15 and 16). In this section the application of the thermal and mechanical stress data to crack growth predictions is discussed. The data are used to investigate the conditions under which thermal cracks can be developed and propagated. Several types of stress cycles need to be considered. First, there is the large number of stress cycles associated with the rotation of the wheel (e.g., a 914 mm (36 inch) wheel rotates 348 revolutions/km (560 rev/mile); 10 million cycles are developed in less than 29,000 km (18,000 miles). Second, there is a stress cycle every time a brake application is made. Third, there are the large stress cycles which occur when a wheel is severely heated due to a prolonged heavy drag brake application.

The procedures are limited to the consideration of thermal cracks which are initiated in the rim of the wheel and lie in a radial plane containing the axis of the wheel. Mode I crack growth is assumed so that the significant fluctuating stresses are the circumferential stresses in the rim of the wheel.

### 6.1 Fracture Mechanics Data

Fracture mechanics principles are used for the examination of crack growth effects. The method is based on the interpretation of a plot of crack extension, per cycle,  $da/dN$ , versus the change in stress intensity ( $\Delta K$ ). A typical curve of this type is shown in Figure 26. Three mechanisms of crack growth are represented by the curve. The left hand side of the curve is affected primarily by the microstructure and the surrounding environment. It includes the initiation of the crack. The middle region of the curve shows the period of crack growth where the growth rate can be represented by  $(\Delta K)^n$ . The right hand side of the curve shows the deviation from the exponential function as the critical stress intensity is approached.

Most crack growth data have been developed for the case where the ratio of minimum to maximum stresses ( $R$ ) is zero. In most real cases materials are not subjected to fluctuating stresses with a zero minimum stress. Stress ranges may cover a wide range of values. This is the case for railroad wheels where the presence of residual stresses may result in relatively high values for the ratio of minimum to maximum stress.

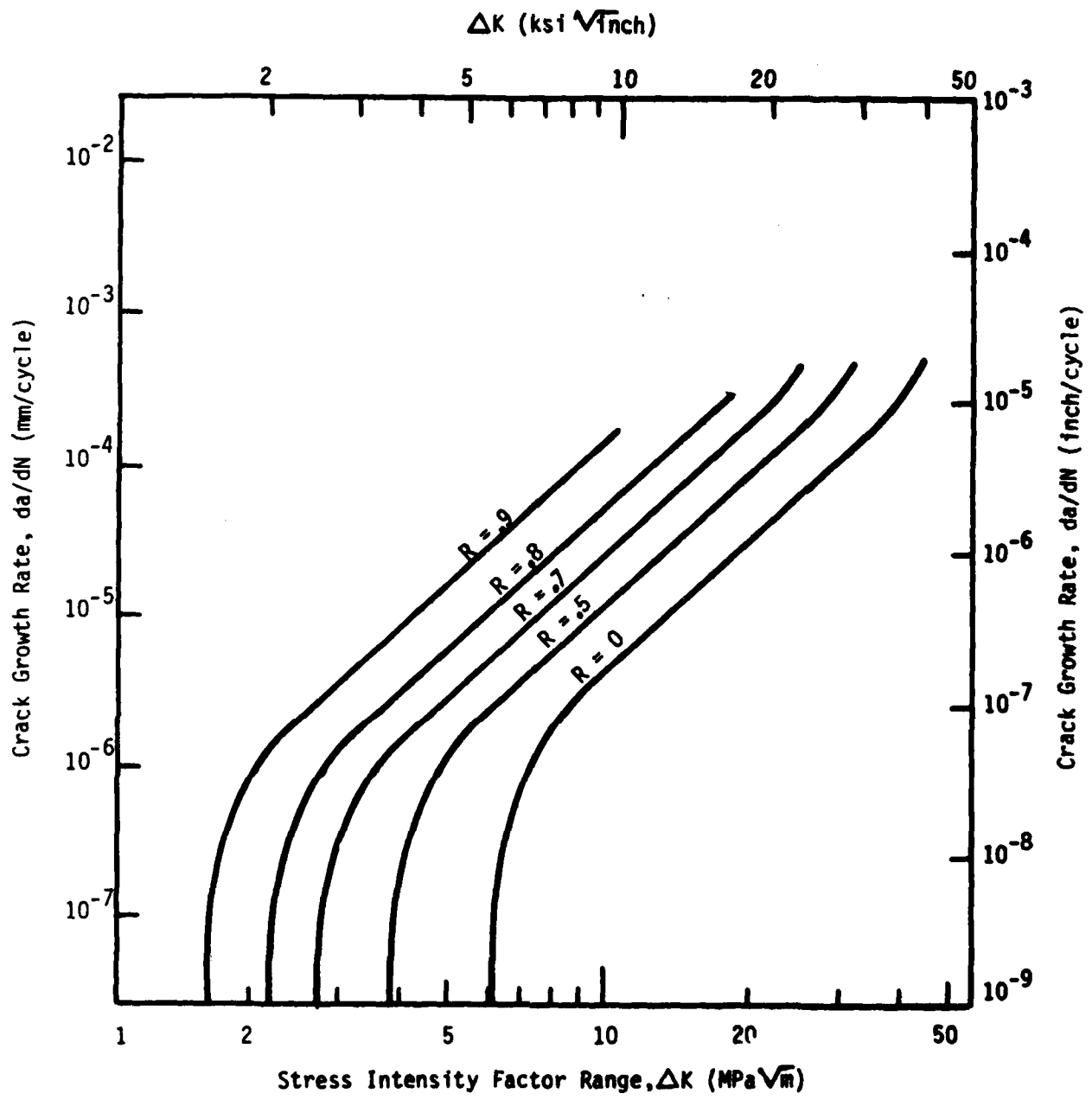


Figure 26 Estimated Crack Growth Curves for Class BR Wheel Steel

Most studies show that the effect of the stress ratio is minimal in the central portion of the crack growth curve. The most significant effect of a high stress ratio is to lower the threshold  $\Delta K$  which will allow the extension of a crack.

Figure 26 has been developed as an estimate of the  $da/dN$  curve for a typical wheel steel (class BR). The basic curve is developed for the  $R=0$  case. The central portion of the curve is based on the data of Opinsky (Ref 18). His work showed the following relationship for crack growth as a function of the stress intensity factor:

$$\frac{da}{dN} = \frac{3.74}{10^9} (\Delta K)^{3.02} \quad (6.1)$$

where  $a$  is the characteristic crack dimension (mm)  
 $N$  is the number of cycles  
 $\Delta K$  is the change in stress intensity as the result of fluctuating stresses ( $\text{MPa}\sqrt{\text{m}}$ )

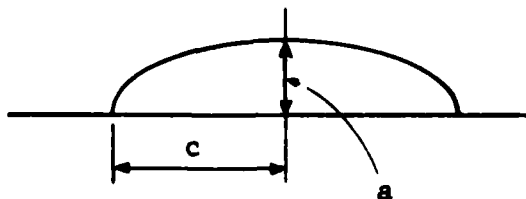
The right hand side of the curve approaches asymptotically the fracture toughness for the steel, which is estimated at  $55 \text{ MPa}\sqrt{\text{m}}$  ( $50 \text{ ksi}\sqrt{\text{inch}}$ ). The left hand side of the curve approaches the threshold value for crack propagation. This is assumed to be  $6.0 \text{ MPa}\sqrt{\text{m}}$  ( $5.5 \text{ ksi}\sqrt{\text{inch}}$ ).

Figure 26 also shows estimates of the crack growth relationship for several values of  $R$ . The development of these curves makes use of the Walker relationship (Ref 19) for modifying Equation (6.1). The effective stress intensity,  $K_{\text{eff}}$ , is calculated as

$$\Delta K_{\text{eff}} = \frac{\Delta K}{\sqrt{1-R}} \quad (6.2)$$

The development of these curves also assumes a decrease in threshold stress intensity,  $\Delta K_{\text{th}}$ , with increasing  $R$  as illustrated in Figure 27.

Knowing  $\Delta K$  and the stress variations one can calculate the minimum size of a crack for crack propagation. For this calculation it is assumed that the crack is elliptical in shape with the major axis,  $2c$ , twice the minor axis,  $2a$ , as illustrated.



For this condition the factor relating stress intensity to nominal stress variations is given as

$$\Delta K = \frac{\Delta \sigma \sqrt{\pi a}}{1.14} \quad (6.3)$$

## 6.2 Crack Threshold Size Analysis

The stress range data for mechanical load stresses combined with thermally induced residual stresses, which were presented in Tables 6 through 11, can now be reviewed to estimate the conditions under which crack propagation can be expected. This is done to assess the susceptibility of wheels to thermal crack initiation. A preliminary evaluation of the data indicates that the most severe conditions occur on one wear wheels at the inside rim position (Position 4 on the straight plate wheel and Position 5 on the curved plate wheel). These results also show the most severe stress condition is associated with the 37 kW (50 bhp) thermal load residual stress.

Table 12 summarizes the stress range data and the threshold crack size calculations for the inside rim position of one wear wheels. The third and fourth columns in this table show the stress range and the stress ratio for the different cases. The threshold  $\Delta K$  for crack propagation is included in the fifth column and is based on Figure 27. Equation (6.3) is then used to calculate the minimum crack depth which is required for crack extension. These data are presented in the right hand column of Table 12. A small crack dimension is indicative of a greater susceptibility to crack initiation.

The minimum crack depth dimensions in Table 12 are shown for the cases of Tables 8b and 10b. These are the cases where lateral load acts in conjunction with the vertical load, but is directed away from the flange. These are loading conditions which are rather unlikely to occur in service for significant periods of time and therefore are not representative of conditions where a large number of stress cycles can be anticipated. Excluding the cases of lateral load directed away from the flange the next smallest critical crack side is associated with Table 7b for the curved plate wheel. A 2.5 mm (0.098 inch) crack dimension is indicated. The loading condition is a vertical edge load with no lateral load. The rest of the results in the table indicate somewhat larger crack dimensions, which suggests that under the assumed conditions there is not a very high probability of crack initiation and growth.

TABLE 12. CONDITIONS FOR CRACK EXTENSION ASSOCIATED WITH STRESS VARIATIONS FROM COMBINED LOADS

Stress Data Table	Wheel Type (CP: Curved Plate, SP: Straight Plate)	Stress Range MPa (ksi)	Stress Ratio R	Threshold $\Delta K$ MPa $\sqrt{m}$ (ksi $\sqrt{in.}$ )	Minimum Crack Depth for Extension mm (in.)
6b	SP	10 (1.4)	0.92	1.4 (1.3)	9.1 (0.36)
	CP	12 (1.8)	0.94	1.3 (1.2)	4.8 (0.19)
7b	SP	19 (2.7)	0.86	1.9 (1.7)	4.3 (0.17)
	CP	20 (2.9)	0.91	1.5 (1.4)	2.5 (0.098)
8b	SP	34 (4.9)	0.75	2.3 (2.1)	2.0 (0.077)
	CP	37 (5.3)	0.84	1.8 (1.6)	1.0 (0.038)
9b	SP	15 (2.2)	0.96	1.8 (1.6)	5.6 (0.22)
	CP	11 (1.6)	0.95	1.3 (1.2)	6.1 (0.24)
10b	SP	47 (6.8)	0.90	1.5 (1.4)	0.5 (0.018)
	CP	43 (6.3)	0.81	2.1 (1.9)	1.0 (0.038)
11b	SP	11 (1.6)	0.94	1.3 (1.2)	6.1 (0.24)
	CP	6 (0.9)	0.97	1.2 (1.1)	16.0 (0.63)

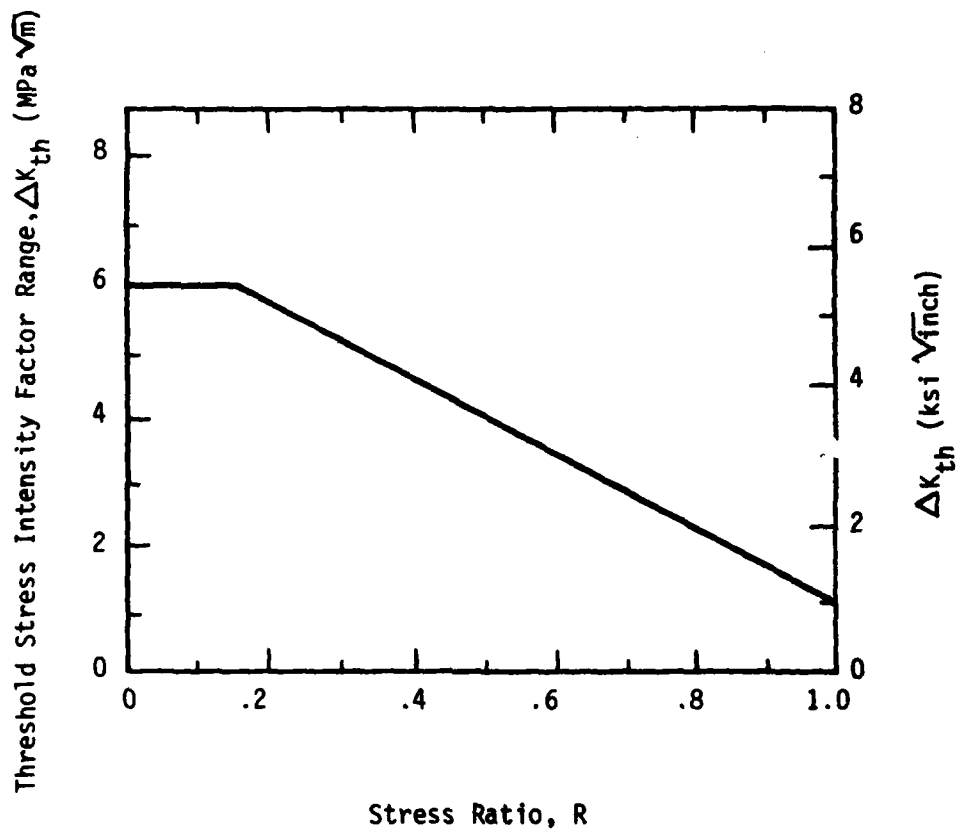


Figure 27 Threshold Stress Intensity Factor Range as a Function of Stress Ratio, R

### 6.3 Consideration of Service Braking Stresses

The relatively large crack sizes which are calculated for the threshold of crack propagation as a result of mechanical, once per revolution, cyclic stresses, leads one to consider other mechanisms for the initiation of the crack. One possibility would be a mechanism dominated by low-cycle fatigue effects, which considers the stress cycle each time the brake is applied. Consider, for example, a wheel which has been overheated so that a tensile residual circumferential stress has been induced in the rim. Each time the tread brake is applied, the rim stresses will be greatly diminished, or even driven into compression so that there would be a large change in stress intensity with each braking cycle. The nature of the stress fluctuation would depend on the position within the rim.

This problem has been examined by looking at combinations of service braking stress data (from Figures 17 and 18) mechanical load stress range data (from Table 4) and the residual stresses associated with severe thermal loads (from Table 2). This set of analyses is limited to the one wear, straight plate wheel because the service braking calculations were performed only on this wheel configuration.

The results are presented in Table 13. The first case considers conditions in the rim at the corner between the outside face and inside surface as the result of combined vertical edge load and service braking stress effects. The tensile portion of the maximum stress range is evaluated. Utilizing the threshold  $\Delta K$  for the given stress conditions a minimum crack depth for extension of 2.2 mm (0.085 inch) is determined.

The second case considers conditions at the tip of the flange as a result of combined vertical center load, service braking and residual thermal stress effects. The relatively high tensile residual stress puts the entire stress fluctuation into the tensile range. Using the threshold  $\Delta K$  for the stress conditions indicated, a minimum crack depth for extension of 4.8 mm (0.189 inch) is determined.

The third case considers conditions on the inside face of the rim, again as the result of combined vertical edge load, service braking, and residual thermal stress effects. The high thermal residual tensile stress puts the entire stress fluctuation into the tensile range. Using the threshold  $\Delta K$  associated with the stress conditions a minimum crack depth for extension of 1.5 mm (0.059 inch) is calculated.

TABLE 13. CONDITIONS FOR CRACK EXTENSION WITH INCLUSION OF SERVICE BRAKING STRESSES

Core	Wheel Position (see Figure 1)	Loads and Stress Ranges, MPa (ksi), Considered	Total Stress Range, MPa (ksi)	Stress Ratio	Threshold $\Delta K$ MPa $\sqrt{m}$ (ksi $\sqrt{in.}$ )	Minimum Crack Depth for Extension mm (in.)
1	1	Vertical Edge Load (Table 4) -24/50 (-3.5/7.2) Service Braking (Figure 17) -10/34 (-1.5/5.0)	0/84 (0/12.2)	0	6.0 (5.5)	2.2 (0.085)
2	3	Vertical Center Load (Table 4) -21/1 (-3.0/0.2) Service Braking (Figure 17) -34/0 (-5.0/0) Thermal Residual (Table 2) 56 (8.2)	1/58 (0.2/8.4)	0.02	6.0 (5.5)	4.8 (0.189)
3	4	Vertical Edge Load (Table 4) -9/10 (-1.3/1.4) Service Braking (Figure 17) -55/0 (-8/0) Thermal Residual (Table 2) 119 (17.3)	55/129 (8.0/18.7)	0.43	4.4 (4.0)	1.5 (0.059)



These results show the importance of considering various load combinations when looking for critical crack growth conditions. The threshold crack sizes indicated by these calculations are slightly smaller than those calculated without the inclusion of the service braking stresses (Table 12). However, when interpreting the results, the fact that there would be fewer stress cycles of this range must be recognized.

#### 6.4 Application to Plate Crack Growth Considerations

Consideration of the cyclic service braking stresses acting alone leads to the calculation of a fairly small threshold crack size for the propagation of circumferential plate cracks in the hub and rim fillets of the wheel. For this condition one is concerned with the radial component of stress, which would be perpendicular to a circumferential crack direction. Figure 18 shows that the service braking results in a tensile stress of 140 MPa (20 ksi) in the outside hub fillet and a tensile stress of 100 MPa (15 ksi) in the inside rim fillet. Using the same procedures followed in the thermal crack calculations for the rim (Table 13) a threshold crack size for propagation of 0.81 mm (0.032 inch) is determined for the hub fillet region and a threshold crack size of 1.4 mm (0.056 inch) is obtained for the rim fillet region. The fluctuating stresses due to vertical and lateral loads in these regions are relatively small and would have a negligible effect on crack propagation by themselves. The complicating factor in the application of this result is the apparent complex state of residual stresses which normally exist in the plate and hub fillet areas. If a wheel has been subjected to a thermal loading which is sufficient to cause a shift in the residual stress field, compressive stresses will be introduced in the hub and plate fillet regions. The residual compressive stresses would inhibit the initiation and growth of circumferential cracks in these regions. Other work (Ref 20) has indicated that the residual stress gradient across the plate of a wheel may be quite complex with large stress gradients or one moves inside the surface. This has been noted in both newly manufactured wheels and wheels that have been subjected to moderate drag braking loads which are sufficient to cause slight shifts of the residual stress field. This situation greatly complicates attempts to make predictions of plate crack growth.

#### 6.5 Crack Growth Calculations

The fracture mechanics and stress range data can be utilized to make crack growth predictions. Two examples are selected from the data in Table 12, namely, the conditions defined for the straight plate and curved plate wheels under stress data Table 7b. Calculations were made utilizing the

crack growth rate data defined in Figure 26. The objective of these calculations was to determine the number of stress cycles (wheel revolutions) required to extend the crack depth by 10 mm (0.4 inch). The effect of the extension of the crack on the stress field was not included in these calculations.

The results are shown in Table 14. Approximately 10 million cycles are indicated for enlarging the depth of the crack by 10 mm (0.4 inch). This normally would represent only a small portion of the life of the wheel. The calculations show that the cyclic fluctuating load stresses, though relatively small in magnitude, can lead to a significant crack growth rate under the right conditions. Note that rate of crack growth becomes larger as the size of the crack increases.

TABLE 14. CRACK GROWTH ANALYSIS

Core (see Table 12)	Number of Cycles (10 <sup>6</sup> )	Crack Depth mm (in.)
Stress Data Core Table 7b	---	2.5 (0.10)
Curved Plate Wheel	2.0	3.0 (0.12)
Inside Rim Position	3.3	3.7 (0.14)
	4.4	4.4 (0.17)
	5.3	5.3 (0.21)
	6.1	6.3 (0.25)
	6.8	7.6 (0.30)
	7.4	9.1 (0.36)
	8.0	10.9 (0.43)
	8.4	12.7 (0.50)
Stress Data Core Table 7b	---	5.1 (0.20)
Straight Plate Wheel	2.3	6.1 (0.24)
Inside Rim Position	4.2	7.3 (0.29)
	5.9	8.8 (0.35)
	7.4	10.5 (0.42)
	8.6	12.6 (0.50)
	9.8	15.2 (0.60)

## 6.6 Limitations of Analyses

The interpretation of results presented in the preceding sections must recognize certain limitations of the analyses. First, much of the required crack growth data are associated with high stress ratios and low changes in stress intensity. This is a condition where limited material property test data are available. The assumed characteristics of the material in this region were extrapolated from test data obtained at larger stress intensity ranges and at  $R=0$ . The extrapolation of the data reduces the confidence in its accuracy. Therefore, the results should be used primarily as an indication of the trends that can be expected. It is obvious that if more accurate predictions are to be made better material data must be obtained.

A reduction in the calculated threshold size of cracks for their propagation would probably result from initial higher residual tensile stresses. However, this puts one further away from conditions where material property data are available.

## 7. VALIDATION ANALYSES

A number of results are available which allow experimental stress values to be compared with elastic analyses. These results include both the effects of mechanical load and low or moderate thermal loads where the yield point of the wheel is not exceeded. (See for example Ref 21 and 22.) These results generally show close correspondence between theoretical and experimental values, which demonstrates the accuracy of these analytic procedures.

### 7.1 Comparison of Predicted and Measured Strains for a Wheel with an Induced Heat Load

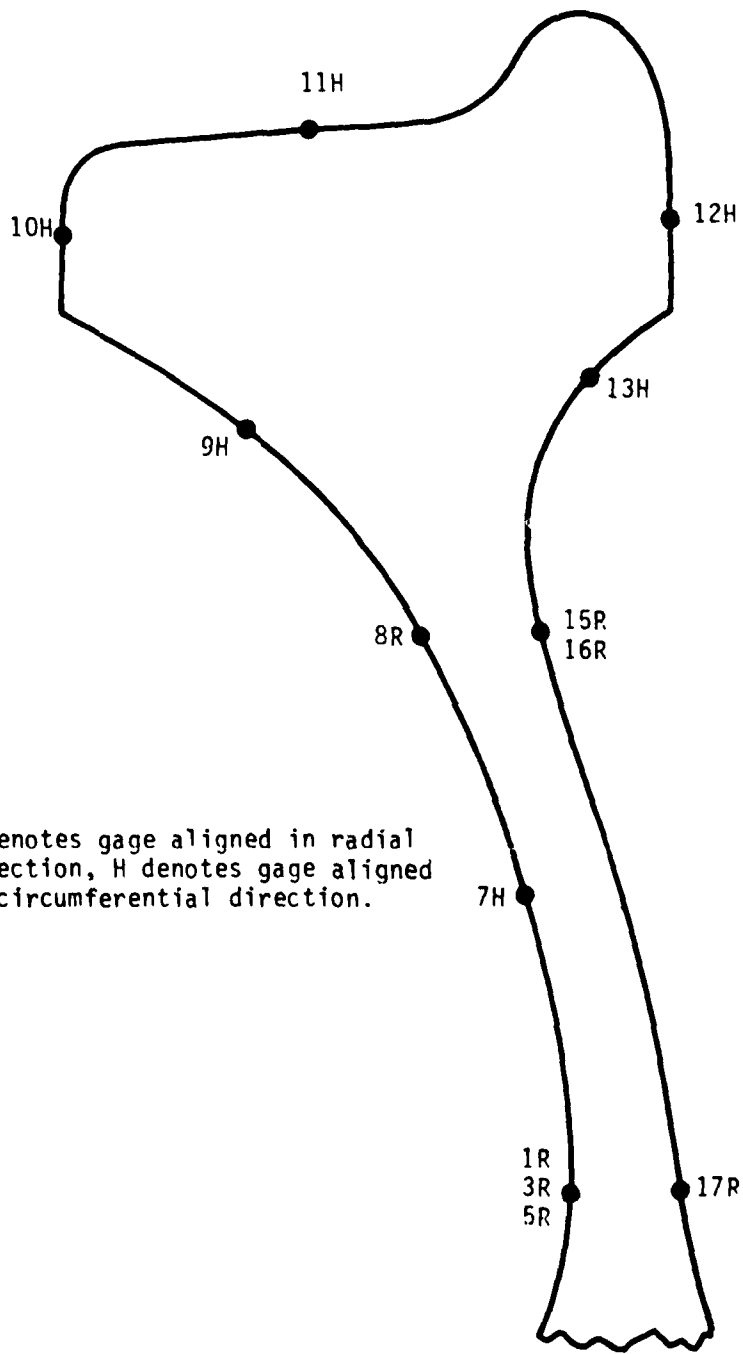
7.1.1 Test Conditions-There have been relatively few opportunities to compare theoretical and experimental results of wheels subjected to severe thermal loads where the yield point of the wheel is exceeded. One opportunity for such a comparison was the AAR Track Train Dynamics sponsored test series with a CH36, one wear, curved plate wheel. The wheel was subjected to several heating loads at the rim by using an induction heater. The most severe thermal load was 37 kW (50 bhp). The results of this test were selected for comparison with analyses\*.

Strain gages were placed on the wheel to measure the response of the wheel to the thermal load. The positions of the strain gages where comparisons can be made with analytic solutions are shown in Figure 28.

7.1.2 Analytic Representation-The elastic-plastic two-dimensional code was used to predict the behavior of the wheel. It was assumed that a 37 kW (50 bhp) thermal loading applied over a 75 mm (3 inch) width of the wheel rim centered on the tape line would simulate the 37 kW induction heating coil load. The duration of the heat load was assumed to be 37 minutes, 41 seconds, the duration of the experimental heat load. Strains were calculated several times during the application of the heat load, at the end of the application of the heat load, and following subsequent cooling of the wheel to ambient conditions. The latter condition gave predictions of the residual stress field remaining in the wheel. The calculation assumed that there was no initial residual strain in the wheel.

---

\*Note: These comparative analyses were conducted under the sponsorship of the AAR Track Train Dynamics Program.



Note: R denotes gage aligned in radial direction, H denotes gage aligned in circumferential direction.

Figure 28 Strain Gage Positions for Induction Heating Test

7.1.3 Material Property Data-Three sets of calculations were made utilizing different material property data. This was done in an attempt to bracket uncertainties in the data, particularly with regard to high temperature properties, and also to determine the sensitivity of the predictions to the values assumed for material properties.

The elastic-plastic program accommodates temperature dependent material properties. The first calculations were based on a standard set of temperature dependent material property data which were used in the other thermal analyses described in this report. The temperature dependent nature of these parameters are given in Table 15.

Some recent AAR test results (Ref 23) indicated that a lower plastic modulus should be considered. Therefore, a second set of calculations were performed using a lower value for the plastic modulus. The data in Ref 23 indicate that a modulus of  $21 \times 10^3$  MPa ( $3.1 \times 10^6$  psi) gives a fair approximation for the second part of a bilinear representation of the stress-strain curve. This is about one-half the comparable values given in Table 15. Consequently the "plastic" modulus values given in Table 15 were divided by two and used for the second set of calculations.

A third set of calculations was performed to determine if a reduction in the dependence of the elastic modulus with temperature would have a significant affect on the residual hoop strains in the rim of the wheel. These calculations utilized the material properties listed in Table 15 except that a constant modulus of  $200 \times 10^3$  MPa ( $29 \times 10^6$  psi) was employed.

TABLE 15. TEMPERATURE DEPENDENT MATERIAL PROPERTIES

Temperature °C (°F)	Elastic Modulus of Elasticity $10^3$ MPa ( $10^6$ psi)	Poissons Ratio	Yield Stress MPa (ksi)	Plastic Modulus $10^3$ MPa ( $10^6$ psi)
-18 (0)	200 (29.0)	0.29	400 (58.0)	43 (6.25)
93 (200)	198 (28.7)	0.29	395 (57.4)	42 (6.15)
204 (400)	190 (27.6)	0.29	383 (55.5)	41 (5.90)
316 (600)	178 (25.8)	0.29	336 (48.8)	39 (5.60)
427 (800)	159 (23.0)	0.29	265 (38.4)	35 (5.00)
538 (1000)	132 (19.1)	0.29	192 (27.9)	28 (4.10)

7.1.4 Results-The results of the analysis for the first two sets of calculations are given in Tables 16 and 17. The thermal strains in these tables have been computed based on an average coefficient of thermal expansion of  $13 \times 10^{-6}$  mm/mm°C ( $7 \times 10^{-6}$  inch/inch°F) and the computed temperature at the node point closest to the strain gage. Results are given at 33 minutes, 41 seconds which was the time when the power source was turned off and also at the end of the test when the wheel was cooled down to approximately 24°C (75°F). Note that the differences between the two sets of calculations are relatively small. This indicates that the values selected for the plastic modulus will not have a major influence on the computed stresses.

The comparison of the computed and test results is reasonably good at the 33 minutes, 41 seconds time considering the difference in the way the thermal loads were introduced. The residual strains also compare favorably except for two circumferential gages in the rim, 10H and 11H. The large residual test strain in gage 11H, 1105  $\mu$ mm/mm ( $\mu$ inch/inch), indicates a major discrepancy between the computed and test results since the computed value at this point was under 30  $\mu$ mm/mm ( $\mu$ inch/inch). The difference could be caused by the way the temperature dependent material properties are idealized in the computer code or from the material parameters that are used. It is more likely that the strain gage results are in error since the temperature at several gages was in excess of the recommended maximum temperature of 260°C (500°F) for these strain gages. For example, the maximum temperature near strain gage 11H was in excess of 427°C (800°F).

The third set of calculations, which were conducted to see if the reduction in the elastic modulus with temperature is a significant factor in affecting the residual hoop strains, showed relatively minor differences with the strains shown in Tables 16 and 17. Thus it can be concluded that the change in the elastic modulus with temperature has little effect on the predicted residual hoop strains.

TABLE 16. COMPARISON OF CALCULATED AND EXPERIMENTAL THERMAL STRAINS FOR 37 kW (50 bhp) INDUCTION COIL THERMAL LOAD TESTS USING IITRI MATERIAL PROPERTIES

Strain Gage	Calculated Temperature after 33 min 41 sec Thermal Load °C (°F)	Strain $\mu\text{m}/\text{mm}$ ( $\mu\text{in.}/\text{in.}$ )							
		Calculated Mechanical		Calculated Thermal	Total Calculated		Residual (cool wheel)		
		Calculated Mechanical	Calculated Thermal	Calculated Mechanical	Calculated Thermal	Calculated Mechanical	Calculated Thermal	Calculated Mechanical	Calculated Thermal
17R	85(185)	-1620	770	-850	-1853	39	179		
1R	87(188)	4465	791	5256	4736	656	364	386	
3R					4814		305		
5R					4940		490		
15R	266(510)	2281	3045	5326	5063	83	132	156	
16R					5015		179		
8R	284(544)	-1015	3283	2268	1283	-42	128		
7H	168(334)	923	1813	2736	2559	93	68		
9H	377(710)	661	4445	5106	3912	20	91		
10H	429(805)	698	5110	5808	5041	6	429		
11H	470(878)	-1540	5621	4081	5235	21	1105		
12H	355(671)	-1955	4172	2217	1835	38	81		
13H	352(665)	-1631	4130	2499	2213	38	77		



TABLE 17. COMPARISON OF CALCULATED AND EXPERIMENTAL THERMAL STRAINS FOR 37 kW (50 bhp) INDUCTION COIL THERMAL LOAD TESTS USING AAR MATERIAL PROPERTIES

Strain Gage	Calculated Temperature after 33 min 41 sec Thermal Load °C (°F)	Strain $\mu\text{mm/mm}$ ( $\mu\text{in./in.}$ )					
		Conditions After 33 min 41 sec Thermal Load			Residual (cool wheel)		
		Calculated Mechanical	Calculated Thermal	Total Calculated	Calculated Mechanical	Calculated Mechanical	Experimental
17R	85(185)	-1607	770	-837	-1853	52	179
1R	87(188)	4691	791	5482	4736	887	364
3R					4814		305
5R					4940		490
15R	266(510)	2303	3045	5348	5063	106	132
16R					5015		179
8R	284(544)	-1030	3283	2253	1283	-58	128
7H	168(334)	957	1813	2770	2559	128	68
9H	377(710)	665	4445	5110	3912	24	91
10H	429(805)	694	5110	5804	5041	2	429
11H	470(878)	-1534	5621	4087	5235	27	1105
12H	355(671)	-1937	4172	2235	1835	57	81
13H	352(665)	-1613	4130	2517	2213	58	77

## 8. CONCLUSIONS AND RECOMMENDATIONS

The objective of this program was to recommend ways of reducing the failure rate of railroad car wheels by considering design changes, the use of new materials, or the specification of operating limits. Fulfilling this objective was found to require a better understanding of the factors which lead to railroad wheel failure. The most serious failures are those from thermal or plate cracks which result in wheel fracture. The phenomena associated with thermal crack initiation and growth have been examined in detail through the use of analytic techniques for studying the stress phenomena in wheels under various types of loading.

The design changes which can be considered for railroad car wheels are limited if the wheels are to remain compatible with the specifications and standards used in present railroad freight car construction. The principal region where there is some freedom for design changes is in the shape of the plate of the wheel. The design of the plate influences the way the wheel responds to tread brake thermal loads. There are two plate design configurations which are used in wheels of U.S. manufacture; the straight plate wheel design, which is used by wrought steel wheel manufacturers, and the curved plate wheel design which is used by cast steel wheel manufacturers. Both types of wheels were thoroughly analyzed under this program. These analyses failed to reveal any significant advantages for one type over the other.

The data presented in Section 4 show that the stress distributions in curved plate and straight plate wheel designs can be substantially different when the wheels are subjected to the same thermal load. While the thermal stresses at the conclusion of the braking period are larger in the straight plate wheel design than in the curved plate design, the residual stresses following the subsequent cooling of the wheel are about the same magnitude in each type of wheel. From one standpoint the residual stress field in the curved plate design may be less satisfactory because of the high tensile stresses on the inside face of the rim, which is a common site for the initiation of thermal cracks.

Some investigators have concluded (e.g., Ref 1) that the curve plate design is to be preferred over the straight plate design because of the lower plate stresses associated with a thermal load, but the effect on residual stresses should also be considered. Reference 1 also states that the superiority of the curve plate design has been established by dynamometer tests. It describes the results of drag brake tests, where notches were cut into the treads of the wheels to promote the initiation of thermal cracks. The wheels were subjected

to severe thermal loads. It took a larger number of drag tests to initiate a failure crack in the curved plate wheel than in the straight plate wheel. The differences in these results may be due to the placement of the notches rather than to any inherent characteristics of the wheel design. For example, comparing the residual stress distribution patterns in Figures 8 and 9, it can be seen that the residual tensile stresses adjacent to the center of the tread are larger for the straight plate design than for the curve plate design. The straight plate design would then be expected to be more sensitive to the placement of a notch in this position. The residual tensile stress on the inside face of the rim is higher for the curve plate wheel than for the straight plate wheel. If notches had been put at this location, the results of the tests may have been different.

It is interesting to note that the development of thermal cracks on dynamometer tests requires that stress concentration features must be introduced to initiate thermal cracks. The test described in Ref 1 required notches on the tread of the wheel in order to develop thermal cracks. An extensive series of tests described in Ref 24 required the placement of saw cuts in the wheel in order for a consistent trend in thermal cracking to be developed. This suggests that the thermal crack phenomenon requires combined loading effects for its initiation. This would include both the effects of large thermal loads from drag braking and the stress fluctuations from vertical and lateral wheel/rail interaction loads. In addition, as previously indicated, the stresses associated with service braking may also be important.

The limitations associated with the application of analytical procedures to the study of wheel failure phenomena have been illustrated by the work conducted under this project. One limitation results from the lack of thermal and material property data for wheel materials at elevated temperatures. The lack of data describing the modification of the yield point and the definition of the stress-strain curve at high temperatures is especially critical. The modification of the residual stress field in the wheels will depend to a large extent on the degree of yielding that takes place during severe thermal loads.

Another limitation is the lack of crack growth data under the conditions which are prevalent in many wheel failures. The analyses have shown that crack initiation and early growth probably takes place as the result of small stress fluctuations about a high average tensile stress. More information must be obtained about the behavior of wheel materials under these conditions because they are not included in most sets of fracture mechanics property data.

There is the need to conduct full-scale experiments on railroad wheels which would provide experimental data on the relative importance of various parameters that affect the initiation of wheel failure mechanisms. This would require the construction of a test fixture on which experiments could be conducted where the failure of the wheel can be tolerated. The present understanding of wheel failure phenomena is that a large number of factors interrelate to cause failures. These cannot be fully evaluated through analytical studies. Experimental studies must go along with the analytical work. Analysis work would provide guidance for suggesting the types of experiments to be conducted and also to explain the observed experimental phenomena.

Severe thermal loading (drag brake) tests which have been conducted on railroad wheel dynamometers have generally failed to cause wheel failure by thermal cracking. In order to get consistent test results it has been necessary to introduce a notch or other stress concentration feature in the wheel. This suggests that the small cyclic stresses associated with mechanical wheel loads play an important role in wheel failure phenomena and that the provision for introducing these loads should be built into any test fixture which is constructed for the study of these wheel failure effects. The test fixture should also have the capability of sustained high energy drag braking loads in excess of 37 kW (50 bhp) for periods of time as long as an hour and for the simultaneous introduction of vertical and lateral forces at a simulated wheel/rail interface. Force levels of 224 kN (50,000 lb) vertically and 112 kN (25,000 lb) laterally may be required for the tests.

## 9. REFERENCES

1. Haley, M. R., Larson, H. R. and Kleeschulte, D. G. "Systems Approach to Failure Resistant Cast Steel Railroad Carwheel Design", ASME Journal of Engineering Materials and Technology (January 1980), pp 26-31.
2. Brazzoduro, L., Brozzo, P., DeMartini, R. and Venturelli, T. "Final Results of the Research Work on a New Solid Wheel Apt to the Most Severe Operative Conditions", 6th International Wheelset Congress, Colorado Springs, Colorado (October 1978).
3. Wetenkamp, H. R. "Thermal Stress Developed in S-Plate, Straight Plate, and Deep Dish Wheels", ASME Paper 73-RT-1 (April 1973).
4. "Manual of Standards and Recommended Practices", Section A Specifications for Materials, Specification M107, Wheels, Wrought Carbon Steel, Association of American Railroads, Mechanical Division.
5. "Manual of Standards and Recommended Practices", Section A, Specification for Materials, Specification M208, Wheels, Cast Carbon Steel, Association of American Railroads, Mechanical Division.
6. "Field Manual of the AAR Interchange Rules", Association of American Railroads, Mechanical Division, (1980).
7. Bruner, J. P., Jones, R. D., Levy, S. and Wandrisco, J. M. "Effect of Design Variation on Services Stresses in Railroad Wheels", ASME Technical Paper 67-WA/RR-6 (November 1967).
8. Bruner, J. P., Benjamin, G. N. and Bench, D. M. "Analysis of Residual, Thermal, and Loading Stresses in a B33 Wheel and Their Relationship to Fatigue Damage", ASME Journal of Engineering for Industry (May 1967), pp 249-258.
9. Novak, G. E. and Eck, B. J. "A Three-Dimensional Finite Difference Solution for the Thermal Stresses in Railcar Wheels", ASME Journal of Engineering for Industry (August 1969), pp 891-896.
10. Novak, G. E., Kucera, W. J., and Eck, B. J. "The Effect of Rim Thickness on Wheel Stresses Caused by Simulated Service Conditions", ASME Paper 73-WA/RT-10 (November 1973).
11. Novak, G. E., Greenfield, L. D. and Stone, D. H. "Simulated Operating Stresses in 28-inch Diameter Wheels", ASME Paper 75-RT-10 (April 1975).
12. Nishioka, K. and Morita, Y. "The Strength of Railroad Wheels", Bulletin of JSME, 14 (67), (1971) pp 11-19.

13. Rusin, T. M., Kleeschulte, D. G. and Coughlin, J. M. "Application of the Finite Element Method in the Development of Improved Railroad Car Wheel Designs", ASME Technical Paper 78-WA/RT-5 (December 1978).
14. Johnson, M. R., Welch, R. E. and Yeung, K. S. "Analysis of Thermal Stresses and Residual Stress Changes in Railroad Wheels Caused by Severe Drag Braking", Journal of Engineering for Industry (ASME) 99 (1), Series B (February 1977), pp 18-23.
15. Novak, G. E. and Eck, B. J. "Asymmetrical Wheel Stresses Caused by Simulated Thermal and Mechanical Service Loads", ASME Paper 72-WA/RT-13 (November 1972).
16. Nishioka, K., Nishimura, S., Hirakawa, K., Tokimasa, K. and Suzuki, S. "Fracture Mechanics Approach to the Strength of Wheelsets", 6th International Wheelset Congress, Colorado Springs, Colorado (October 1978).
17. Wetenkamp, H. R. and Kipp, R. M. "Safe Thermal Loads", 6th International Wheelset Congress, Colorado Springs, Colorado (October 1978).
18. Opinsky, A. J. "Fracture Mechanics Data for Three Classes of Railroad Wheel Steels", 6th International Wheelset Congress, Colorado Springs, Colorado (October 1978).
19. Walker, K. "The Effects of Stress Ratio During Crack Propagation and Fatigue for 2024-T3 and 7075-T6 Aluminum", ASTM STP 462, American Society for Testing and Materials, 1970, pp 1-14.
20. Johnson, M. R. Development of Data to Improve Design Criteria of Railroad Wheels. Final Report Contract DOT-TSC-855 for Transportation Systems Center, 1978.
21. Rusin, T. M. "Experimental Verification of Computer Predicted Temperatures and Elastic Thermal Strains in Railroad Wheels", 6th International Wheelset Congress, Colorado Springs, Colorado (October 1978).
22. Johnson, M. R. "Predicted and Measured Wheel Strains Resulting from Prolonged Drag Braking", 6th International Wheelset Congress, Colorado Springs, Colorado (October 1978).
23. Park, Y. J. Cyclic Behavior of Class U Wheel Steel, Association of American Railroads Report R-342, December 1978.
24. Wetenkamp, H. R., Sidebottom, O. M. and Schrader, H. J. "The Effect of Brake Shoe Action on Thermal Cracking and on Failure of Wrought Steel Railway Car Wheels", University of Illinois Bulletin 47 (77), (Series 387), (June 1950).

DISTRIBUTION LIST

<u>No. of Copies</u>	<u>Organization</u>	<u>No. of Copies</u>	<u>Organization</u>
12	Commander Defense Technical Info Center ATTN: DDC-DDA Cameron Station Alexandria, VA 22314	1	Commander US Army Communications Rsch and Development Command ATTN: DRDCO-PPA-SA Fort Monmouth, NJ 07703
1	Commander US Army Materiel Development and Readiness Command ATTN: DRCDMD-ST 5001 Eisenhower Avenue Alexandria, VA 22333	1	Commander US Army Electronics Research and Development Command Technical Support Activity ATTN: DELSD-L Fort Monmouth, NJ 07703
2	Commander US Army Armament Research and Development Command ATTN: DRDAR-TSS (2 cys) Dover, NJ 07801	1	Commander US Army Missile Command ATTN: DRSMI-R Redstone Arsenal, AL 35809
1	Commander US Army Armament Materiel Readiness Command ATTN: DRSAR-LEP-L, Tech Lib Rock Island, IL 61299	1	Commander US Army Missile Command ATTN: DRSMI-YDL Redstone Arsenal, AL 35809
1	Director US Army ARRADCOM Benet Weapons Laboratory ATTN: DRDAR-LCB-TL Watervliet, NY 12189	1	Commander US Army Tank Automotive Rsch and Development Command ATTN: DRDTA-UL Warren, MI 48090
1	Commander US Army Aviation Research and Development Command ATTN: DRDAV-E 4300 Goodfellow Boulevard St. Louis, MO 63120	1	Director US Army TRADOC Systems Analysis Activity ATTN: ATAA-SL, Tech Lib White Sands Missile Range NM 88002
1	Director US Army Air Mobility Research and Development Laboratory Ames Research Center Moffett Field, CA 94035	10	Department of Transportation Federal Railroad Administration ATTN: Mr. Don Levine RRD-33 7th and D Streets, SW Washington, DC 20590

DISTRIBUTION LIST

<u>No. of Copies</u>	<u>Organization</u>
2	Department of Transportation Federal Railroad Administration ATTN: Mr. Dave Dancer Mr. John Mirabella 7th and D Streets, S.W. Washington, DC 20590
3	IIT Research Institute ATTN: Dr. Milton R. Johnson 10 West 35th Street Chicago, IL 60616
2	Transportation Test Center ATTN: Mr. Pete Cramer Mr. Thomas Loucks Pueblo, CO 81001
2	Micro-Tec, Inc. ATTN: Mr. Monte Johnson Mr. Dave Carey 15 N. Bond Street 2nd Floor Bel Air, MD 21014

Aberdeen Proving Ground

Dir, USAMSAA  
ATTN: DRXS-D  
      DRXS-MP, H. Cohen

Cdr, USATECOM  
ATTN: DRSTE-TO-F

Dir, USACSL, Bldg. E3516, EA  
ATTN: DRDAR-CLB-PA



USER EVALUATION OF REPORT

Please take a few minutes to answer the questions below; tear out this sheet, fold as indicated, staple or tape closed, and place in the mail. Your comments will provide us with information for improving future reports.

1. BRL Report Number \_\_\_\_\_

2. Does this report satisfy a need? (Comment on purpose, related project, or other area of interest for which report will be used.)

\_\_\_\_\_  
\_\_\_\_\_  
\_\_\_\_\_

3. How, specifically, is the report being used? (Information source, design data or procedure, management procedure, source of ideas, etc.) \_\_\_\_\_

\_\_\_\_\_  
\_\_\_\_\_

4. Has the information in this report led to any quantitative savings as far as man-hours/contract dollars saved, operating costs avoided, efficiencies achieved, etc.? If so, please elaborate.

\_\_\_\_\_  
\_\_\_\_\_

5. General Comments (Indicate what you think should be changed to make this report and future reports of this type more responsive to your needs, more usable, improve readability, etc.) \_\_\_\_\_

\_\_\_\_\_  
\_\_\_\_\_  
\_\_\_\_\_

6. If you would like to be contacted by the personnel who prepared this report to raise specific questions or discuss the topic, please fill in the following information.

Name: \_\_\_\_\_

Telephone Number: \_\_\_\_\_

Organization Address: \_\_\_\_\_

\_\_\_\_\_  
\_\_\_\_\_